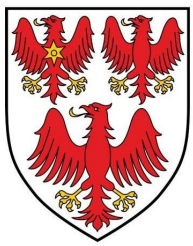



# Spacetime Connectomics for Describing and Modelling Complex Dynamics of Human Brain States

Jakub Vohryzek

The Queen's College



University of Oxford

A thesis presented for the degree of

*Doctor of Philosophy*

Trinity 2021

Copyright © 2021 by Jakub Vohryzek
All Rights Reserved

Most men will not swim before they are able to. Is that not witty? Naturally, they won't swim! They are born for the solid earth, not for the water. And naturally they wont think. They are made for life, not for thought. Yes, and he who thinks, what's more, he who makes thought his business, he may go far in it, but he has bartered the solid earth for the water all the same, and one day he will drown.

— Herman Hesse, Steppenwolf

From argument comes light

— Portuguese proverb

# Acknowledgements

No bird soars too high, if she soars with her own wings.

— W. Blake, The Marriage of Heaven and Hell

Nothing comes more easily than the expression of gratitude to those who have supported me throughout this amazing, albeit challenging, journey.

To my anchors in life, whose love wills me on in the pursuit of scientific passions while reminding me of what counts beyond cerebral matters. Mum and dad, thank you for the excitement with which you share any journey I embark on, Jan and Matěj, thank you for being my brothers in arms; BabiJana and BabiHelka, for your calm, wisdom and open arms whenever my flitting mind comes home to Prague.

I have been privileged to see ideas one so enthusiastically writes about being manifested in other walks of life. Just as the brain balances flexibility to engage with the word and stability to consolidate concepts and knowledge, so Morten has done exactly that during my DPhil, guiding me through the shifting sands of human knowledge and supporting me in times of doubt while granting me freedom to wonder about the world (and to be creative in doing so). For this I am very grateful. This gratitude also extends to Gustavo, who welcomed me in Barcelona for my visiting studentship and entrusted me with my next chapter of postdoctoral position in Barcelona.

A bow of thanks to the postdoctoral triumvirate of the Hedonia Research Group for their friendship and provision of a safe space to think together freely; to Joana for the vigour and passion through which we have discussed scientific matters, to Selen for the comfort and calm she always exuded when discussing ideas on

the Hedonia sofa, and finally to Henrique, for exemplifying the scientific balance between rigour and creativity.

My DPhil has been a story of many exchanges of ideas and meetings of minds, and I feel honored to have glimpsed the Oxford temper of playing gracefully with ideas. This has been made possible through many discussions on various topics with friends James, Adrien, František and Lena, the Hedonians L.D., Marina, Angus, Eloise and Jetro. My friends and colleagues in Switzerland Emeline, Alessandra, Ruxandra and Patric, and in Spain Thomas, Ludovica and Josephine. Friends and collaborators on scientific papers and other related matters Leonardo, Louis, Andrea, Pedro, Fernando, Yonatan and Enzo. Friends at home Kryštof and Cyril, whose discussions have allowed me to see my scientific expertise in a larger, societal context. The Brainhack community for sharing the sense of inclusive and community-led vision of scientific inquiry.

When the coronavirus pandemic came, you took me under your wings and gave me a safe space to concentrate on my Thesis, and shared with me Cornwall surfing escapades that kept me sane during the final stages of writing. A testament of a unique friendship for which I will be forever grateful - thank you Fraser and Matthew. Finally to you Atilla, who has always believed in me and provided me with so much needed mental and scientific support going all the way back to my Master's Thesis, when whole-brain models were exotic beasts to me.

# Abstract

Spacetime Connectomics for Describing and Modelling Complex Dynamics of Human Brain States

Jakub Vohryzek

The Queen's College

The human brain is poised to maintain reproducible behaviours while simultaneously allowing for flexible adaptability. Such characteristics are realised in complex systems endowed with metastable dynamics. The central tenet of this Thesis is to investigate rich and spontaneous brain dynamics in terms of their spatial and temporal properties in different brain states, namely the psychedelics-induced and depressive state.

In Chapter 2, I formalise spatio-temporal dynamics as a temporal trajectory evolving in a space of phase-locking substates. I define temporal characteristics of those substates in terms of fractional occupancy, life times and transition probability. I show functional relevance of the phase-locking substates, recurrence across recording sessions, and a moderate reliability for potential personalised fingerprinting. These results provide theoretical underpinning of spatio-temporal dynamics and motivate use of this particular representation in diagnosis and prognosis of various brain states.

Chapter 3 builds on Chapter 2 studying how whole-brain models, fitted to the spatio-temporal description of brain states, can be used for intervention with psychedelics for treatment-resistant depression. I build and validate whole-brain models for responders and non-responders to treatment and by systematic perturbation stimulation I analyse how different regions permit (or not) a transition to healthy brain function. The results demonstrate a subset of regions unlikely to transit to the healthy state. Moreover, these regions correlate with the $5HT_{2a}$ and $5HT_{1A}$ density maps known to be mediators of the psychedelic neuropharmacology. This study is a proof-of-concept of the viability in using whole-brain modelling of the brain's spatio-temporal representation, to inform potential avenues in clinical treatments.

In Chapter 4, I analyse the psychedelic state induced by N,N-Dimethyltryptamine (DMT) from a perspective of Connectome Harmonic Decomposition. Here, spatio-temporal dynamics are described in terms of temporal contributions of spatial frequencies realised on the structural connectivity of the brain. The results show changes in the harmonic spectrum in line with previous findings with psilocybin and Lysergic Acid Diethylamide (LSD). Furthermore, the DMT-induced state broadens the repertoire of connectome harmonics and enhances signatures of critical dynamics in the brain. These results provide further evidence of whole-brain spatial and temporal changes under the psychedelic-induced state and offer further evidence of the brain being tuned closer to critical dynamics.

In Chapter 5, I consider functional substates implicitly derived from the brain's communication structure. I call this method HArmonic DEcomposition of Spacetime (HADES). I demonstrate how large proportion of the data can be reconstructed with just a few of the spatial substates and their temporal contributions. By using the same dataset as in Chapter 4, I show suppression of functional hierarchies and an increase of global integration under the influence of DMT. This method promises an exciting avenue for the analysis of gradient-like and locally specialised functional activity in time.

The proposed and applied methods in this thesis demonstrate the necessity of describing brain dynamics across space and time from a complexity science perspective. I show how psychedelics-induced states such as DMT, psilocybin and LSD, change spatial and temporal characteristics of brain activity towards more integrative and flexible functioning, and outline how whole-brain models might inform future clinical interventions for treatment of depression.

***Keywords—*** Complexity - Brain States - Spacetime Connectomics - Complex Dynamics - Whole-brain Modelling

# Contents


**1 Introduction** **1**

1.1 The Brain as a Complex System . . . . . 2

1.1.1 Characteristics . . . . . 2

1.1.2 Insights from Neuroimaging . . . . . 7

1.1.3 Whole-brain Modelling . . . . . 13

1.1.4 Dynamical Landscape . . . . . 17

1.2 Theoretical Models of Brain Function . . . . . 17

1.2.1 The Entropic Brain . . . . . 19

1.2.2 REBUS and the Anarchic Brain . . . . . 21

1.3 The Psychedelic State . . . . . 23

1.3.1 Neural Correlates of the Psychedelic-induced State . . . . 24

1.3.2 Pharmacology of Psychedelic Drugs . . . . . 26

1.4 Depressive State . . . . . 29

1.4.1 Behavioural and Neuropharmacological Symptoms of Depression . . . . . 29

1.4.2 Resting-state Networks Implicated in Major Depressive Disorder . . . . . 32

1.4.3 Treatment with Psychedelics . . . . . 34

1.4.4 Moving forward . . . . . 35

**2 Brain Spatio-Temporal Dynamics as a Temporal Trajectory in a Landscape of Phase-Locking Substates**[1] **37**

2.1 Introduction . . . . . 37

2.2 Methods . . . . . 39

2.2.1 Dataset . . . . . 39

2.2.2 Phase dynamics . . . 40
2.2.3 Leading Eigenvector of Phase Dynamics . . . 40
2.2.4 Phase Space Partition . . . 42
2.2.5 Comparison with Canonical Resting-state Networks . . . 45
2.2.6 Validation Dataset . . . 45
2.2.7 Measures of the Substate-based Representation . . . 46
2.2.8 Intra-Class Correlation . . . 48
2.3 Results . . . 48
2.3.1 Functional Relevance . . . 49
2.3.2 Repertoire Exploration . . . 51
2.3.3 Recurrence . . . 53
2.3.4 Reliability . . . 55
2.4 Discussion . . . 56
2.5 Chapter Summary . . . 63

**3 Rebalancing the Depressive Brain State with Psilocybin 64**
3.1 Introduction . . . 64
3.2 Methods . . . 66
3.2.1 Experimental Data . . . 66
3.2.2 Probabilistic Metastable Substates (PMS) . . . 66
3.2.3 Whole-brain Computational Model . . . 69
3.2.4 Objective Function . . . 71
3.3 Results . . . 72
3.3.1 Experimental Analysis . . . 73
3.3.2 Optimization of the Whole-brain Model to PMS Space . . . 75
3.3.3 Perturbation Protocol . . . 75
3.3.4 Correlation with 5HT Maps . . . 78
3.4 Discussion . . . 80

3.5 Summary . . . . . 83

**4 DMT Psychedelic State Revealed by Connectome Harmonics Decomposition 84**

4.1 Introduction . . . . . 84
4.2 Methods . . . . . 86
4.2.1 DMT dataset . . . . . 86
4.2.2 Psilocybin Dataset . . . . . 88
4.2.3 LSD Dataset . . . . . 89
4.2.4 Structural Connectome Construction . . . . . 89
4.2.5 Derivation of Connectome Harmonics . . . . . 90
4.2.6 Connectome Harmonic Decomposition of Resting-state fMRI . . . . . 92
4.2.7 Measures . . . . . 92
4.3 Results . . . . . 95
4.3.1 The DMT-induced State Suppresses Low-level Harmonics and Increases High-level Harmonics . . . . . 95
4.3.2 DMT-induced State Enhances Signatures of Criticality . . 97
4.3.3 DMT-induced Changes in CHD Compare to LSD and Psilocybin . . . . . 100
4.4 Discussion . . . . . 102
4.5 Summary . . . . . 106

**5 HArmonic DEcomposition of Spacetime (HADES) 108**

5.1 Introduction . . . . . 108
5.2 Methods . . . . . 112
5.2.1 Data . . . . . 112
5.2.2 Dense Functional Connectome . . . . . 112

5.2.3 Resting-state fMRI Timeseries and DMT . . . . . 113
5.2.4 Functional Harmonics . . . . . 113
5.2.5 Functional Harmonic Decomposition . . . . . 114
5.2.6 Parcellation and Reference Functional Networks . . . . . 115
5.2.7 Power . . . . . 115
5.2.8 Dynamic Measures . . . . . 117
5.3 Results . . . . . 117
5.3.1 Functional Relevance . . . . . 117
5.3.2 Signal Reconstruction . . . . . 118
5.3.3 Power across Functional Harmonics . . . . . 120
5.3.4 Dynamic Measures of HADES . . . . . 122
5.4 Discussion . . . . . 123
5.5 Summary . . . . . 126

**6 Discussion** **127**
6.1 Novel Insights . . . . . 128
6.1.1 Brain Spatio-temporal Dynamics as a Temporal Trajectory in a Landscape of Phase-locking Substates . . . . . 128
6.1.2 Rebalancing the Depressive Brain State with Psychedelics 128
6.1.3 DMT-induced Psychedelic State Revealed by Connectome Harmonic Decomposition . . . . . 129
6.1.4 HArmonic DEcomposition of Spacetime (HADES) . . . . 130
6.2 Perspective . . . . . 130

**Appendix A Supplementary Information** **169**

# List of Figures


1.1 Brain as a Complex System . . . . . 5
1.2 Methods Across Spacetime . . . . . 10
1.3 Whole-brain Neuroimaging . . . . . 11
1.4 Insights from Whole-brain Modelling . . . . . 16
1.5 Dynamical Landscape . . . . . 18
1.6 The Entropic Brain . . . . . 20
1.7 REBUS and Anarchic Brain . . . . . 22
1.8 Phenomenology of Psychedelic Experience . . . . . 24
1.9 Psychedelics in Space and Time . . . . . 27
1.10 Symptoms of Depression . . . . . 30
1.11 Depression in Space and Time . . . . . 32
1.12 Brain Serotonin Function . . . . . 34

2.1 Time-evolving Patterns of Phase Dynamics . . . . . 41
2.2 N-dimensional Phase Space Partition into a K-dimensional Substate-based Space . . . . . 43
2.3 Centroids Overlap with RSNs . . . . . 50
2.4 Repertoire of Phase Locking Substates Obtained Using K = 5 . . . 52
2.5 Trajectories of Brain Activity in Substate Space. . . . . 54
2.6 Individual Reliability of the Phase-Locking Substates' Measures . 57

3.1 Experimental Design . . . . . 67
3.2 Study Overview . . . . . 68
3.3 PMS in Treatment-resistant Depression with Psilocybin Intervention 73
3.4 Model Validation . . . . . 74
3.5 Perturbation Protocol . . . . . 76

3.6 Inability of Nodes to Force a Transition to the Healthy State . . . 78
3.7 Correlations with Serotonergic Receptors . . . . . 79

4.1 Experimental Design . . . . . 87
4.2 Study Overview . . . . . 93
4.3 DMT-induced Energy Changes in the Connectome Harmonic Spectrum . . . . . 96
4.4 Repertoire of Connectome Harmonic and Repertoire Entropy . . . 98
4.5 Power-laws of Connectome Harmonics in the DMT-induced State 100
4.6 Connectome Harmonic Decomposition across Psychedelic-induced States . . . . . 101

5.1 Overview of HADES . . . . . 111
5.2 Functional Harmonics . . . . . 116
5.3 Signal Reconstruction . . . . . 119
5.4 Power Results . . . . . 120
5.5 Dynamic Measures of HADES . . . . . 121
5.6 Fractional Occupancy and Life Times . . . . . 122

6.1 Summary of Methods . . . . . 132

A.1 Centroids Overlap with RSNs - Top view . . . . . 170
A.2 Individual Transition Probability . . . . . 171
A.3 Clustering Quality Measures . . . . . 172
A.4 Empirical Results - GBC, Synchrony, Metastability, FCD . . . . . 173
A.5 Model Validation - GBC, Synchrony, Metastability, FCD . . . . . 174
A.6 Connectome Harmonic Decomposition Based on 32 HCP Subjects; an Effect of Connectome Template . . . . . 175

A.7 Energy Spectrum of Connectome Harmonics Between Post-DMT and Post-placebo Conditions . . . . . 176
A.8 Functional Harmonics of HADES and (Glomb et al., 2019) . . . . 176

# List of Abbreviations

**5HT** . . . . . Serotonin or 5-hydroxytryptamine

**BOLD** . . . . . Blood-Oxygen Level-Dependent

**CN** . . . . . Control Network

**DAN** . . . . . Dorsal Attention Network

**DMN** . . . . . Default Mode Network

**DMT** . . . . . N,N-Dimethyltryptamine

**DSI** . . . . . Diffusion Spectrum Imaging

**DSM** . . . . . Statistical Manual of Mental Disorders

**DTI** . . . . . Diffusion Tensor Imaging

**EEG** . . . . . ElectroEncephaloGram

**FC** . . . . . Functional Connectivity

**FCD** . . . . . Functional Connectivity Dynamics

**fMRI** . . . . . functional Magnetic Resonance Imaging

**FPN** . . . . . Fronto-Parietal Network

**GABA** . . . . . Gamma-AminoButyric Acid

**HADES** . . . . . HArmonic DEcomposition of Spacetime

**HMM** . . . . . Hidden Markov Models

**ICD** . . . . . International Classification of Diseases

**KOP** . . . . . Kuramoto Order Parameter

**LEiDA** ..... Leading Eigenvector Dynamic Analysis

**LN** ..... Limbic Network

**LSD** ..... Lysergic Acid Diethylamide

**MDD** ..... Major Depressive Disorder

**MEG** ..... MagnetoEncephaloGram

**MRI** ..... Magnetic Resonance Imaging

**PCI** ..... Perturbation Complexity Index

**PET** ..... Positron Emission Tomography

**PMS** ..... Probability Metastable Substates

**REBUS** ..... RElaxed Beliefs Under pSychedelics

**sFC** ..... static Functional Connectivity

**SN** ..... Salience Network

**TMS** ..... Transcranial Magnetic Stimulation

**TRD** ..... Treatment Resistant Depression

**VAN** ..... Ventral Attention Network

**VIS** ..... Visual Network

# 1 | Introduction

The whole process of nature is an integrated process of immense complexity and it is really impossible to tell whether something that happens in it is good or bad. Because you never know what will be the consequences of the misfortune. Or, you never know what will be the consequences of good fortune.

— Alan Watts, The Story of the Chinese Farmer

Complex systems are full of interdependencies - hard to detect - and nonlinear responses.

— Nassim Nicholas Taleb, Antifragile

The reason that being healthy and robust equates with greater variance and larger fluctuations, and therefore a larger fractal dimension as in an EKG, is closely related to the resilience of such system, Being overly rigid and constrained means that there isn't sufficient flexibility for the necessary adjustments needed to withstand the inevitable small shocks and perturbations to which any system is subjected.

— Geoffrey West, Scale

## 1.1 The Brain as a Complex System

### 1.1.1 Characteristics

To engage with the world, the human brain relies on reproducible behaviours related to internal and external stimuli, and simultaneously adapts with endowed flexibility to the ever-changing environmental conditions. Such capabilities are enabled by rich and spontaneous brain dynamics necessary for maintaining a certain degree of order (stability), for consistent functioning, as well as disorder (flexibility), for functional adaptability (Plenz, 2013; Atasoy et al., 2017b). For instance, while bike-riding for the first time, the brain engages in reproducible neuronal activity associated with learnt behaviour of motor coordination and gait, and at the same time allows for sufficient adaptability of learning to balance on two wheels. Accordingly, such rich and spontaneous dynamics will be altered in various states of brain functioning such as in minimally conscious state, sleep or neuropsychiatric disorders (Laureys, 2005). More specifically, a psychedelic-induced state will be highly suggestive to the incoming information, and in contrast a depressive state will be excessively rigid in ruminative thought (Carhart-Harris et al., 2014; Carhart-Harris, 2018; Carhart-Harris and Friston, 2019). Indeed, recent developments in systems neuroscience have started to make inroads into the characterisation of these complex dynamics in space and time with special focus on the underlying mechanisms (Deco et al., 2011; Cocchi et al., 2017; Tognoli and Kelso, 2014).

To appreciate the brain's ability to (re)produce a plethora of behaviours emerging from spatio-temporal dynamics, it is pertinent to consider the brain from a complex system perspective (Turkheimer et al., 2021). The brain consists of approximately 100 billion neurons with about 100 trillion synapses between them. This

dense network of interactions has been named the human connectome (Sporns et al., 2005; Hagmann et al., 2008). Recent advances in transcriptomics have further demonstrated the heterogeneity of neuronal anatomy across the human brain (Burt et al., 2020; Hawrylycz et al., 2012). The arising dynamics of neuronal interactions on the structural scaffold are further modulated by numerous neurotransmitter systems (Shine, 2019). It is therefore not surprising that many novel approaches ranging from dynamical system theory (Deco et al., 2011), information theory (Rosas et al., 2020), turbulence (Deco and Kringelbach, 2020) to statistical mechanics (Deco et al., 2021b; Lynn et al., 2020; Ponce-Alvarez et al., 2021) have been deployed to understand the brain's complex spatio-temporal dynamics in its entirety (Turkheimer et al., 2021).

Indeed, this has meant a paradigm shift away from looking at the brain and its function solely in terms of individual neurons or brain regions to a system-based interaction of a multiplicity of interacting units. One of the fields to emerge from this conceptual leap has been network neuroscience that has focused on describing large-scale structural and functional networks in terms of their properties and relevance for creating complex behaviour (Bullmore and Sporns, 2009; Bassett and Sporns, 2017) (See Figure 1.1 A).

Such complex systems usually consist of a multitude of interacting units, each of which potentially exhibits non-linear dynamics (Chialvo, 2010). Instances of non-linear responses within the brain to physiological stimulation have been demonstrated both at the level of single neurons and brain regions (Williams and Shapley, 2007; Loggia et al., 2012) with perhaps the most striking complex effects to the whole brain's response having been shown with external Transcranial Magnetic Stimulation (TMS). A short TMS pulse was administered to clinical populations exhibiting varying levels of consciousness. The resulting complex spatio-temporal dynamics recorded with electroencephalography (EEG) were successfully used to

distinguish between the different groups and individuals (Casali et al., 2013) (Figure 1.1 B). Another perspective is to consider how the brain as a whole responds to systemic challenges. With metabolic demands, stress-induced pressures and immune challenges within the system, structural and functional observables will inadvertently reflect non-linear behaviours of constituent parts. This has been suggested to play a role in non-linear trajectories in brain development and ageing, as well as the emergence of brain disorders (Turkheimer et al., 2021).

At the right balance, a complex system can further demonstrate self-organising properties across space and time from non-linear interactions of the parts (Turkheimer et al., 2021; Bak and Paczuski, 1995; Chialvo, 2004). Interestingly, this happens in a distributed manner without a centralised control dictating the emerging order (Kelso, 1995). In the brain, such spatio-temporal organisation has been demonstrated across scales with characteristics of spatial and temporal invariance (Expert et al., 2011) (Figure 1.1 C). Importantly, such organisation is believed to happen at the edge of criticality - a dynamical regime where long-range spatial and temporal correlations are made possible (Tagliazucchi et al., 2012). To date such scale-freeness has been observed across spatial dimensions - from the microscopic scale of cortical slices of individual neurons (Beggs and Plenz, 2003), to the macroscopic scale of the degree distribution of a functional Magnetic Resonance Imaging (fMRI) network (Eguíluz et al., 2005), as well as across temporal dimensions - both at the fast scale of magnetoencephalography (MEG) recordings (Shriki et al., 2013), in microstates of EEG (Van De Ville et al., 2010), and at the slow scale of fMRI data (Kitzbichler et al., 2009). It is further relevant to appreciate the properties that the brain is endowed with close to criticality, as in this regime the dynamic range, capacity and transmission of information are optimised (Shew and Plenz, 2013; Shew et al., 2011). Furthermore, it is in this range that spatio-temporal metastability (a notion of dynamical flexibility) has been hy-

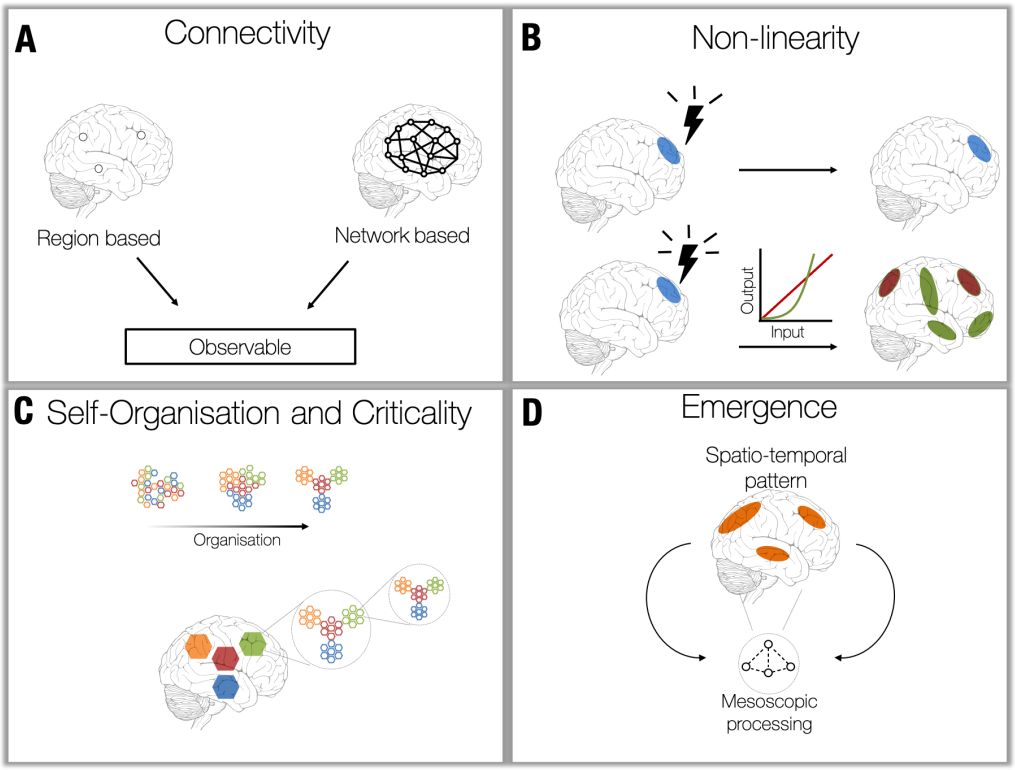



Figure 1.1: ***The Brain as a Complex System.*** ***A)*** *A shift in perspective towards considering the brain's function and structure as an integrated network of relationships as opposed to solely localised descriptions of individual regions of interest.* ***B)*** *In many biological systems such as the brain, interactions between stimuli and measurement outputs are mostly non-linear.* ***C)*** *The brain is thought to show self-organisation across many spatial and temporal scales. Furthermore, such organisation is considered scale-free in space and time with dynamics characteristic of a system near criticality - a balanced regime between orderly and disorderly activity.* ***D)*** *Constituent parts at the mesoscopic scale give rise to emergent ensembles of brain activity that cannot be merely explained by the summation of the individual parts. These are said to be computationally irreducible and causally emergent (adapted from (Turkheimer et al., 2021))*

pothesised to be maximal (Yang et al., 2012; Tognoli and Kelso, 2014; Bressler and Tognoli, 2006).

Furthermore, complex systems, exhibiting self-organising properties, give rise to emergent phenomena with various examples across nature - flocks of startles, swarms of bees or ant colonies. Such collective behaviour emerges as an interaction of a large number of constituent parts of the system but the behaviour in its entirety is unexplainable by simply looking at localised spatio-temporal interactions of the individual elements - the behaviour is said to be computationally irreducible. In the brain, such characteristics are representative of higher-order cognition which cannot be simply reduced to the underlying neurophysiology. Specifically, in resting-state brain activity, a condition without any external task, spatially synchronised systems, termed Resting-State Networks (RSNs), are hypothesised to be emergent from the underlying neuronal activity (Turkheimer et al., 2015) (Figure 1.1 D). These emergent properties (examples of weak-emergence (Turkheimer et al., 2019)) result in creating their own rules through which they interact with the environment (causal decoupling) and at the same time allow for causally influencing the behaviour of the underlying parts (downward causation) (Rosas et al., 2020).

To summarise, understanding the brain as a complex system has profound conceptual implications for its study. It is important to describe its basic properties, such as non-linear spatio-temporal interactions, emergent phenomena of higher-order cognition and dynamics at the edge of criticality and relate them to empirical structural and functional brain data.

### 1.1.2 Insights from Neuroimaging

Much of the progress in understanding large-scale brain networks has come out from studying the brain with Magnetic Resonance Imaging (MRI). Here, I describe two of the most popular MRI techniques, namely fMRI and Diffusion Tensor Imaging (DTI). With respect to fMRI, I will further discuss how progress in dynamic functional connectivity (FCD), as opposed to the static functional connectivity (sFC), has paved the way to a more complete understanding of many complexity questions.

FMRI is a non-invasive technique measuring the blood-oxygen level-dependent (BOLD) signal. The BOLD signal has been considered as an indirect measure of neuronal activity through the principle of neurovascular coupling. In brief, heightened neuronal activity leads to a cascade of events starting with increases in cerebral blood flow and cerebral blood volume that results in an increase in the cerebral metabolic rate of $O_2$. This has an effect on the ratio of oxygenated to deoxygenated haemoglobin which in turn affects the local magnetic fields. The BOLD-tuned ($T_2^*$-weighted) MRI is sensitive to these inhomogeneities in the local magnetic fields (Logothetis, 2002; Logothetis and Wandell, 2004). Such signal is characterised by very slow fluctuations, usually below frequency of 0.15Hz (Josephs and Henson, 1999).

The voxel-based signal is usually pre-processed before considered for analysis. However it still isn't clear what the best pre-processing of the fMRI dataset is. A nice example to illustrate this point, which is relevant to this Thesis, is that of global signal regression (Murphy et al., 2009). While it is not a desirable step from the complex system perspective as important background activity might be lost, many scientists argue for global signal regression on the basis of artifact removal (Murphy and Fox, 2017). All considered, there has been a growing

consensus on the minimal pre-processing pipeline (Glasser et al., 2013), as well as pre-processing workflows unifying the different pre-processing steps (Esteban et al., 2019). Standard steps usually involve, but are not limited to, slice-timing correction, spatial smoothing, physiological artifact removal, motion correction and temporal filtering (Daducci et al., 2012). Movement induced distortions in fMRI scanner are also highly debated topic (Power et al., 2017). Recent work has shown that idiosyncratic motion of participants can accurately predict anthropometric and cognitive factors (Bolton et al., 2020a).

After pre-processing, fMRI signal is parcellated using atlas-based delineation of the cortex. Functionally (Schaefer et al., 2018) and anatomically (Tzourio-Mazoyer et al., 2002) pre-defined atlases or data-driven templates (Beckmann and Smith, 2004) are usually considered. However, it is still unclear what the relevant number of brain regions should be and so approaches assessing regional homogeneity have been proposed (Zang et al., 2004). Furthermore, the notion of a brain region, as a sharply defined anatomical location, has been challenged in favour of gradient-like representation of cortical organisation (Margulies et al., 2016; Glomb et al., 2019) (also see Figure 1.3, B).

Static functional connectivity has been a common approach of analysing functional activity from the perspective of network neuroscience. Connectivity is estimated as the similarity between the timeseries of pairs of atlas-based regions, often using the correlation coefficient (Hlinka et al., 2011). Other, more elaborate methods have been proposed to account for spurious correlations and edge directionality, such as partial correlation and effective connectivity respectively, but the idea of static representation of functional brain networks remains the same. Despite the initial success of shifting the perspective from regional activations to network based methods, it has remained challenging to tease apart different brain states with sufficient subject specificity (Preti et al., 2016; Bolton et al., 2020b;

Tagliazucchi et al., 2012). Since the brain is a dynamic process that evolves in time, static or grand average functional connectivity might miss important time-varying characteristics of the functional signal (Preti et al., 2016; Allen et al., 2014). Indeed this has been hinted at by studies focusing on the variability of individual functional connections (Zalesky et al., 2014).

To this date, many methods have been developed to characterise the fMRI spatial organisation varying in time (Preti et al., 2016). Commonly, various features of time-varying activity are exploited but largely they converge on quantification of signal variability, spatial substate-based representations and topology of temporal graphs. Spatial resolutions of these methods vary from voxel and vertex-level to regional and even global representations. Temporal resolutions range from a single timepoint (sampling size) to correlated fluctuations all the way to the full recording timescale (Bolton et al., 2020b). Here, I focus predominantly on substate-based representations of functional connectivity dynamics. However, it is to be noted that there are other approaches considering dynamics from a continuous point-of-view such as spatio-temporal connectomes (Griffa et al., 2017; Vohryzek et al., 2019) and auto-regressive models (Liégeois et al., 2017).

Due to its simplicity, the most widely used technique is a sliding-window approach (Allen et al., 2014) that considers windows of correlated activity in time, and then clusters those into substates of varying connectivity. Notably, other techniques have described functional activity by maintaining the fastest temporal resolution possible through point-process analysis or similar approaches, by considering the main activation or transient events of the BOLD series before obtaining the substate-based representation through clustering (Tagliazucchi et al., 2012; Karahanoglu and Van De Ville, 2015). Another method worth mentioning is the Hidden Markov Model (HMM) that infers states as a multivariate normal distribution reoccurring at different points in time (Baker et al., 2014; Vidaurre et al.,

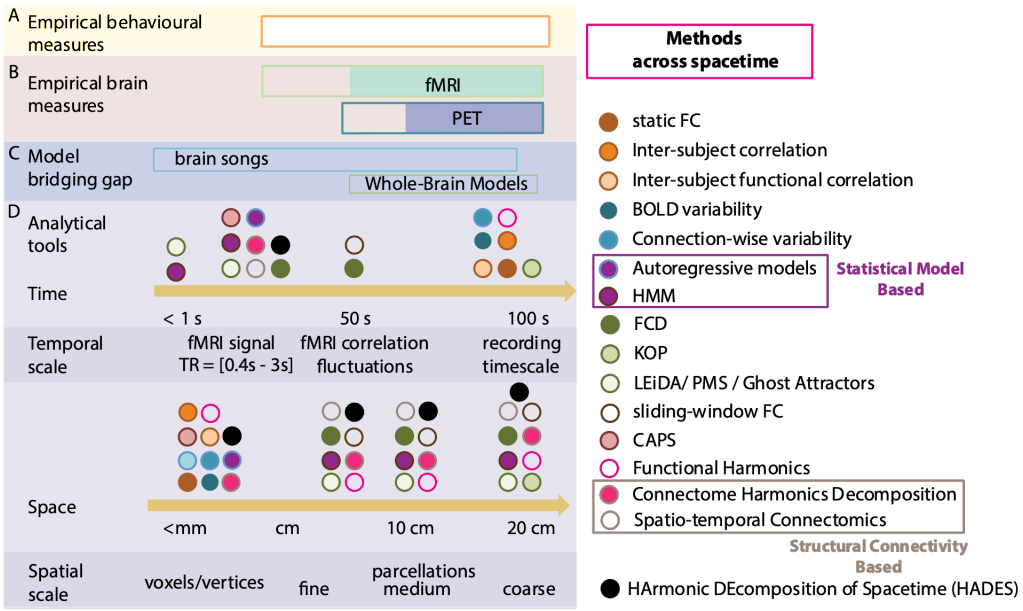



Figure 1.2: ***Methods Across Spacetime.*** *Summary of various methods and their spatial and temporal resolutions.* ***A)*** *In fMRI empirical behavioural measures are only limited by the haemodynamic response of approximately one to two seconds.* ***B)*** *Neuroimaging modalities considered in the thesis are fMRI with sub-millimeter and sub-second spatial and temporal resolution respectively, and PET with less precise resolutions in space and time but delivering important additional information about neurotransmitter expression within the brain.* ***C)*** *Modelling approaches linking underlying mechanisms to the empirical measures.* ***D)*** *Top, Temporal properties of different methods within the fMRI temporal range.* ***D)*** *Bottom, Spatial properties of different methods within the fMRI spatial range.* ***Methods across space time*** *- FC (Functional Connectivity), BOLD (Blood-Oxygenated-Level-Dependent), HMM (Hidden Markov Models), FCD (Functional Connectivity Dynamics), KOP (Kuramoto Order Parameter), LEiDA (Leading Eigenvector Dynamic Analysis), PMS (Probabilistic Metastable Substates), CAPs (Co-Activation Patterns). (adapted from (Kringelbach et al., 2020))*

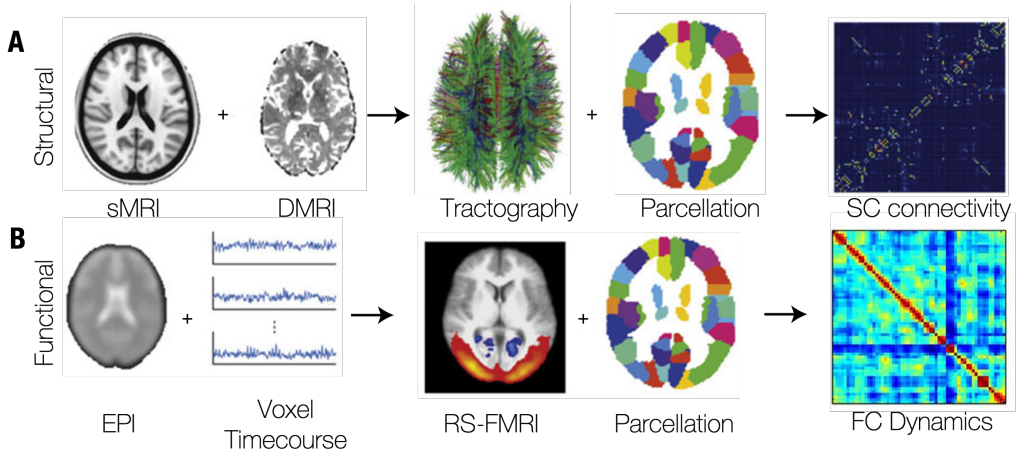



Figure 1.3: ***Whole-brain Neuroimaging.*** ***A)*** *A structural connectome (SC matrix) is obtained from structural and diffusion MRI by mapping white-matter fibers between pairs of cortical regions using tractography algorithms.* ***B)*** *Functional Connectivity Dynamics are obtained from fMRI recordings measuring BOLD signal. Here, FCD represents spatial correlations across different timepoints to highlight the temporal aspects of brain activity (adapted from (Lord et al., 2017)).*

2017). Lastly, taking inspiration from dynamical system theory, an instantaneous phase-based approach considers pairwise regional connectivity described in terms of its phase relationships. This is achieved by taking the analytical signal and clustering the leading eigenvector of the phase relationships into a meaningful substate representation (Cabral et al., 2017b). While methodological considerations might differ based on a specific approach, they carry a similar outlook on the FCD as a series of successive spatio-temporal brain substates. Once such a description is achieved, it is possible to describe spatial substates varying in time in terms of their Fractional Occupancy, Life Times and Transition Probability amongst other summary measures, and in turn create a more accurate description of the dynamic processes that the brain engages in.

While FCD tries to represent spatio-temporal patterns from brain activity recordings alone, an active area of research has focused on understanding how underly-

ing white-matter fibers, through which brain activity propagates, give rise to these complex dynamics. Recent developments in diffusion imaging have allowed to trace large-scale axonal bundles. This is achieved by mapping anisotropic water diffusion in brain-white matter. Appropriate modelling of the diffusion direction is then used in tractography algorithms to map white-matter tracts across the brain (Daducci et al., 2012; Tournier et al., 2019). Together with brain atlases, a comprehensive map of large-scale structural connectivity, termed the connectome, is created (Sporns et al., 2005; Hagmann et al., 2008). Tractography algorithms are still considered error-prone with fiber-crossing and axonal fanning among the outstanding issues (Jbabdi and Johansen-Berg, 2011). Furthermore, there is yet to be a consensus on the use of deterministic or probabilistic tractography (Sarwar et al., 2019). Despite these challenges DSI has been a powerful imaging modality to non-invasively map white-matter organisation of the brain (Griffa et al., 2013) (also see Figure 1.3, A).

Early studies have demonstrated a structure-function relationship based on a comparison between functional and structural connectivity profiles (Hagmann et al., 2010; Honey et al., 2009). How structure sculpts function is far from clear with path-ensembles and indirect pathways being also relevant (Avena-Koenigsberger et al., 2018). However, it is commonly accepted that brain structure constrains the space on which dynamics emerge. The idea can be put forward in Aristotle's quote "the shape of water is determined by its container". Methods from graph signal theory provide a more general framework through which different neural activity patterns can be expressed from the laplacian eigenmodes of the structural connectome(Atasoy et al., 2016; Preti and Van De Ville, 2019). Specifically, the connectome harmonics framework has shown that a few of the low-frequency building blocks can accurately describe the known resting-state networks (Atasoy et al., 2016). Incidentally, these buildings blocks of brain activity can be used to

represent complex spatio-temporal patterns of brain activity in mental disorders, as well as in different states of consciousness (Atasoy et al., 2018).

### 1.1.3 Whole-brain Modelling

Whilst FCD is an encouraging framework for fingerprinting and biomarking various clinical populations, its explanatory power lies in a realm of description and thus prevents mechanistic interpretations relevant to fully understand the drivers of mental disorders. Similarly, it is crucial to move beyond merely comparative approaches to understand how complex dynamics emerge from structural brain topology. So that such insights can deliver clinical use, it is important to construct computational models that will enable to simulate and predict emerging brain dynamics from the structural connectome. Not only would this disentangle mechanisms underlying pathologies, but also provide fundamental observations about the structural, functional and dynamical properties of healthy brain activity (Deco et al., 2014).

Whole-brain computational models describe neural activity of individual brain regions as a set of differential equations representing the desired neurophysiology or dynamic profile. To strengthen biological plausibility of the model, a structural connectome is used to reflect the strength of connections between individual brain regions. The choice of the brain regional model often depends on striking a delicate balance between model complexity and realism. In particular cases, emergent brain dynamics can be addressed through mean-field approximations of neural mass activity or phenomenological models of coupled oscillators (Honey et al., 2009; Cabral et al., 2017b). Several different solutions have been proposed, with conductance-based and excitatory-inhibitory neuron-based models describing aspects of brain physiology (Honey et al., 2007; Deco et al., 2009b) to phenomenological models depicting synchronization mechanisms, such as Ku-

ramoto and Hopf models (Cabral et al., 2011; Deco et al., 2017b). As mentioned in the previous paragraph, one of the important aspects of the emerging richness of spatio-temporal activity is its underlying structural connectivity. It has been shown that the optimal fit between empirical and simulated data emerges when modularity and efficiency are balanced (Deco et al., 2015). This is relatable to the small-world properties of the structural connectome (Bassett and Bullmore, 2006). Importantly, when such topology is disrupted through lesioning of the underlying connectivity, many important properties of the dynamics are lost (Vasa et al., 2015). Moreover, when simulating dynamics across a range of network architectures, from the regular lattice topology to random network organisation, the optimal working point emerges in the intermediate small-world regime demonstrating both high modularity and high efficiency (Deco et al., 2015).

Another important aspect of the emergence of spatio-temporal features, symbolised by resting-state networks, is the coupling strength of the different neuronal populations. At their optimal weakly-coupled point, local dynamics have the ability to influence and be influenced by other neuronal populations. At one extreme, strong coupling results in complete synchronisation of the neuronal populations and thus functional specificity is lost. On the other hand, very little coupling will be governed by the local description of the neuronal populations without much influence on the overall dynamics rendering the emergent spatial patterns structureless (Deco et al., 2017b). At the optimal weakly-coupled point such spatial organisation has been demonstrated when compared to empirical findings of sFC (Honey et al., 2009) and RSNs maps (Deco et al., 2009b). Furthermore, the delays arising from the finite conduction velocity of (simulated) neuronal signals have also been shown to be relevant, although they seem to affect the temporal disintegration and coalescence of RSNs rather than their integrity (Deco et al., 2011).

Funtional Connectivity (FC) also evolves over time, and therefore it is pertinent to consider the mechanisms giving rise to such spatio-temporal fluctuations. In other words, applied whole-brain models should further illuminate FCD features beyond static FC or the emergence of RSNs. Recently, it has been demonstrated that at an optimal level of coupling between brain regions, structured noise alone (combined with the SC) can explain the static FC, but not the non-stationary dynamics (Messé et al., 2014; Hansen et al., 2015). This begs the question: "What are the additional principles giving rise to such spatio-temporal dynamics?" This has been attributed to stochastic non-linear dynamics embedded in each region. Accordingly, the spatio-temporal dynamics emerge from noise-induced fluctuations of regional non-linear models poised at the edge of instability (Deco et al., 2013). As such the model becomes endowed with characteristics of critical systems such as an increase in the repertoire of possible brain substates and long-range temporal correlations (Cocchi et al., 2017; Tagliazucchi et al., 2016a). Indeed such characteristics have been demonstrated with the supercritical Hopf bifurcation where the model was able to recapitulate spatio-temporal measures including FCD (Deco et al., 2017b) and PMS (Deco et al., 2019).

To summarise, the spatio-temporal dynamics can be seen along the two axes of space and time. On one hand, the brain must balance the spatial segregative and integrative tendencies to optimally engage different specialised regions in a distributed network. On the other hand, the brain has to exhibit enough temporal persistence to create weak and strong temporal correlations evolving in time (Cabral et al., 2017a). In other words the brain's spatio-temporal structure should "live" in a metastable regime where spatial patterns wax and wane alongside its temporal dimension.

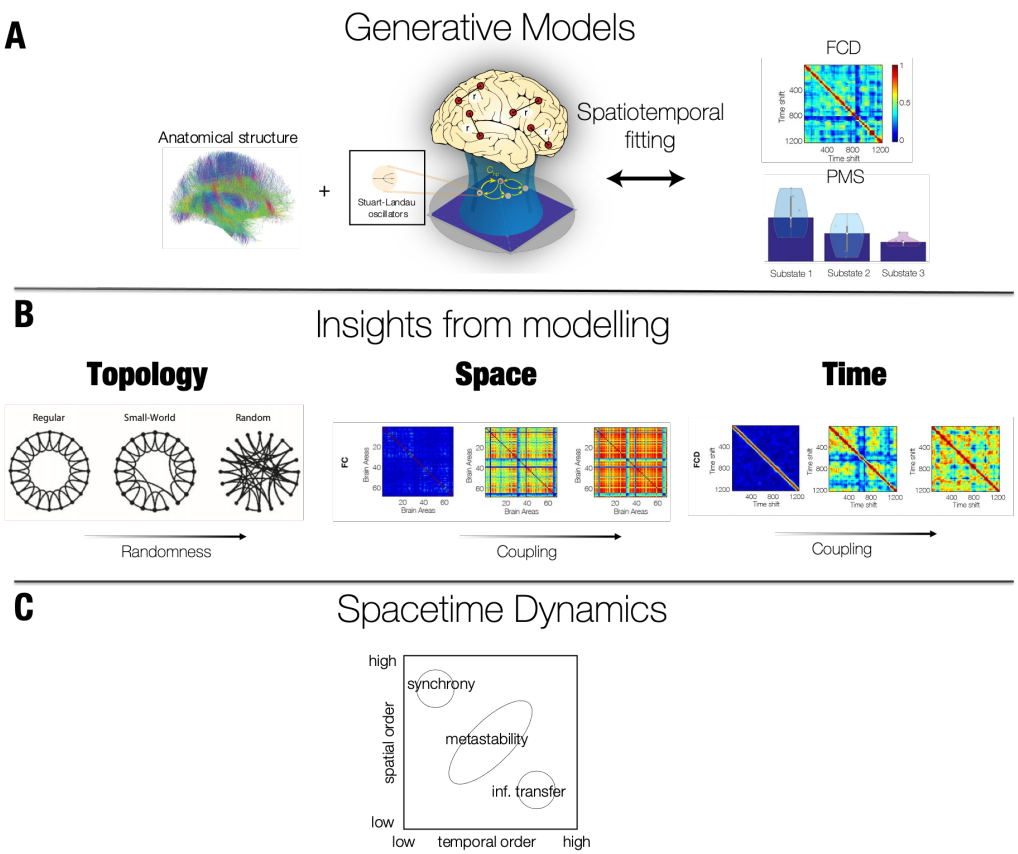



Figure 1.4: ***Insights from Whole-brain Modelling.*** ***A)*** *Whole-brain models describe spatio-temporal dynamics in terms of stochastic non-linear dynamics embedded in each region, which interact with other regions through the anatomical structure represented by the connectome. An important step in the description of such models is validation with empirical FC features. Here, I focus on spatio-temporal properties such as FCD and PMS.* ***B)*** *Spatial and temporal organisation of brain dynamics is preserved in models with structural connectomes exhibiting small-world properties (Watts and Strogatz, 1998), weakly-coupled interactions between regions of interest and local dynamics poised at the edge of instability (Deco et al., 2017b).* ***C)*** *The metastable regime of rich spontaneous brain dynamics can be perceived along extreme cases of the spatial and temporal order continuum.*

### 1.1.4 Dynamical Landscape

Taken together the brain's spatio-temporal dynamics can be perceived as a temporal trajectory through an n-dimensional dynamic landscape of weakly-coupled substates constrained by the structural connectome. Furthermore, it happens at the edge of criticality where the brain can explore a plethora of substates and maintain long-range temporal correlations. The characteristics of individual basins of attraction (substates) are described in terms of their prominence of occurrence (Fractional Occupancy), temporal stability (Life Times) and proximity to other substates (Transition Probability). In healthy brain functioning, the landscape will manifest enough stability to meaningfully visit substates but at the same time sufficient flexibility not to become trapped in one particular substate. In the depressive state such landscapes will exhibit stable temporal trajectories with certain attractors being more prominent implying aberrant dwellings in certain parts of the landscape. On the contrary, the psychedelic state will result in the 'flattening' of the landscape with less predictable temporal trajectories implying novel reroutings through the underlying landscape.

## 1.2 Theoretical Models of Brain Function

How consciousness arises within the brain has been one of the long-standing questions across many fields of inquiry. Yet the appreciation of a purely neurobiological interpretation has gained prominence with the publication of the Astonishing Hypothesis by Francis Crick, about 30 years ago (Crick and Clark, 1994). Over the years many neural correlates have been suggested to account for various aspects of the conscious experience (Tononi and Koch, 2008; Koch et al., 2016). One of the traditional classifications of the conscious experience has been in terms of conscious content and level (Seth et al., 2008). While there is still

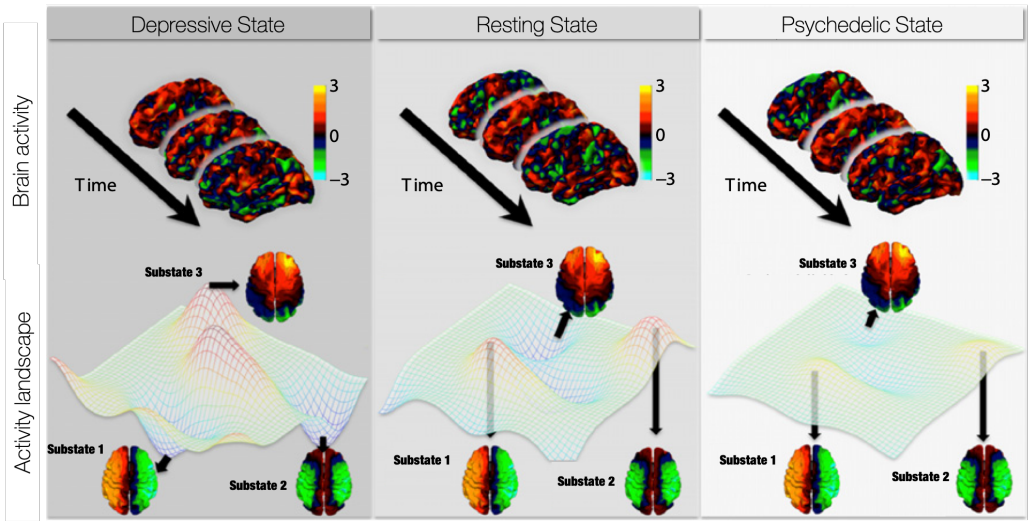



Figure 1.5: ***Dynamical Landscape.*** *Brain activity in different brain states as described by fMRI. Here, the depressive state, resting-state and psychedelic state. Activity landscape where the brain's spatio-temporal dynamics can be perceived as a temporal trajectory through an n-dimensional terrain of weakly-coupled substates constrained by the structural connectome. Optimal healthy functioning is expected to be observed in the resting-state with enough stability and flexibility. In depressive states, specific attractors become pronounced, making it more difficult to escape from their vicinity. On the contrary, psychedelic-induced states will result in a 'flattened' landscape and thus will allow for more flexibility to move within the landscape (adapted from (Atasoy et al., 2018)).*

an ongoing debate on the appropriate characterisation of consciousness given its multi-dimensional nature (Bayne et al., 2016), it has brought forth a novel understanding of the make-up of different brain states as one of the important aspects pushing the field of consciousness forward. With the development of whole-brain non-invasive neuroimaging techniques, it has been recognised that different brain states can be characterised by their complex dynamics. These are made up of waning and waxing of evolving spatio-temporal patterns that are constrained by condition-dependent self-organisation (Kringelbach et al., 2020). A growing body of neuroimaging literature has been looking into the different aspects of complex dynamics across space and time in various brain states - for example; disorders of consciousness, anesthesia, sleep, psychedelics as well as many psychiatric disorders (Demertzi et al., 2019; Barttfeld et al., 2015; Stevner et al., 2019; Atasoy et al., 2017b; Fu et al., 2020). In this section, I describe two theoretical models, the entropic brain hypothesis and the RElaxed Beliefs Under pSychedelics (REBUS) with the anarchic brain model to give a conceptual understanding in the context of brain states considered in this Thesis - the depressive and psychedelic brain states.

### 1.2.1 The Entropic Brain

The entropic brain hypothesis posits that the level of entropy of complex brain activity indexes the richness of informational content of brain states with upper and lower boundaries marking the cessation of ordinary waking consciousness. Positioned in a critical zone, the normal/healthy waking conscious state (resting-state) is observed with a sufficient stability and flexibility. In the psychedelic state, entropy is enhanced resulting in more susceptible and malleable brain dynamics. The spontaneous brain dynamics are believed to move closer to criticality with a broadening of the repertoire of possible substates that the brain engages in (Atasoy et al., 2018). Conversely, in the depressive state such dynamics are

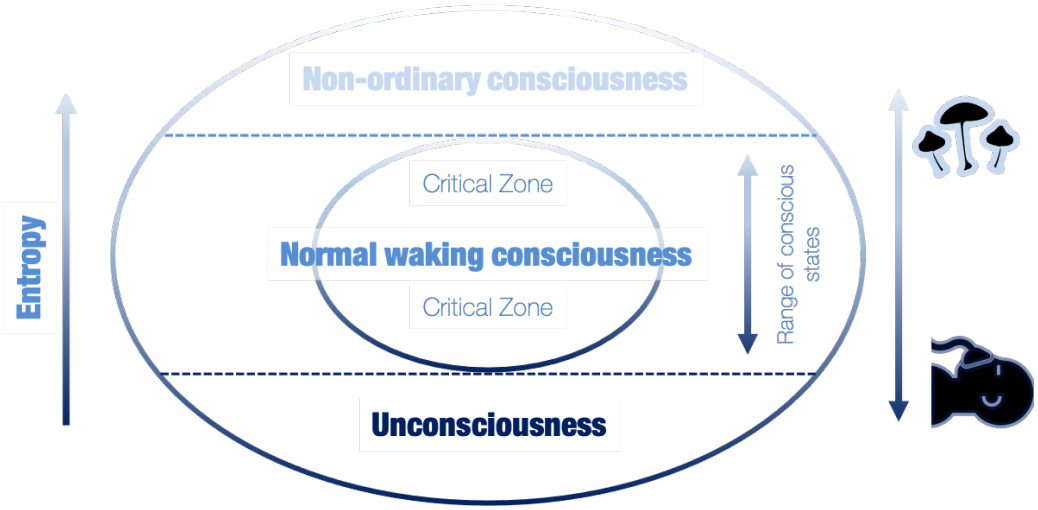



Figure 1.6: ***The Entropic Brain.*** *The entropic brain hypothesis posits that the entropy of spontaneous brain activity marks informational richness of brain states, with lower and upper limits beyond which a loss of consciousness is expected. The psychedelic state can be perceived on the high-entropy end of the spectrum with the depressive state on the opposite (low-entropy) side. Other reduced states of consciousness consist of anesthesia, dreamless sleep and minimally conscious states for example - adapted from (Carhart-Harris, 2018; Carhart-Harris et al., 2014). .*

characteristically inflexible with ruminative and self-critical periods of thinking resulting in diminished entropy. In this respect the ability to flexibly engage in divergent thinking becomes impaired. One possibility is that the brain dynamics become less metastable, with a given substate, for example the Default Mode Network (DMN), coming to control most of cognition (Carhart-Harris et al., 2014; Carhart-Harris, 2018).

### 1.2.2 REBUS and the Anarchic Brain

One of the recent developments in the description of brain states and their representation in terms of large-scale networks and spatio-temporal dynamics is the RElaxed Beliefs Under pSychedelics (REBUS) model. In this perspective, psychedelics are acting to relax high-level priors and thus make them more sensitive to the bottom-up information inputs that would otherwise be omitted, potentially revising and cultivating aberrant priors. These high-level priors are encoded in spontaneous activity of neuronal hierarchies, especially in high-level associative regions as well as the DMN. One can look at these whole-brain functional organisations as compressive or summary models that constrain the content of the levels below. By relaxing/decompressing these priors one can allow the unheard or suppressed information to travel freely through the neuronal hierarchies and be noticed in higher levels (Carhart-Harris and Friston, 2019).

The REBUS principle implies the anarchic brain whereby the intrinsic hierarchy of information processing is disrupted mainly at the higher levels, as represented for example by the DMN. This results in bottom-up information flows being put on the same footing with higher levels of the hierarchy. In this sense, there is no longer any "central control", as implied by the term *anarchic*, resulting in the loss of the functional hierarchy, enhanced brain entropy as well as enhanced effective connectivity of the bottom-up informational flows (Carhart-Harris and Friston,

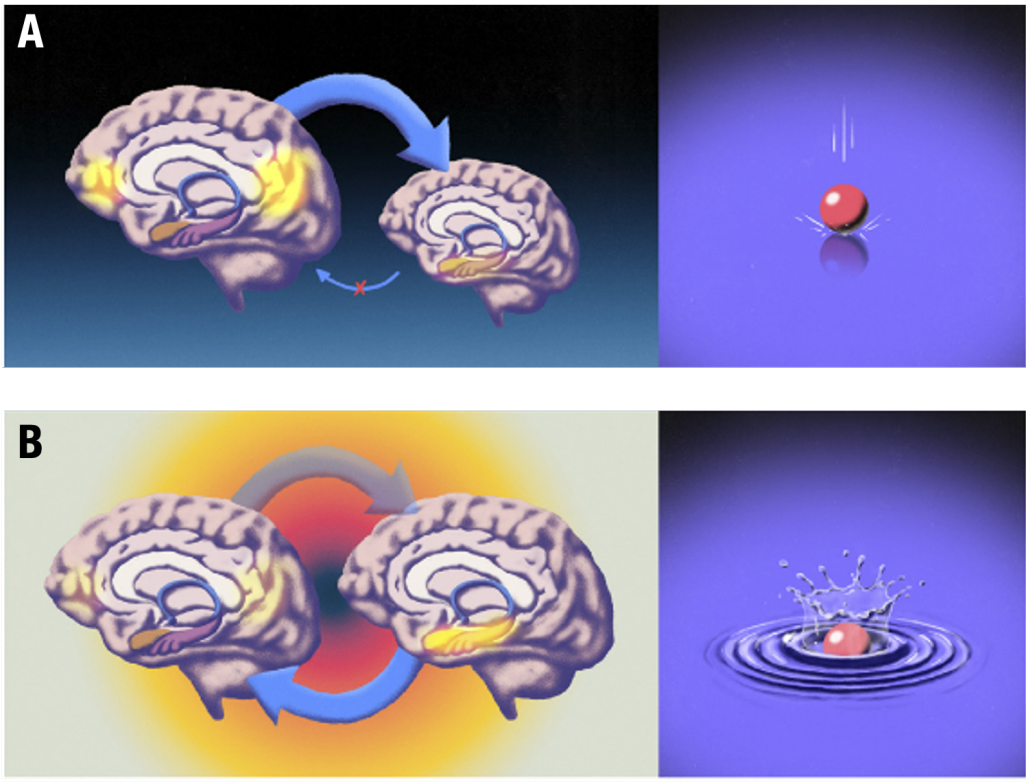



Figure 1.7: ***REBUS and Anarchic Brain.*** *Schematic description demonstrating the concepts of REBUS and Anarchic Brain in depressive and psychedelic states.* ***A)*** *In a depressive state, aberrant high-level priors represented by large-scale network organisation (for example the default mode network) suppress and desensitise any incoming information. Graphically, it can be perceived as a representation of a rigid state expected in pathologies such as depression.* ***C)*** *Relaxation of high-level priors in psychedelic state results in more sensitivity for incoming bottom-up signalling. The idea of the anarchic brain is that high-level priors and bottom-up signalling are put on the "same footing". Graphically, a representation of a flexible state expected under the influence of psychedelics. (Carhart-Harris and Friston, 2019)*

2019).

## 1.3 The Psychedelic State

In a letter conversation in the 1950s, Humphry Osmond and Aldous Huxley have coined the word "psychedelic" as an attempt to describe the mind-manifesting (from the greek $psukhē$, breath, life, soul and $delōs$, to clear, manifest) experiences of these substances (Huxley, 1977; Pollan, 2019). Indeed, psychedelics have a unique place amongst neuropharmacological agents due to their profound changes to both levels and contents of consciousness (Schartner et al., 2017). Probably the most commonly known synthesised psychedelic is Lysergic acid diethylamide (LSD), but remarkably psychedelics widely occur in nature as psilocybin - an active compound of "magic mushrooms", mescaline - an alkaloid in peyote, and N,N-dimethyltryptamine (DMT) - a part of the ayahuasca beverage alongside monoamine oxidise inhibitors (MAOIs) (Nutt et al., 2013; Nichols, 2016). Commonly, their mind-manifesting effects have been related to experiences of "vivid imaginations", "ego disintegration" and "feelings of supernatural" in subjective reports of participants taking psychedelics. Such cognitive alterations have been associated with the brain's shift towards more elated and encompassing modes of greater conscious content, flexibility of mind and emotional lability (Carhart-Harris, 2018; Swanson, 2018). Unsurprisingly, psychedelics have been used in many different cultures in religious and divinatory rituals for their revelatory properties (Nichols, 2016). Perhaps more surprising is their hiatus in terms of scientific inquiry into their mind-altering effects and potential benefits in treating psychiatric disorders. This is due to their legal status as Class A drugs, going back to Nixon's Controlled Substances Act of 1970, effectively hindering any potential scientific research into their clinical benefits. Since then,

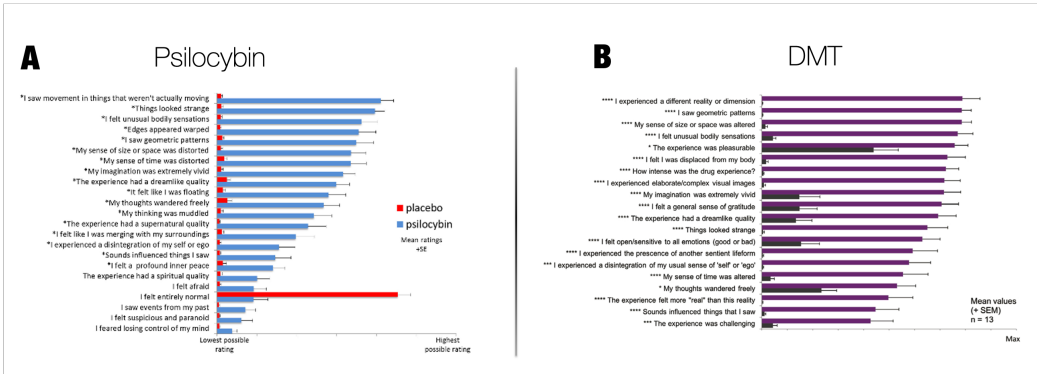



Figure 1.8: ***Phenomenology of Psychedelic Experience***. *Subjective ratings of participants undergoing the psychedelic experience of intravenously administered psilocybin (Muthukumaraswamy et al., 2013) and DMT (Timmermann et al., 2019). **A)** Many aspects of the phenomenological experience pertaining to psychedelics are enhanced under psilocybin such as "The experience had a supernatural quality" and "My imagination was extremely vivid": (**Blue** - subjects undergoing psilocybin infusion. In the placebo group the prominent bar pertains to "I felt entirely normal": **Red** - subjects undergoing saline infusion (placebo)). **B)** Also, many aspects of the phenomenological experience (different questions to the psilocybin dataset) pertaining to psychedelics are enhanced under DMT such as "I experienced a different reality or dimension" and "The experience had a dreamlike quality": (**Purple** - subjects undergoing DMT infusion. In the control group there were no prominent enhancements in subjective experiences **Dark Purple** - subjects undergoing saline infusion (placebo))*

psychedelic research has been experiencing a new renaissance largely focused on clinical trials with psychedelics for the treatment of depression (Carhart-Harris et al., 2016b)(Carhart-Harris et al., 2021), addictive disorders (Morgan et al., 2017; Johnson et al., 2017), anxiety (Reiche et al., 2018), Obsessive Compulsive Disorder (OCD) (Moreno et al., 2006) as well as for symptoms of depression and anxiety in patients with life-threatening diseases (Griffiths et al., 2016).

### 1.3.1 Neural Correlates of the Psychedelic-induced State

Over the last decade several neuroimaging studies have been carried out exploring the neural correlates of the psychedelic experience across various substances. To

this day studies have investigated brain activity under the influence of psilocybin - in both healthy (Carhart-Harris et al., 2012) and depressed populations (Carhart-Harris et al., 2016a), LSD (Carhart-Harris et al., 2016b), ayahuasca (Palhano-Fontes et al., 2015) and DMT (Timmermann et al., 2019). These data provide a unique opportunity to describe the brain activity of the psychedelic experience across space and time.

Along the spatial dimension, FC of fMRI activity has been demonstrated to broaden the repertoire of possible brain patterns, as described by connectome harmonics, both in the LSD and psilocybin states (Atasoy et al., 2018). Similarly, an enhanced repertoire of dynamic connectivity substates has been observed under the influence of psilocybin (Tagliazucchi et al., 2014). Furthermore, another study on the effects of psilocybin using algebraic topology demonstrated an increase in number of low-stability and an emergence of unique stable homological scaffolds (Petri et al., 2014). From the perspective of functional systems, FC between the medial prefrontal cortex (mPFC) and posterior cingulate cortex (PCC) (anterior-posterior regions of the DMN), and functional activity of anterior cingulate cortex (AAC) and mPFC, have been shown to decrease in psilocybin induced state (Carhart-Harris et al., 2012). Further changes have been observed in increases of between network connectivity, as described by FC, among most of the resting-state networks (RSNs) with the exception of lower-cognitive, visual and somatomotor, networks (Roseman et al., 2014). In the LSD-induced state, further increases in FC density (averaged static functional connectivity between a region of interest and the rest of the brain) have been demonstrated in higher associative networks, partially matching with the Default Mode, Salience and Frontoparietal Attention networks, and thalamus, as well as between-network connectivity of the aforementioned networks and their lower-cognitive counterparts (Visual, Auditory and Somatomotor networks) (Tagliazucchi et al., 2016b). This has been complimented

by decreases in within-network connectivity of the DMN and other resting-state networks (medial and lateral visual, occipital pole, somatomotor, parietal cortex, posterior opercular, dorsal attention, left and right fronto-parietal networks) (Carhart-Harris et al., 2016b). From the graph-theoretical perspective the LSD-induced state revealed increased global integration (Tagliazucchi et al., 2014), while increased Shannon entropy of the degree distribution has been demonstrated in the ayahuasca-induced state (Viol et al., 2017). Taken together, these studies suggest that the psychedelic experience leads to a broader repertoire of brain substates. This is further supported by within-network disintegration and increased between-network cohesion.

Along the temporal dimension, decreases in oscillatory power have been observed across many frequency bands, including alpha and gamma bands in EEG data in the ayahuasca-induced state (Schenberg et al., 2015), different frequency-bands in MEG recordings (1-4 Hz delta band, 4-8 Hz theta band, 8-15 Hz alpha band and 15-30 Hz beta band) and slow fluctuations of fMRI signal in the LSD-induced state (Carhart-Harris et al., 2016b; Tagliazucchi et al., 2014), and lastly in the 1-100Hz frequency band of MEG in the psilocybin-induced state (Muthukumaraswamy et al., 2013). Interestingly, signal complexity, as described by Lempel-Ziv complexity, has been demonstrated to increase in LSD, psilocybin and ketamine-induced states (Schartner et al., 2017). Surprisingly, changes in temporal correlations have been observed in co-activation of various spatial frequency-specific brain substates as described by connectome harmonic decomposition, suggesting a spatial grouping in non-trivial manner (Atasoy et al., 2017a).

### 1.3.2 Pharmacology of Psychedelic Drugs

Pharmacologically, all of the classically known psychedelics, such as psilocybin, LSD and DMT, are mediated through the serotonergic receptors (Carhart-Harris

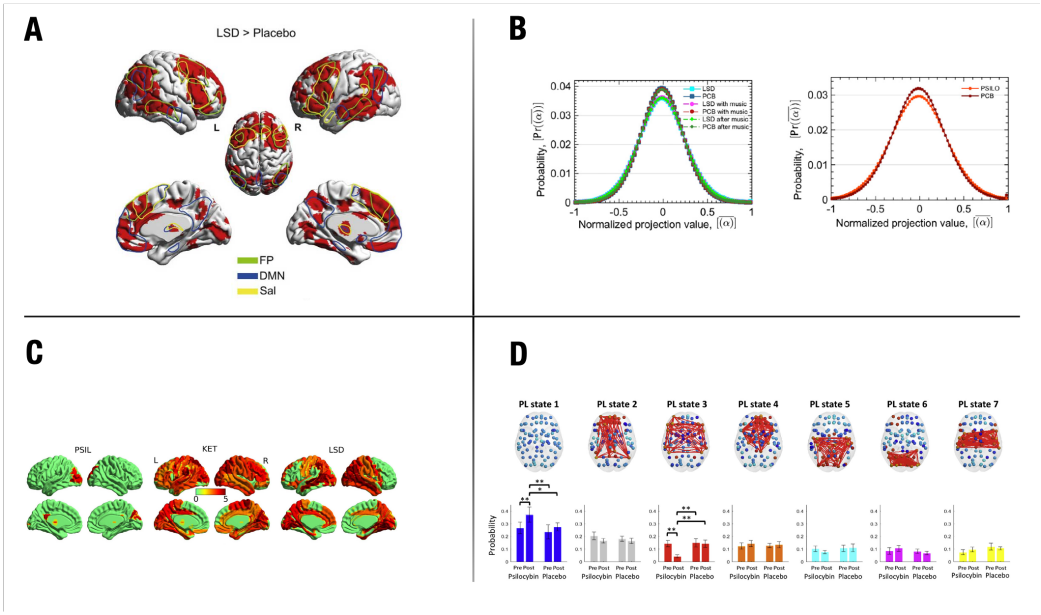



Figure 1.9: ***Psychedelics in Space and Time***. *Neuroimaging studies demonstrating various aspects of spatio-temporal dynamics under the influence of psychedelics.* ***A)*** *LSD increases dynamic functional density, defined by averaged static functional connectivity between a region of interest and the rest of the brain, specifically in functional systems pertaining to the frontoparietal, default-mode and salience networks (Tagliazucchi et al., 2016b).* ***B)*** *Repertoire broadening of brain substates, as described by connectome harmonics, in LSD and psilocybin-induced states (Atasoy et al., 2018).* ***C)*** *Temporal complexity, as defined by LZ-complexity, increases under psilocybin, ketamine and LSD-induced states (Schartner et al., 2017).* ***D)*** *Spatio-temporal dynamics alterations, as described by LEiDA, under the influence of psilocybin. Global integration becomes more prominent in time, as described by the global substate, and frontoparietal networks become less frequently visited (Lord et al., 2019).*

et al., 2017; Halberstadt, 2015) and are known to act as their agonists (Glennon et al., 1984). The 5HT serotonergic receptors have been placed into seven receptor groups with fourteen subtypes, out of which the most prominent and researched ones are the $5HT_{2a}$ and $5HT_{1a}$ (Nichols, 2016). The former is known to be overwhelmingly the main mediator of the hallucinogenic experience. Indeed, an administration of ketanserin, a $5HT_{2a}$ receptor antagonist, has blocked the psychedelic experience in psilocybin, LSD and ayahuasca-induced states in humans, as typically observed on the 5-Dimensional Altered States of Consciousness Rating Scale (Vollenweider et al., 1998; Kometer et al., 2013; Kraehenmann et al., 2017; Valle et al., 2016). As mentioned above, psychedelics act as $5HT_{2a}$ receptor agonists, mainly expressed on the glutamatergic pyramidal neurons of layer V in the cortex, with the result of depolarisation of the cells, and thus increase cortical excitation. Indeed, this has been recently demonstrated in a whole-brain modelling study where PET maps of $5HT_{2a}$ cortical expression were used to describe rich spontaneous resting-state fMRI activity (Deco et al., 2018). Although the excitatory-inhibitory ratio in the psychedelic state is to be tipped towards more excitation, it is to be noted, that $5HT_{2a}$ receptors are also expressed on the GABAergic inhibitory interneurons, and thus, a more complex picture of the neuronal-neurotransmitter interaction worth exploring in the future emerges (Andrade, 2011). Furthermore, other 5HT receptors and neurotransmitter systems have been shown to be relevant for mediating partial aspects of the psychedelic-induced experience and further studies will be needed to demonstrate their specific involvement (Preller et al., 2017; Nichols, 2016). Broadly, these findings corroborate the entropic brain hypothesis discussed in Section 1.2.1 (Carhart-Harris et al., 2014; Carhart-Harris, 2018). The pronounced richness of spatio-temporal complexity of brain activity in the psychedelic-induced state relates to repertoire broadening and increases in temporal complexity. On the RSN level, it results

in suppression of within-network connectivity while enhancing their between-network connectivity.

## 1.4 Depressive State

Major Depressive Disorder (MDD) is a brain condition with vast health implications affecting approximately 300 million people worldwide (World Health Organisation, 2017), and is projected to become the leading cause of burden of disease by 2030 (Malhi and Mann, 2018). Even with recent advances in understanding the neuropharmacology of MDD, only $60 - 70\%$ of patients respond to the first-line of treatment with antidepressants and a further $10 - 30\%$ of patients show treatment-resistant symptoms (Saad Al-Harbi, 2012). Since much of MDD burden is related to the latter group, treatment-resistant depression (TRD) has been recently defined as "*an inadequate response to at least 2 antidepressant trials of adequate dose, duration and adherence*" to separate it from the broader MDD group (Gaynes, 2009).

### 1.4.1 Behavioural and Neuropharmacological Symptoms of Depression

Commonly there are two diagnostic systems for classification of MDD. Namely, the Statistical Manual of Mental Disorders (DSM) and International Classification of Diseases (ICD). As none of the symptoms pertains exclusively to depression, its definition is based on the symptoms leading up to the disorder and those related to the functional dysfunction. The symptoms most commonly associated with MDD are dysfunctions in experiencing pleasure (anhedonia), time-variations in depressive intensity (diurnal variation) and feelings of guilt (see Figure 1.10). Further symptoms worth mentioning are of neurovegetative nature such as sleep depriva-

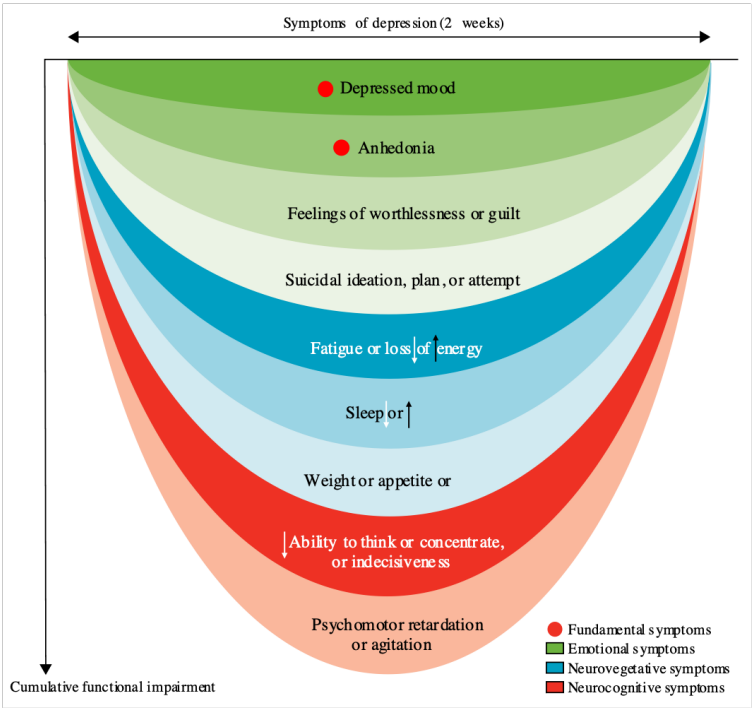



Figure 1.10: ***Symptoms of Depression.*** *Description of Major Depressive Disorder (MDD) syndromes as described by the Statistical Manual of Mental Disorders (DSM) and International Classification of Diseases (ICD). For patients to be considered suffering from MDD, they have to have depressive mood and anhedonia with at least three other symptoms over the duration of two weeks (adapted from (Malhi and Mann, 2018)).*

tion, fatigue, lack of appetite and weight-loss, and neurocognitive nature such as ability to concentrate and focus. Unlike transient feelings of sadness or unhappiness, depression is defined as having at least three of the symptoms mentioned in Figure 1.10 with anhedonia or depressed mood for a duration of two weeks (Malhi and Mann, 2018).

Traditionally, onset of Major Depressive Disorder has been associated with a reduction in the concentration of monoamine neurotrasmitters such as serotonin, dopamine and noradrenaline (Malhi and Mann, 2018). This hypothesis has been further supported with the discovery of antidepressants, such as monoamine oxidase inhibitors (MAOIs) and tricyclic antidepressants (TCAs), known to increase the levels of synaptic monoamines. Furthermore, the first direct evidence of the involvement of the serotonergic system in depression has been demonstrated in joint anti-depressant outcomes of MAOIs and tryptophan - a precursor to 5HT. The involvement of serotonergic pathways in depressive treatment over other antidepressants has gained in prominence with the success of selective serotonin reuptake inhibitors (SSRIs), that block the reuptake of serotonin in the synaptic cleft, showing higher efficacy and safety (Carhart-Harris and Nutt, 2017). Importantly, neuropsychological studies with SSRI administration to both healthy and depressed participants have shown a positive shift in the appraisal of emotionally-valenced information in the brain (Harmer et al., 2009). Moreover, a computational model by Dayan and colleagues has demonstrated the significance of serotonin in the inhibition of chains of thoughts with negative emotional connotations (Dayan and Huys, 2008). Unlike more traditional approaches to depression suggesting that changes in serotonin activity directly relate to depressive syndromes, the emerging picture is of serotonin relevance in functional operability that is reflected in decreased depressive symptoms (Cowen and Browning, 2015)

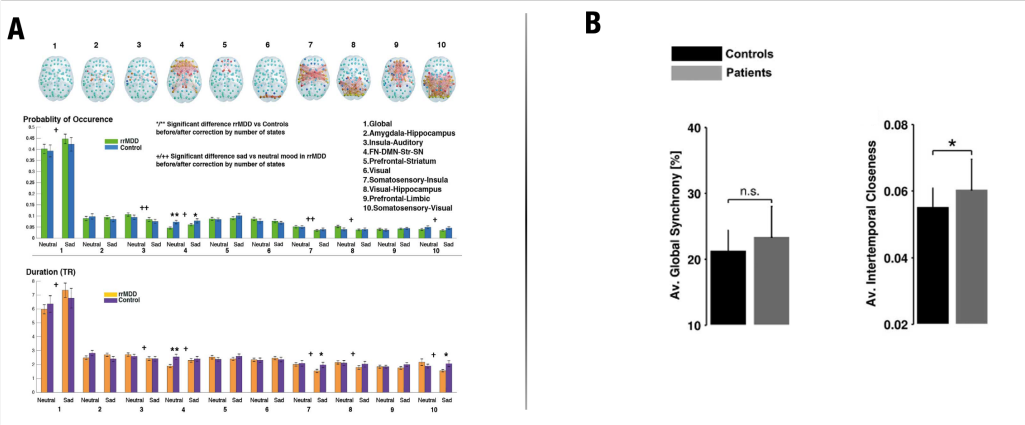



Figure 1.11: ***Depression in Space and Time.*** *Neuroimaging studies demonstrating various aspects of spatio-temporal dynamics in Major Depressive Disorder.* ***A)*** *Spatio-temporal dynamics alterations, as described by LEiDA. A brain network consisting of frontoparietal, default-mode and salience regions becomes visited less frequently and for shorter periods of time when watching neutral pictures in vulnerable remitted-MDD patients compared to healthy controls (Figueroa et al., 2019).* ***B)*** *Global synchrony and temporal stability are both increased in MDD patients (Demirtas et al., 2016)*

### 1.4.2 Resting-state Networks Implicated in Major Depressive Disorder

Recent development in non-invasive neuroimaging started to paint a system-level perspective of brain function in different brain disorders (Williams, 2016). In MDD, aberrant functional network interactions have been associated with the control network (CN) responsible for cognitive control and outward interaction with the world, the DMN engaged in internal mental processes and introspection, and the Salience Network (SN) involved in evaluating valence of relevant cognitive and biological events. Indeed, a description of the interactions amongst these three functional networks, dubbed the triple-network model, has been proposed to explain affective and cognitive dysfunction in several major brain disorders (Menon, 2011).

A recent study, focused on FCD, has shown an impaired recruitment and duration of a network (consisting of frontoparietal, default-mode, salience and striatum regions) in vulnerable remitted-MDD patients compared to controls when watching neutral images. This network has been considered important for switching between internally and externally oriented attention (Figueroa et al., 2019). Furthermore, an increase of within-network connectivity in DMN regions as well as more persistent resting-state FC between prefrontal and temporal regions of the DMN indicate a stronger prevalence of the DMN (Demirtas et al., 2016; Kaiser, 2017). In terms of switching capabilities at the system level, an increase in variability has been observed between mPFC of the DMN and anterior insula and decreased variability between DMN and FPN suggestive of enhanced sensitivity to emotional information resulting in a ruminative state (Demirtas et al., 2016; Kaiser, 2017). Globally, more pronounced synchronisation and temporal stability has been observed in MDD patients compare to healthy participants (Demirtas et al., 2016).

These results corroborate the idea of the REBUS and anarchic brain models whereby DMN exercises abnormal control over bottom-up signalling leading to excessive within-network connectivity and disrupted between-network connectivity with salience and control networks. Such scenario results in inflexible brain functioning both in space and time revealed by ruminative states. Furthermore, the temporal inflexibility and global spatial synchrony also corroborates the entropic brain hypothesis. The loss of patients' ability to think in a flexible manner might result in predictable, less entropic brain dynamics as the DMN constraints the types of self-referential and introspective thinking processes (Carhart-Harris et al., 2014; Carhart-Harris, 2018).

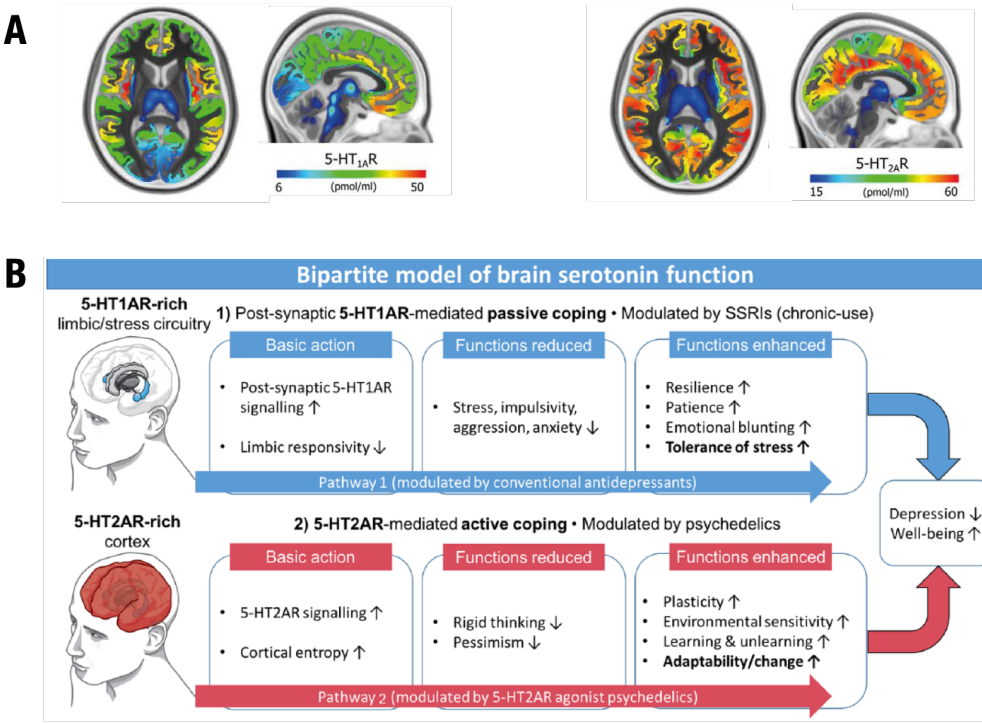



Figure 1.12: ***Brain Serotonin Function.*** ***A)*** *Average density maps of $5HT_{1a}$ and $5HT_{2a}$ neuroreceptors (Beliveau et al., 2017).* ***B)*** *The bipartite model of brain serotonin function proposes two mechanisms for serotonin function based on the $5HT_{1a}$ and $5HT_{2a}$ neuroreceptor signalling. In this model, post-synaptic $5HT_{1a}$ mediates passive coping resulting in decreased depressive symptoms. This signalling is predominantly modulated by SSRIs. Conversely, $5HT_{2a}$ mediates active coping resulting in an increase in well-being. This signalling is mainly modulated by serotonergic psychedelics (Carhart-Harris and Nutt, 2017)*

### 1.4.3 Treatment with Psychedelics

As discussed above, MDD has been conventionally treated with SSRI anti-depressants acting on $5HT_{1a}$ post-synaptic signalling. Such mechanisms result in decreased limbic system responsiveness which has been behaviourally associated with reduced stress and anxiety levels, and increased psychological resilience and emotional moderation or "blunting" (Carhart-Harris et al., 2017). Similarly, psychedelics also act through serotonergic modulation with resulting effects on the altered re-

lationship to the environment. However, their serotonergic modulation mainly comes from direct agonism of the $5HT_{2a}$ receptors resulting in possibly very different coping mechanisms. In other words, psychedelics have been shown to increase the cortical entropy with decreases in inflexible thinking and increases in emotional release and environmental sensitivity, and thus employ an active coping mechanism (Carhart-Harris et al., 2017; Carhart-Harris and Nutt, 2017). Indeed, newly constructed clinical trials have been encouraging in treating depression (Carhart-Harris et al., 2016a)(Carhart-Harris et al., 2021).

### 1.4.4 Moving forward

In the Introduction, I have argued for a perspective of the brain as a complex system (Section 1.1), and as such a clear need to interpret and understand the underlying mechanisms of brain states along both spatial and temporal dimensions. Importantly, this is made possible with non-invasive imaging (Section 1.1.2) and whole-brain modelling (Section 1.1.3), respectively mapping and modelling the rich spatio-temporal dynamics of the brain. Conceptually, these insights fit in with the entropic brain hypothesis, RElaxed Belief Under pSychedelics and the Anarchic Brain (Section 1.2). Experimentally, the psychedelics-induced state (Section 1.3.1) and the depressive state (Section 1.4) are hypothesised to be on the opposite sides of a spectrum of spatio-temporal dynamics.

An improved spatio-temporal description of brain states is needed. In Chapter 2, I therefore mathematically formalise brain spatio-temporal dynamics as a temporal trajectory in a landscape of phase-locking substates, and show its utility in predicting different brain states. Building on the previous Chapter, Chapter 3 applies Probabilistic Metastable Substates to explain changes in spatio-temporal dynamics of responding and non-responding treatment-resistant depression patients to treatment with psychedelics. Moreover, I use whole-brain modelling to mecha-

nistically probe brain regions for a successful transition between depressive and healthy states.

Subsequently, in Chapter 4, I further consider how functional substates and their temporal propagation can be realised from structural connectivity of the human brain by using Connectome Harmonic Decomposition to discern the spatio-temporal dynamics of the DMT-induced state. From this perspective, I describe changes to the DMT-induced space across spatial and temporal features. Chapter 5 builds on the previous methods by considering building blocks of communication structure of the brain and their temporal unfolding - HArmonics DEcomposition of Spacetime (HADES). Leveraging on the rich informational content of the communication structure, I explore the DMT-induced state along both temporal and spatial dimensions. Finally, in Chapter 6, I consolidate the different Chapters and suggest perspectives for future investigations.

# 2 | Brain Spatio-Temporal Dynamics as a Temporal Trajectory in a Landscape of Phase-Locking Substates[1]

## 2.1 Introduction

For healthy human cognition, the brain needs to engage in functionally meaningful activity through an integration of information incoming from various segregated brain areas (Tononi and Edelman, 1998; Sporns et al., 2000). At rest, brain activity has been shown to reveal the spontaneous activation of meaningful functional subsystems, sharing spatial features with networks of brain areas typically activated during task (Beckmann et al., 2005; Fox et al., 2005; Damoiseaux et al., 2006). These spatially activated coalitions of brain regions, dubbed resting-state networks (RSNs), have been remarkably consistent across neuroimaging studies and utilised in describing functional changes in disruptions to the healthy brain functioning (Greicius, 2008; Fox and Greicius, 2010; van den Heuvel and Hulshoff Pol, 2010; Vargas et al., 2013; Kaiser et al., 2015). However, while RSNs represent spatially meaningful information, in order to further investigate the generative mechanisms of RSNs and their functional role, it is important to characterize their behavior in the temporal domain as well (Preti et al., 2016; Cabral et al., 2017b).

Indeed, recent advances have focused on how spatially coherent functional patterns can explain the complex brain dynamics evolving in time (Chang and Glover,

[1]Material in this Chapter has been published in: Vohryzek, J., Deco, G., Cessac, B., Kringelbach, M. L., & Cabral, J. (2020). Ghost Attractors in Spontaneous Brain Activity: Recurrent Excursions Into Functionally-Relevant BOLD Phase-Locking States. Frontiers in Systems Neuroscience, 14(April), 1-15. doi: 10.3389/fnsys.2020.00020

2010; Hutchison et al., 2013; Allen et al., 2014). However, the most appropriate way to characterize network dynamics at the whole brain level is still unclear. Here, I build on work by Cabral and colleagues who have proposed to represent the instantaneous relationships between brain regions using the largest magnitude eigenvector of BOLD phases (a $1 \times N$ vector for each time point) instead of the $N \times N$ phase synchronization matrix (Cabral et al., 2017b). By representing whole brain activity over time as a succession of discrete Phase-Locking (PL) substates, it is possible to quantify fractional occupancy (FO), Transition Probability Matrix (TPM) as well as the Life Times (LT) of individual substates. Importantly, these measures have shown to be significantly related with cognitive performance (Cabral et al., 2017a), altered in clinical populations of patients suffering with major depressive disorder (Figueroa et al., 2019), as well as describe network-specific modulation of resting-state activity by the psychoactive compound psilocybin (Lord et al., 2019). As such, this representation turns out to be a useful tool to quantitatively characterize individual fingerprints in FCD, reinforcing a mechanistic scenario proposed by theoretical works where RSNs are the expression of a repertoire of FC configurations emerging from complex non-linear interactions in the whole-brain network (Ghosh et al., 2008; Cabral et al., 2011; Deco and Jirsa, 2012; Deco et al., 2013; Haimovici et al., 2013; Hansen et al., 2015).

Here, I explore this mechanistic hypothesis using mathematical formalism from dynamical systems theory and Markov chains in order to characterize spatio-temporal dynamics of spontaneous brain activity in terms of probabilistic trajectories between recurrent PL substates. I validate functional role of the obtained patterns by comparing them with known RSNs. Furthermore, I evaluate stability of PL substates based on their Fractional Occupancy, Life Times and Transition Probabilities. While previous works have applied this representation to condition-specific datasets, with reduced sample sizes, here I make secondary use of a large

open source dataset of healthy participants, demonstrating recurrence and reliability of the yielded metrics across subjects and consecutive fMRI recording sessions.

## 2.2 Methods

### 2.2.1 Dataset

I used data from a publicly available database - the Human Connectome Project, WU-Minn Consortium (Principal Investigators: David Van Essen and Kamil Ugurbil; 1U54MH091657) with funding from the sixteen NIH Institutes and Centers supporting the NIH Blueprint for Neuroscience Research; and by the McDonell Center for Systems Neuroscience at Washington University.

I focused on the 100 unrelated participants (mean age 29.5 years old, 55% females) (Glasser et al., 2013) with each participant undergoing four resting-state fMRI sessions lasting 14 min 30 s with a repetition time (TR) of 0.72 s, on a 3-T connectome Skyra scanner (Siemens) - two during the first day and two during the second day. The 2 fMRI sessions acquired on the same day differ only in the oblique axial acquisition phase encoding, one being from Left to Right (LR) and the other from Right to Left (RL). The acquisition and pre-processing of the data are fully described in detail at the HCP website www.humanconnectome.org/. Here, I used the fMRI data acquired on the first day of scanning. One subject was excluded because of one session missing. In total, two same-day resting-state fMRI sessions from 99 of the 100 unrelated participants' sessions were used for the analysis.

To reduce the dimensionality of the voxel-based data (Voxels $\times$ Time), Anatomic

Automatic Labeling (AAL) atlas was used to define $N = 90$ anatomically distinct cortical and sub-cortical regions covering whole brain (excluding the cerebellum). Data was reduced to size N $\times$ Time, with Time = 1200 TR per session, by averaging the BOLD signals in all the voxels associated to each brain region (Figure 2.1, A).

### 2.2.2 Phase dynamics

To compute phase relationship between brain regions, for each region n with $n = 1...N$, a BOLD phase $\theta(n,t)$ varying in time $t$, was computed via Hilbert transform (Glerean et al., 2012). The analytical signal expresses regional signal $x(t)$ as $x(t) = A(t) * \theta(t)$ with $A$ and $\theta$ representing time-varying amplitude and phase respectively (Figure 2.1, B). The first and last time points were removed from each time series, to exclude the boundary artifacts induced by the Hilbert transform. Subsequently, for every pair of brain regions $n$ and $m$ at time $t$ the phase coherence matrix $dPC$ is computed as follows: $dPC(n,m,t) = cos(\theta(n,t) - \theta(m,t))$, where $cos(0) = 1$ represents the case when two brain areas $n$ and $m$ are aligned at time $t$ (Figure 2.1, E). Conversely, $\cos(\pi) = -1$ indicates two brain areas $n$ and $m$ are anti-aligned at time $t$. Lastly, $cos(\pi/2) = 0$ shows two brain areas $n$ and $m$ at time $t$ to be orthogonal to each other and therefore their phase relationship being $0$.

### 2.2.3 Leading Eigenvector of Phase Dynamics

I used reduced representation of the signal, where only the $1 \times N$ leading eigenvector $V_1(t)$ of the $dPC$ is considered in the analysis, to describe phase coherence pattern of the $(N \times N)$ $dPC(t)$ at every time-point $t$ with reduced dimensionality. In other words, I computed the eigendecomposition of $dPC(t)$ at every time $t$

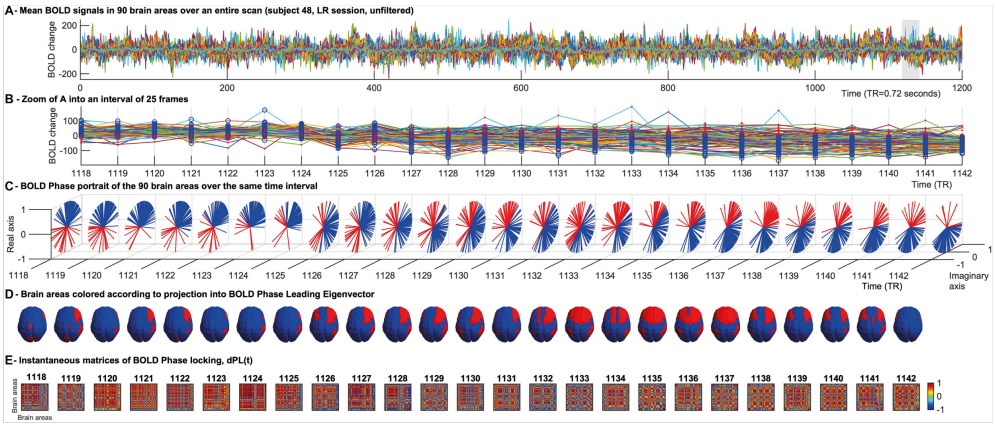



Figure 2.1: ***Time-evolving Patterns of Phase Dynamics.*** *(A) signals from a representative fMRI scan of the HCP dataset averaged over all voxels within each region of interest (ROI). ROIs were defined using anatomically-based parcellation scheme (AAL) covering the entire brain (here excluding the cerebellum). (B) To illustrate phase dynamics, I select a representative interval of TRs. At each TR, blue circles represent the brain areas whose phase projects into the main phase direction (captured by the leading eigenvector, see (C), and red dots represent the brain areas whose phase projects into the opposite direction of the main phase orientation. It serves to illustrate that the phase-shifted signals (in red) do not directly correspond to supra-threshold increases. (C) Phase portraits of the analytic signal at each TR, where the real and imaginary axis represent the cosines and sines of the Hilbert phase at each TR. (D) Representation of brain patterns captured by the signs of the leading eigenvector at each TR, illustrating how phase-locking patterns evolve smoothly over several TRs, whereas the corresponding BOLD signals (shown in panel B) exhibit significantly different activation patterns over the same range of TRs. (E) Representation of the instantaneous phase coherence matrices obtained at each TR as the cosine of the phase difference at each instant of time*

$dPC(t) = V(t)D(t)V^{-1}(t)$, where columns of $V(t)$ are the corresponding eigenvectors of $dPC(t)$ and $D(t)$ is the diagonal matrix of the eigenvalues of $dPC(t)$, and I took the first (most dominant) eigenvector $V_1(t)$ to represent the PL substate at each time point with size $1 \times N$. Since $dPC(t)$ is symmetric, its eigenvectors are orthogonal $V^{(-1)}(t) = V^T(t)$ and the eigenvalues are real. Each element in the eigenvector can be associated to a specific brain area (i.e.,in Figure 2.1, B-D) each brain area is colored according to its sign in $V1(t)$. The $N \times N$ dominant connectivity pattern at every time $t$ captured by $V_1(t)$ can simply be retrieved by calculating the matrix product of the eigenvector with its transpose as $V_1 * V_1^T(t)$ (Cabral et al., 2017b).

With the aforementioned reduction, whole-brain activity at each time point $t$ is represented by a $1 \times N$ vector, where $N$ is the number of brain regions defined by the applied parcellation. Each vector $V_1(t)$ can be seen as an observation of the dynamical system and can be represented as a point in an N-dimensional space $R^N$ (see Figure 2.2, A, represented in $R^3$ for illustration). Each fMRI experiment is thus characterized by a trajectory of the leading eigenvector $V_1$ in this N-dimensional space. To get a graphical representation, I project each vector $V_1(t)$ on the space determined by the first three principal components of all $V_1 s$, (i.e., the $x$, $y$, and $z$ coordinates are given by the cosine distance between each $1 \times N$ $V_1(t)$ and the first 3 $N \times 1$ eigenvectors of the $N \times N$ covariance matrix of all $V_1$s (with size $N \times T$) (see Figure 2.2, A and B).

### 2.2.4 Phase Space Partition

In order to achieve a substate-based representation, the leading eigenvectors obtained from all 99 participants in the Left-Right (LR) fMRI scanning session - corresponding to a total of $T$ = 118602 observations ($99 \times 1198$ TRs) with $N$ = 90 dimensions each - are partitioned into a set of discrete substates. Importantly, I

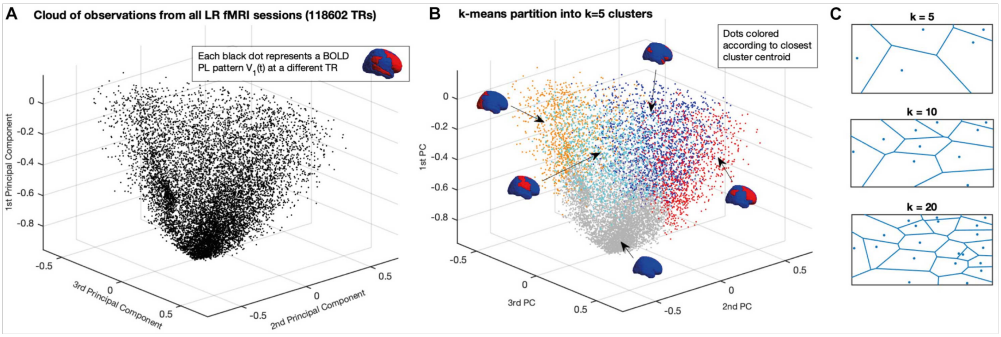



Figure 2.2: ***N-dimensional phase space partition into a K-dimensional substate-based space.*** *Representation of all PL substates captured at each TR in a reduced 3-dimensional perspective of the phase space. Since each observation is a* $1 \times N$ *vector - corresponding to the leading eigenvector of signal phases at each TR - the full phase space is N-dimensional, where N = 90 is the number of ROIs used to parcellate the brain). Each dot corresponds to one fMRI volume recorded over time (TR = Repetition Time = 0.72 s). Dots are placed according to their cosine distance with respect to the first three principal components (i.e., the first 3 eigenvectors of the covariance matrix) of all observations. (B) Partition of the Phase Space using K-means clustering decomposes the space of observations into k clusters, where each observation from an fMRI experiment is assigned to a cluster given its closest proximity to the corresponding centroid. The centroids obtained for K = 5 are represented by coloring each brain area using the same color scheme as in Figure 1, representing distinct whole-brain phase-locking substates. (C) Illustration of the partition of a 2D plane into k Voronoi cells, where each point in a given cell is closer to its centroid than to any other centroid.*

do not include in this partition the Right-Left (RL) fMRI scanning sessions from the same $99$ participants recorded on the same day, which will serve to test the validity and consistency of the results, as described in the following section. I use the k-means algorithm, which relies on an iterative process to find the solution that minimizes distance between each $(1 \times N)$ observation and the closest $1 \times N$ cluster centroid (I note that, given the large number of dimensions, I use Cosine distance, which significantly reduces the computation time with respect to City Block or Euclidean distances). As such, k-means algorithm is used to iteratively cluster leading eigenvectors into $k$ = 2 to $k$ = 20 clusters (resulting in 19 partitions), repeating each calculation 100 times to ensure stability in the results. Since each observation represents a time point, the output vector of cluster assignments - where each observation is assigned to its closest $1 \times N$ cluster centroid $\alpha$ = $1 \ldots k$ - can be approached as a trajectory $\underline{x}(t)$ in substate space.

In Figure 2.2, I show how k-means clustering algorithm divides the phase-space (here represented in only three dimensions for illustration) into $k$ = 5 (Voronoi) cells, where each location in the phase space is assigned to the closest centroid. Using colors to represent regions of the phase space assigned to each cluster $R^{\alpha}$, I represent in Figure 2.2,B the same observations from panel A, while highlighting the cluster assignment at each time point. Although the 3-dimensional representation serves to illustrate the partition of the phase-space, there is a clear overlap of colors given that the phase-space, defined in $N$ = 90 dimensions, cannot be adequately represented in three dimensions only. To illustrate the decomposition into k-means clustering algorithm I show, in Figure 2.2, C , the partition of a 2D plane into k Voronoi cells, where each region in space is assigned to the closest centroid. Each cluster $R^{\alpha}$ (with $\alpha$ = $1 \ldots k$) is now represented by its cluster centroid $V_{c\alpha}$, each corresponding to a distinct phase-locking substate (which will be described in detail in the section in the Results 2.3). To assess the quality of cluster sepa-

ration, silhouette value is computed for each k, which estimates how similar each observation $V_1(t)$ is to its own cluster compared to other clusters.

### 2.2.5 Comparison with Canonical Resting-state Networks

The existence of functionally dependent subsystems, where subsets of brain areas consistently activate together even during rest, has been widely explored in studies of resting-state FC. Resting-state networks, typically assessed using correlation analysis, have been consistently detected in large cohorts of resting-state fMRI experiments (Yeo et al., 2011). Here, I verify if the centroids obtained from clustering the phase leading eigenvectors obtained at TR resolution share spatial similarities with the seven resting-state networks as defined by (Yeo et al., 2011). To do so - and since the PL substates $V_\alpha$ are defined in AAL parcellation - I take the mask of Yeo parcellation (seven non-overlapping functional networks defined in MNI152 space) and the mask of AAL parcellation (in the same MNI152 space), and compute, for each of the $90$ AAL brain areas, a proportion of voxels assigned to each of the seven RSNs, obtaining in this way $7$ $1 \times 90$ vectors representing RSNs in AAL space. Subsequently, I compute Pearson's correlation between RSNs and the PL substates $V_\alpha$ obtained from our clustering analysis across a whole range of $k$ explored (setting all negative values of the centroids' vectors to zero, to only consider the areas whose phase is shifted from the main orientation).

### 2.2.6 Validation Dataset

I used the second fMRI scanning session from each of the $99$ participants recorded on the same day as the primary dataset - differing only in the oblique axial acquisition phase encoding, being Right to Left (RL) instead of Left to Right (LR) - to verify the validity and consistency of the partition performed in the previous

session. To do so, I obtained all the $1 \times N$ leading eigenvectors from the the Right-Left (RL) scanning session - totaling 118602 observations (1198 TRs $\times$ 99 subjects) - using the same methodology as before, but instead of running the k-means algorithm, I compute cosine distance between each $1 \times N$ eigenvector $V_1(t)$ and the $k$ $1 \times N$ cluster centroids $V_{c\alpha}$ obtained from the previous analysis, and define the trajectory vector $\underline{x}(t)$ by assigning each $V_1(t)$ to its closest cluster centroid $V_{c\alpha}$.

### 2.2.7 Measures of the Substate-based Representation

#### Fractional Occupancy

Following the cluster partition into $k$ PL substates evolving in time $t$, the probabilities - or Fractional Occupancies $\prod_{\alpha}^{S}$ associated to each PL substate $\alpha$ and each scan $S$, can be computed as follows:

$$\prod_{\alpha}^{(S)} = \frac{1}{T} \sum_{t=1}^{T} \chi[\underline{x}(t) \in R^{\alpha}] \tag{2.1}$$

where $\chi$ is the indicator function - $\chi(A) = 1$ if the event A is true, and $\chi(A) = 0$ otherwise, and $T = 1198$ is the number of time points (TRs) corresponding to each fMRI scan ($S$). In other words, the equation counts the number of times when the trajectory $\underline{x}(t)$ is assigned to each of the defined clusters $R^{\alpha}$, divided by the total number of time points $T$. Furthermore, given that participants are constantly in resting state condition - i.e. without performing any task, stationarity is assumed in the data within each scan (justifying the time average in Eq. 2.1). Cluster probabilities are estimated separately for each individual fMRI scan.

### Life Times

To describe the average time periods when a given PL substate $\alpha$ is being visited in each fMRI scan $S$, Life Times $LT_{\alpha}^{S}$ are defined as the mean of all the consecutive periods of each substate, i.e.,

$$\mathrm{LT}_{\alpha}^{(S)} = \frac{1}{p_{\alpha}} \sum_{1}^{p_{\alpha}} \mathrm{C}_{p_{\alpha}} \tag{2.2}$$

where $\mathrm{LT}_{\alpha}$ is the Life Time of PL substate $\alpha$, $p_{\alpha}$ is the number of consecutive periods assigned to PL substate $\alpha$ and $\mathrm{C}_{p_{\alpha}}$ is the duration of each consecutive period.

### Transition Probability Matrix

Following the same rational as in Equation 2.1, the definition of a probability $\prod_{\alpha\beta}$ to be in the PL substate $\alpha$ at time bin $t.$ and in the PL substate $\beta$ at time bin $t$ = 1 can be written as follows:

$$\prod_{\alpha\beta}^{(S)} = \frac{1}{T-1} \sum_{t=1}^{T-1} \chi[\underline{x}(t) \in R^{\alpha}, \underline{x}(t+1) \in R^{\beta}] \tag{2.3}$$

and thus, the Transition Probability Matrix $\prod_{\alpha\beta}^{(S)}$ of each fMRI scan $S$ is defined as:

$$\mathrm{W}_{\alpha\beta}^{(S)} = \mathrm{W}[\underline{x}(t+1) \in R^{\beta} | \underline{x}(t) \in R^{\alpha}] = \frac{\prod_{\alpha\beta}^{(S)}}{\prod_{\alpha}^{(S)}}. \tag{2.4}$$

$\mathrm{W}_{\alpha\beta}$ defines the Transition Probability Matrix from substate $\alpha$ to substate $\beta$. This defines a homogeneous Markov chain, characterizing the transition between PL substates. The Tranisition Probability Matrix $\mathrm{W}_{\alpha\beta}^{(S)}$ is estimated separately for each scan $S$. To each matrix $\mathrm{W}_{\alpha\beta}^{(S)}$ is associated a transition graph with an oriented

arrow from $\alpha$ to $\beta$ if $W_{\alpha\beta}^{(S)} > 0$. To illustrate the transitions at a group level, I represent the transition graph of the average transition matrix $W_{\alpha\beta}$ across all scans in the LR sessions (see Section 2.5, B and C). In Supplementary Figure A.2, I report the first 20 participants' TPMs.

### 2.2.8 Intra-Class Correlation

In order to compute reliability of the computed measures between LR and RL fMRI sessions recorded on the same day, I computed Inter-Class Correlation (ICC) (Landis and Koch, 1977; Xing and Zuo, 2018). ICC describes the proportion of within-subject variability versus between-subject variability across recording conditions as follows:

$$\mathrm{ICC} = \frac{\mathrm{MSE}_b - \mathrm{MSE}_w}{\mathrm{MSE}_b + \mathrm{MSE}_w}, \tag{2.5}$$

where $\mathrm{MSE}_w$ and $\mathrm{MSE}_b$ are the within-subject and between subject mean squared errors, respectively (Xing and Zuo, 2018). Positive ICC values (i.e., when within-subject MSE is smaller than the between-subject MSE) indicate individual reliability, which, depending on its value, is categorized as low ($0 < \mathrm{ICC} < 0.2$), fair ($0.2 < \mathrm{ICC} < 0.4$), moderate ($0.4 < \mathrm{ICC} < 0.6$), substantial ($0.6 < \mathrm{ICC} < 0.8$) and almost perfect ($0.8 < \mathrm{ICC} < 1$) (Landis and Koch, 1977).

## 2.3 Results

A set of PL substates is obtained from the first session of resting-state fMRI of 99 unrelated subjects (see Section 2.2 for details). Each PL substate is represented as a vector with $N$ elements, each element representing the projection of a phase of a brain area into the leading eigenvector of all phases (here $N = 90$ since I use 90

non-cerebellar brain regions from the AAL atlas).

### 2.3.1 Functional Relevance

Firstly, I verify the overlap between PL substates obtained across clustering solutions (with $2 < k < 20$) to seven RSNs defined in the literature (Yeo et al., 2011). In Figure 2.3, A, I report for all partitions into $k$ substates (rows), the $k$ cluster centroids obtained (columns). The cluster centroids $V_{c\alpha}$ (representing PL substates) are represented in the brain by coloring only brain areas whose phase projects in the opposite direction from the main orientation of phases (negative elements in $V_{c\alpha}$). PL substates are color-coded according to the most significantly correlated RSNs used as a reference (shown in Figure 2.3, B), given a corrected threshold of $p < 0.05/k$, and in black otherwise.In Supplementary Figure A.1, I show the top view perspective.

Sorting the substates according to their Fractional Occupancy, I find consistently across clustering solutions a most prevalent substate, occupying the first column of Figure 2.3, A, in which the phase of all brain areas project into the same direction. Since it does not reveal the separation of any particular subsystem, and does not significantly overlap with any reference RSNs, this so-called global substate (substate 1) is represented as a transparent brain.

The remaining substates are all characterized by a phase shift in the signal of a given subset of brain areas, which are highlighted as colored patches. Notably, most of the obtained cluster centroids demonstrate a close statistical similarity to reference RSNs, revealing a strong and highly significant overlap (up to r = 0.89, with p-values down to $10^{30}$) with the different RSNs used as reference. I also find that some partitions show different PL substates overlapping with the same reference RSN. When no significant overlap is found, the patches are colored in

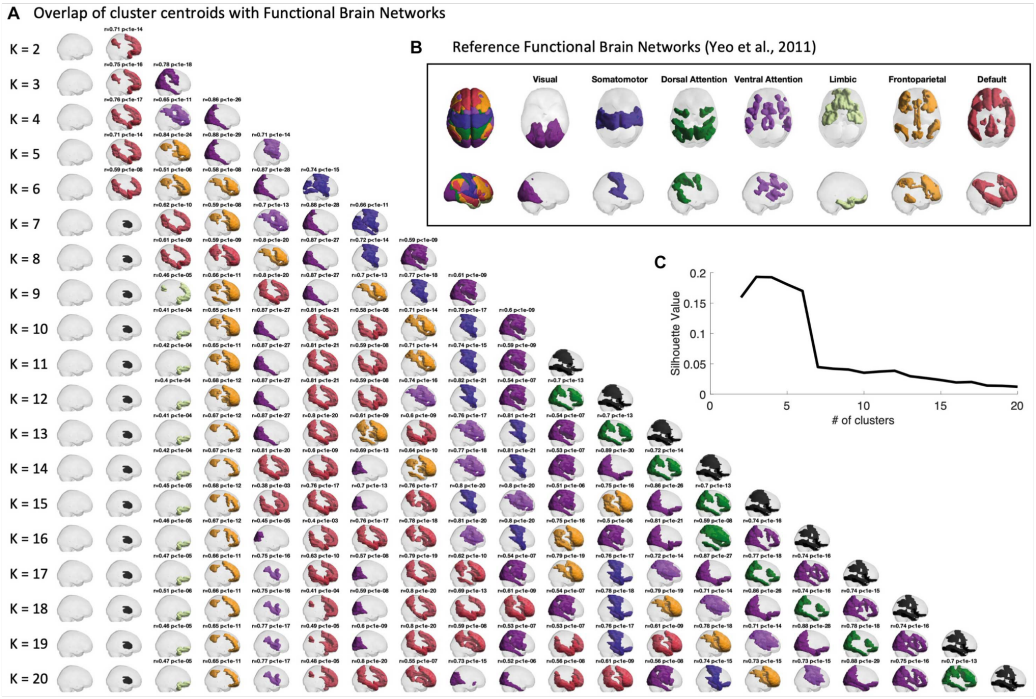



Figure 2.3: ***Centroids Overlap with RSNs.*** *(A) Representation of the centroids obtained for each k-means clustering solution with K ranging between 2 and 20. Centroids are represented in cortical space, rendering only the ROIs whose BOLD phase is shifted* $> \pm\pi/2$ *with respect to the leading direction. ROIs are colored according to the reference Functional Brain Network (shown in panel B) to which they relate to with the most significance. Pearson's r and corresponding p-value are reported as titles only when surviving a conservative threshold of* $p < 0.05/K$*, to correct for the number of independent hypotheses tested in each partition model. Centroids not significantly overlapping with any of the reference Functional Brain Network are colored in black. Top view perspective of the same centroids are reported in Supplementary Figure A.1. (B) Reference Functional Brain Networks estimated from 1000 subjects from correlation-based intrinsic FC (Yeo et al., 2011). (C) Silhouette value, used to evaluate a clustering performance, shows a peak for partitions into 2 to 6 clusters.*

black. One example is the second most prominent substate appearing in all clustering solutions with $k > 7$, which involves regions of basal ganglia, which have been omitted in the analysis of RSNs from (Yeo et al., 2011). I chose to focus on the clustering solution with $k = 5$ within the range of best clustering performance according to the silhouette value (Figure 2.3, C), as it reveals a meaningful partition of the PL substates into four representative functional networks. For $k = 5$ I found substate 2 to correlate with the Default Mode Network (r = 0.71, p = $10^{14}$), substate 3 to correlate with the Fronto-Parietal Network (r = 0.84, p = $10^{21}$), substate 4 to correlate with the Visual Network (r = 0.88, p = $10^{29}$) and finally substate 5 to mostly correlate with the Ventral Attention Network (r = 0.71, p = $10^{14}$). In Supplementary Figures A.1, I also report the overlap of cluster centroids with reference functional brain networks from a top view perspective.

### 2.3.2 Repertoire Exploration

In Figure 2.4, A, I show the different representations of the PL substates and their properties. Each PL substate is represented in two ways: on the left I plot $N = 90$ vector elements as arrows representing the magnitude of projection of each brain area into the leading eigenvector of phases $V_1$. On the right, I render and color brain regions shifted from the main orientation (corresponding to the red arrows on the left) according to the relevant RSNs, to which they overlap maximally with (Figures 2.4, A and E). The PL substates can also be represented in the form of a matrix by computing the matrix product of each centroid's vector $V_{c\alpha}$ and its transpose, describing the pairwise relationship between individual brain regions in each PL substate (Figure 2.4, B).

Assuming stationarity of the brain's dynamical regime during rest, I compute Fractional Occupancy of PL substates as well as their mean Life Times within each fMRI scan (see Section 2.2). In Figure 2.4 C and D, I show the Fractional

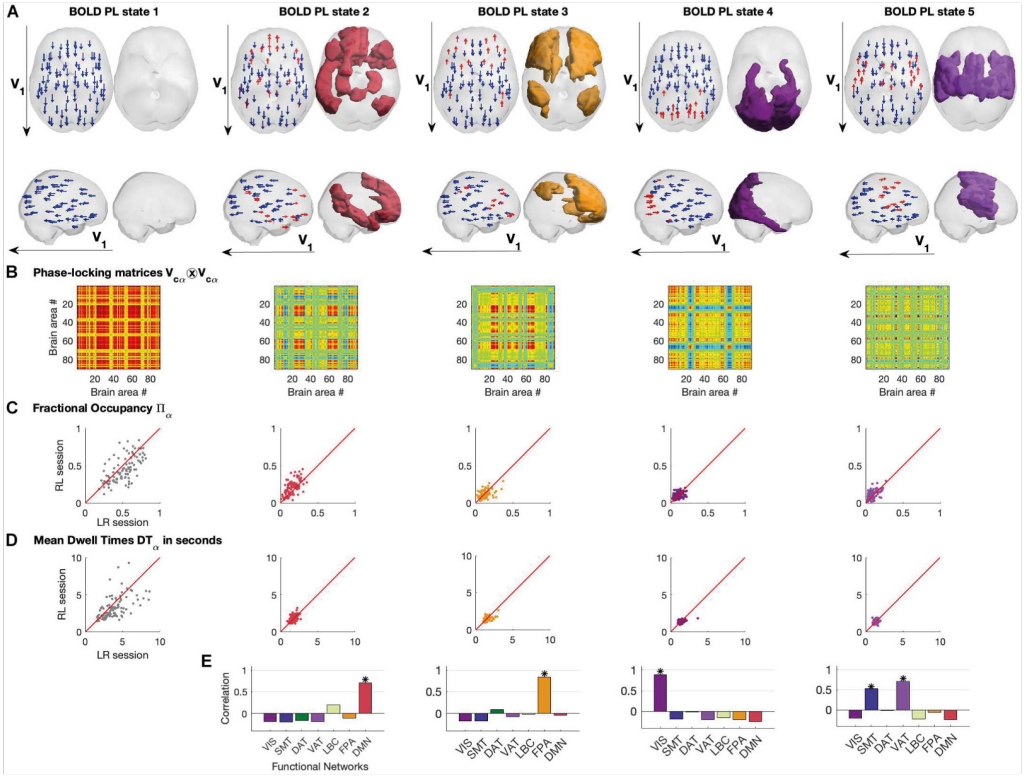



Figure 2.4: ***Repertoire of Phase Locking Substates Obtained Using K = 5.*** *(A) Phase Locking substates represent recurrent patterns of phase alignments across the whole brain. Each centroid is a vector $V_C$ of size $1 \times N$ whose elements indicate how each brain area projects into it. Each centroid is represented in the brain in two different ways: (left) by placing an arrow at the centre of gravity of each brain area and setting its size, direction and color according to the magnitude and sign of the corresponding element in $V_C$ (coloring in red for positive projections into $V_C$, and blue otherwise). (right) Rendering all brain areas with positive values in $V_C$ colored according to the functional network to which they show maximal overlap (see Figure 2.3 and/or panel E below). (B) Phase-locking matrices computed as the outer product of the centroid vectors $V_C$. (C) Scatter plots of substate Fractional Occupancy, plotting the values obtained for the 99 fMRI scans in the LR scanning session versus the values from the RL session. (D) Scatter plots of mean substate Life Times, plotting the values obtained for the 99 fMRI scans in the LR scanning session versus the values from the RL session. (E) Correlation between each PL substate and the seven networks of intrinsic FC from (Yeo et al., 2011). * indicates significance corrected for multiple comparisons with Pearson's p-value < 0.05/7.*

Occupancies and Life Times of each PL substate obtained for each participant, plotting the values obtained from the first fMRI session (LR) versus the values obtained from the second same-day fMRI session (RL). I find that, in both LR and RL sessions, substate 1 shows high variability both in terms of Fractional Occupancy (mean = 0.51, standard deviation (std) = 0.16) and Life Times (mean = 3.94 s, std = 1.73 s), with some subjects spending as little as 20% of the time in this globally coherent substate, whereas others spend up to 80% of the time, with some occurrences lasting up to 10 s (the reliability of metrics across recordings will be addressed in a following subsection). Interestingly, the other 4 substates show consistently lower Fractional Occupancies, with substate 2 (overlapping with the DMN) occurring on average 16.6 $\pm$ 7.6% of the time (mean $\pm$ std), being slightly more prevalent than the other substates (substate 3: 12.7 $\pm$ 6.2%; substate 4: 9.9 $\pm$ 4.7%; substate 5: 9.5 $\pm$ 5.5%). Not only do these functionally relevant PL substates occur less often, but they also show, consistently across subjects, much shorter Life Times, lasting on average around 2 TRs (substate 2, 1.71 $\pm$ 0.34 s; substate 3 1.57 $\pm$ 0.37 s; substate 4, 1.4 $\pm$ 0.34 s; substate 5, 1.3 $\pm$ 0.22 s).

In Figure 2.4, E, I report the correlation between each PL substate and the seven RSNs used as reference (see Section 2.2). I observed substate 2 to correlate only with Default Mode Network (r = 0.71, p = $10^{14}$), substate 3 to correlate with the Fronto-parietal Network (r = 0.84, p = $10_{24}$),substate 4 to correlate with the Visual Network (r = 0.88, p = $10^{29}$) and finally substate 5 to mostly correlate with the Ventral Attention Network (r = 0.71, p = $10^{14}$) but also with the Somatomotor Network (r = 0.53, p = $10^{8}$).

### 2.3.3 Recurrence

Similar to the probability of occurrence of a given substate, I can quantitatively characterize the temporal trajectories by the probabilities of transition between

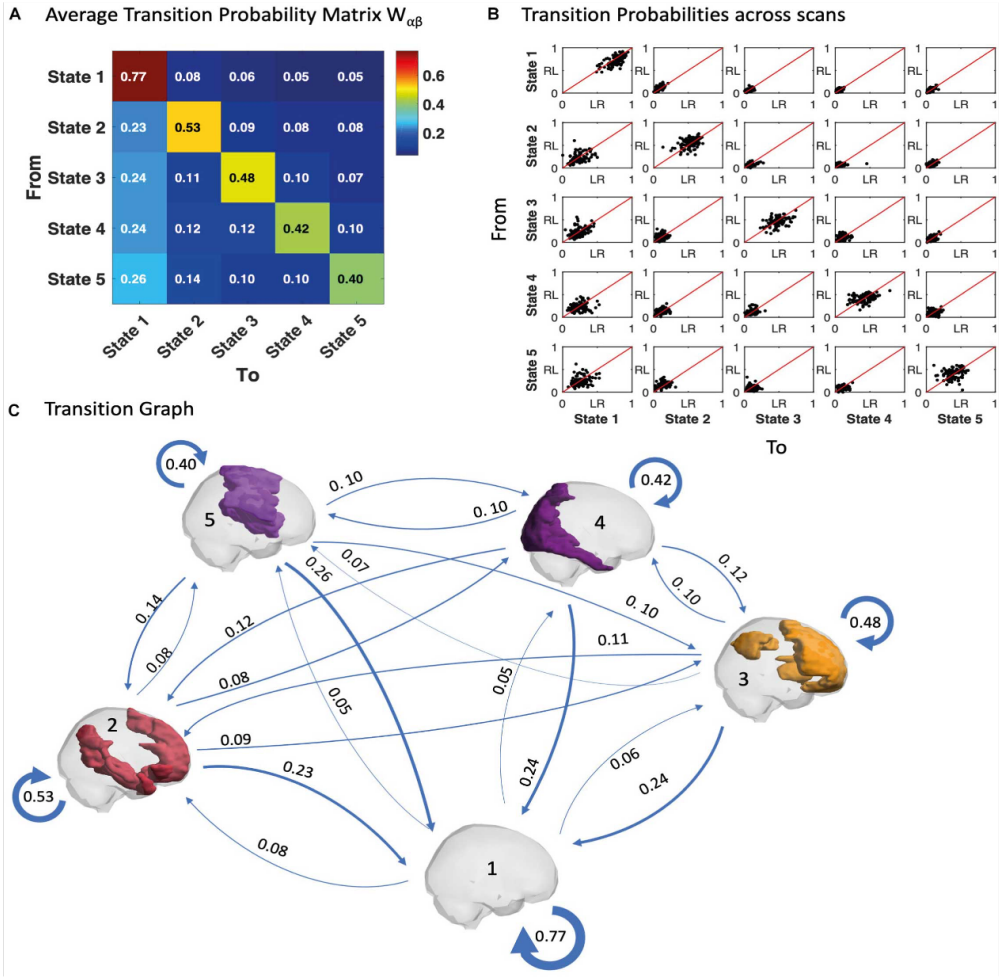



Figure 2.5: ***Trajectories of Brain Activity in Substate Space.*** *(A) Transition matrix quantifying the probability of the trajectory transiting from one substate to another as defined in Equation 2.4, averaged across the scans from all 99 participants in the LR session. (B) Transition probabilities estimated for each fMRI scan, each dot corresponding to one participant, plotting the probabilities of switching in the LR fMRI session versus the RL fMRI session. (C) Transition Graph is constructed from transition matrix W where edges $\alpha \rightarrow \beta$ are directed and weighted with weight $W_{\alpha\beta}$.*

the different PL substates. In Figure 2.5, A, I show the average transition matrix, W$\alpha\beta$, as the probability of switching from substate $\alpha$ to state $\beta$. I noted that the highest probabilities of transition (W$\alpha\beta$ > 0.5) were along the diagonal (representing the probability to remain in the same substate) as well as along the first column (representing the transitions back to the substate 1). The characteristic self-transitions ($\alpha \rightarrow \alpha$) along the diagonal are a distinctive feature of the system, indicating the relative stability of each substate. Substate 1 reveals the highest stability (with 77% probability of remaining in it in the following TR), whereas the probability of remaining in the other substates is close to chance levels. The scatter plots in Figure 2.5, B show the transition probabilities obtained for each of the 99 participants (LR session vs. RL session), revealing consistency of the results across participants and scanning sessions.

Another relevant feature is the asymmetry of the transition matrix, which is indicative of an imbalance in the reciprocity of transitions both to and from a given substate, as can be observed with the apparent proclivity for switching into the (global) substate 1, whereas the probability to leave from it is much smaller. In Figure 2.5, C, a Transition Graph is constructed from the transition matrix W shown in Figure 2.5, A, where edges $\alpha \rightarrow \beta$ are directed and weighted with weight $W_{\alpha\beta}$. This gives a good insight into the spontaneous transition dynamics and motivates the use of the Markov chain transition matrix beyond the probability of occurrence alone.

### 2.3.4 Reliability

To assess the metric's reliability across same-subject same-day recordings when compared to other subjects, I computed the Intra-Class Correlation (see Section 2.2) for each measure above, namely, Fractional Occupancies, Life Times and Transition Probabilities. In Figure 2.6, A, I show the Fractional Occupancy for all

5 substates to have moderate reliability values (substate 1: ICC = 0.59, substate 2: ICC = 0.47, substate 3: ICC = 0.42, substate 4: ICC = 0.39 and substate 5: ICC = 0.51). The Life Times for the first three states have moderate values of ICC and substates 4 and 5 showed poor values (substate 1: ICC = 0.55, substate 2: ICC = 0.37, substate 3: ICC = 0.4, substate 4: ICC = 0.32, and substate 5: ICC = 0.28 (Figure 2.6, B).

Regarding the transition matrix, Figure 2.6, C shows that the probability of remaining in the (global) substate 1 has one of the highest ICC values (ICC = 0.61), with most of the transition to and from the substate 1 showing a range of fair to moderate ICC values ($0.29 < ICC < 0.62$). substates 2 and 3 have border-line moderate values of ICC in the self-transitions (substate 2: ICC = 0.39, substate 3: ICC = 0.40) and some of the transitions to other substates were also in the moderate range. substates 4 and 5 seem to have relatively poor, but still positive, ICC values for the probability of transitions metric (Figure 2.6, C).

Taken overall, the ICC results show that all the measures evaluated have smaller within-subject error than the between-subject error (given ICC values are positive for all measures), indicating that the measures proposed herein capture individual fingerprints of FCD.

## 2.4 Discussion

The challenge of describing spatio-temporal dynamics for a mechanistic understanding of the brain processing as well as for its potential use in clinical research, has been of great interest to the neuroimaging community (Hutchison et al., 2013; Preti et al., 2016; Bolton et al., 2020b). With the advent of open multimodal neuroimaging data, it is possible to address and validate these approaches in representative datasets (Van Essen et al., 2013; Poldrack and Gorgolewski, 2014). In this

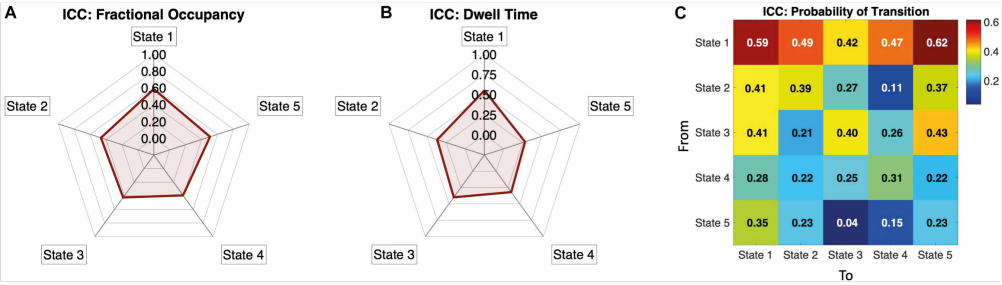



Figure 2.6: ***Individual Reliability of the Phase-Locking Substates' Measures*** *(A) Intra-Class Correlation (ICC) computed for the Fractional Occupancy, showing positive ICC values for all five PL substates, meaning that the within-subject error is smaller than the between-subject error. All values are within a moderate range of within-subject reliability (i.e., 0.4 < ICC < 0.6) according to the categorization by Landis and Koch (1977). (B) Intra-Class Correlation for Life Times for all five substates showing the substates 1,2 and 3 to be in the moderate reliability range. (C) ICC for the normalized Probability Transition Matrix showing positive ICC values in all transitions, with the probabilities of transition from substate 1 being the most reliable, whereas other transitions, particularly between substates 2 to 5, showing lower reliability. The ICC is categorized, based on (Landis and Koch, 1977) as low (0 < ICC < 0.2), fair (0.2 < ICC < 0.4), moderate (0.4 < ICC < 0.6), substantial (0.6 < ICC < 0.8) and almost perfect (0.8 < ICC < 1).*

work, I apply, formalize and validate the Leading Eigenvector Dynamics Analysis (LEiDA) to a large cohort of 99 healthy unrelated HCP subjects (Glasser et al., 2013). I describe spatio-temporal brain activity during rest as a time evolving trajectory in a low-dimensional substate space, where spatial substates are defined according to characteristic whole-brain configurations of BOLD phase-locking. Furthermore, I validate these PL substates to reference RSNs ((Yeo et al., 2011)) and compute their properties of Fractional Occupancy, Life Times and Transition Probabilities. I subsequently assess the reliability of these measures across the two same-day fMRI recordings (using Intra-Class Correlation) and show that all measures have a smaller within-subject error than the between-subject error (ICC values > 0). I argue that such interpretation of spatio-temporal brain activity, validated with reliability analysis, has the potential to identify individual-specific fingerprints in the brain's dynamical landscape and thus serve personalized clinical applications in diagnostics and therapeutics of patients with cognitive disorders.

Concepts and methods from dynamical systems theory are proving useful in the analysis of spatio-temporal brain activity at the macroscopic scale, as they serve to formally characterize the complex dynamics emerging from the collective behavior of billions of interacting neurons, exhibiting features such as multi-stability, meta-stability and self-organized criticality, that may serve helpful to identify the underlying principles coordinating cognition at the whole-brain level (Deco and Jirsa, 2012; Tognoli and Kelso, 2014; Cocchi et al., 2014; Roberts et al., 2019). Here, I aimed at a different characterization of the dynamical properties of the RSNs emerging spontaneously and consistently during rest. The analysis revealed a repertoire of phase-locking substates through which the trajectory of brain activity consistently returns in time and across subjects.

By analyzing the PL substate's Fractional Occupancy, Life Time and Probability of Transitions, the results revealed that the PL substates can be divided in

two groups according to their dynamical properties: On one hand, the algorithm consistently detects a substate where all the ROI-averaged BOLD signals project into the same direction captured by the leading eigenvector (substate 1 for all clustering solutions). This substate exhibits longer Life Times and shows high between-subject variability but also high within-subject reliability. On the other hand, I detect for all k-means clustering solutions, a set of k-1 substates where the BOLD signals of some brain areas project into the opposite direction from the main BOLD phase orientation. These substates occur consistently less often and last for shorter times than the global substate, but reoccur consistently across subjects and sessions. Given the reduced stability of these PL substates with respect to the meta-stable globally synchronized substate, I refer to this second group as 'ghost' attractor substates. In other words, ghost attractors in this framework refer to short-lived (or weakly stable) spatial configurations that consistently reoccur across time.

Regarding the functional relevance of these "ghost" PL substates, the results show a clear and highly significant overlap of most cluster centroids (obtained for the whole range of partitions explored) with a set of seven previously identified RSNs used as reference (Yeo et al., 2011). This finding indicates that these PL substates, despite being obtained from a different analytic perspective than more conventional correlation-based analyses, are closely related to the RSNs. Yet, unlike correlation-based analyses that reveal only the spatial map of these functional networks, the LEiDA approach allows characterizing their properties over the temporal dimension. As the reference RSNs are computed from the correlation-based sFC, a perfect match to the PL substates detected herein is not expected. Rather, they can be considered for validation of the functional relevance of the PL substates and served to guide the choice of the number of substates or further analysis. The number of substates chosen is a trade-off between more fine-grained

but less robust substate solutions as demonstrated by the increasing specificity of functional subsystems for higher $k$. Here, the clustering solution with $k$ = 5 was chosen for being within the range of maximal Silhouette value and for revealing a separation into distinct functionally meaningful RSNs such as the Default Mode Network, Frontoparietal Network, Ventral Attention Network and Visual Network. However, a partition into a higher number of substates may prove necessary when addressing particular conditions that affects a particular subsystem optimally defined for higher $k$. For instance, in a previous work using LEiDA, the partition into $k$ = 10 was chosen for detecting the network that most significantly distinguished patients in remission from major depressive disorder and controls (Figueroa et al., 2019), whereas another study found the solution with $k$ = 7 to optimally highlight the effects of psilocybin-induced state (Lord et al., 2019).

For all partitions into $k$ > 7, the algorithm consistently detected a functional subsystem involving the basal ganglia (colored in black in Figure 2.3, A, and Supplementary Figure A.1) for not overlapping with any of the reference RSNs) as the second most prevalent PL substate. This indicates that resting-state activity also involves connectivity to subcortical areas, which appears particularly important for the study of psychiatric disorders, such as anxiety-related disorders involving the basal ganglia. Following previous LEiDA studies, I chose here a coarse parcellation into N = 90 brain areas and did not include the BOLD signal detected in the cerebellum. The Anatomic Automatic Labeling Atlas has been validated in many studies and has shown consistency in the LEiDA results across datasets (Cabral et al., 2017a; Figueroa et al., 2019; Lord et al., 2019). However, it is based on an anatomic definition of the brain regions and as such might not generalize adequately to the dynamic functional connectivity analysis. I expect to extend to finer-grained and fMRI-derived parcellations in future studies, potentially including other substructures such as the cerebellum, in order to gain a wider insight

into the network configurations observed in spatio-temporal brain activity at the macroscopic scale (Cammoun et al., 2012; Glasser et al., 2016; Schaefer et al., 2018).

The mechanistic interpretation of the empirical data proposed herein serves as a great candidate for further theoretical exploration by whole-brain computational models (Ghosh et al., 2008; Honey et al., 2009; Deco et al., 2009a). To this date, many models have demonstrated well-matched dynamics to the brain activity as represented by sFC in a critical range of parameters where the brain is poised between noisy and oscillatory spatio-temporal activity. Furthermore, different properties were shown to have an impact on the emerging dynamics such as propagation delays, local vs. global connections, signal-to-noise ratio, and local inhibitory rules (Deco et al., 2014; Honey et al., 2009; Cabral et al., 2011). Extending such modeling endeavors away from sFC to a spatio-temporal dynamic representation of the experimental data is currently becoming a possible new avenue into understanding the underlying principles governing FCD (Hansen et al., 2015; Cabral et al., 2017a; Deco et al., 2018). Recently, Deco et al. have shown how the dynamic representation of resting-state data in wakefulness and sleep (characterized using Probabilistic Metastable Substates) can serve to explore a whole-brain model perturbation for an identification of the brain regions responsible for the transition between awake and sleep state (Deco et al., 2019).

Representing FCD through the prism of dynamical system theory hypothesizes the existence of attractors in N-dimensional space through which the functional activity evolves in time. Assuming this hypothetical scenario, it describes a substate-based propagation of the data, rendering the underlying dynamics in a discrete sense (Baker et al., 2014; Karahanoglu and Van De Ville, 2015; Preti et al., 2016; Cabral et al., 2017b). However, other methods have considered FCD from a continuous point-of-view, such as the spatio-temporal connectome where brain activ-

ity is described as a temporal graph (Griffa et al., 2017; Vohryzek et al., 2019) and auto-regressive models (Liégeois et al., 2019) (See Figure 1.2). I acknowledge that looking at the brain spatio-temporal activity in a discrete sense is only one of the interpretations currently proposed in trying to describe the emergent complex phenomena observed in whole-brain dynamics.

It is to be noted that the applied clustering algorithm is just one amongst many decomposition methods that can partition the leading eigenvectors into meaningful substates. Indeed (Cabral et al., 2017a) compared the results from k-means algorithm to the HMM, in their paper on cognitive performance of patients, showing similar results with both approaches (Cabral et al., 2017a). However, k-means was chosen here for its relatively simple implementation and its relatively low computational cost, revealing functionally meaningful cluster centroids.

New imaging methods benefit greatly from the reliability analysis that investigates individual variabilities across recordings sessions. Especially in clinical applications, reliability is crucial to obtain stable measures across time for individual subjects (i.e., low within-subject variability) and at the same time distinguishable differences between subjects (i.e., high between-subject variability) (Xing and Zuo, 2018; Zuo et al., 2019). In this work, Intra-Class Correlation is used to compute the desirable ratio between between-subject variability and within-subject variability across recording sessions. One of the Intra-Class Correlation scales proposed by Landis and Koch (1977) to assess reliability for clinical applications suggests that values $1.0 > ICC > 0.8$ have excellent reliability, $0.8 > ICC > 0.6$ substantial reliability, $0.6 > ICC > 0.4$ have moderate reliability and, $0.4 > ICC > 0.2$ poor substantial reliability. In other words, it is desirable to obtain high reliability values for the method's possible clinical application.

## 2.5 Chapter Summary

To summarize, this Chapter has described the spatio-temporal brain dynamics during rest as a time-evolving trajectory in a low-dimensional substate space, where spatial substates are defined in terms of their whole-brain phase-locking characteristics. This formalism allows to describe the PL substates in terms of Fractional Occupancy, Life Times and Probability of Transitions. Furthermore, the results demonstrate the PL substates to be functionally relevant, recurrent across subjects and moderately reliable across scanning sessions. This suggests the potential to identify the brain dynamical landscape of individual participants and thus serve as a diagnostic and therapeutic application for patients with cognitive disorders.

# 3 | Rebalancing the Depressive Brain State with Psilocybin

> Mind at Large has to be funnelled through the reducing valve of the brain and nervous system. What comes out at the other end is a measly trickle of the kind of consciousness which will help us to stay alive on the surface of this particular planet...
>
> — Aldous Huxley, The Doors of Perception

## 3.1 Introduction

More than half a century later, Aldous Huxley's Reducing Valve analogy still maintains its relevance in glimpsing the wonders of the psychedelic experience. Moreover, could it be that in a depressive state ever more tightening of the Reducing Valve is experienced? Of course, in reality the picture is likely more complicated, and so here, I argue that the psychedelic-induced and depressive state can be perceived on opposite sides of the entropic continuum as defined by the entropic brain hypothesis (Carhart-Harris et al., 2014; Carhart-Harris, 2018). Indeed, the recent revival of psychedelic therapy has started making inroads into potential treatments of these so called rigid or less entropic brain states (Carhart-Harris et al., 2016a; Carhart-Harris and Goodwin, 2017; Carhart-Harris, 2018).

As discussed in the Introduction 1.1.2, recent advancements in neuroimaging techniques have started describing complex spatio-temporal dynamics in terms of their spatial and temporal correlations. Every brain state, here defined in its broadest sense as a psychedelic-induced or depressive state, has its own characteristic spatio-temporal dynamics of large-scale spatial communities temporally evolving

as '*stable, quasi-stable, high or low activities, and transient arrangements*' (Deco et al., 2019; Kringelbach et al., 2020). The challenge for contemporary neuroscience is to understand what is the most appropriate description of such brain states and how they manage to shift between each other.

The common picture of a brain state has been that of static FC (Perl et al., 2020). Such approach has successfully defined variety of brain states in terms of their spatial relationships known as resting-state networks (Fox et al., 2005; Damoiseaux et al., 2006). But importantly, as I have argued in my Thesis, time is a crucial ingredient in the depiction of brain states. As such many efforts have been devoted to moving beyond the mere stationary representation of spatio-temporal dynamics. To this date, there has been a growing taxonomy of different approaches (Kringelbach et al., 2020; Preti et al., 2016; Bolton et al., 2020b) from data-driven heuristic clustering methods across time (Karahanoglu and Van De Ville, 2015; Allen et al., 2014; Hutchison et al., 2013), dynamical systems informed phase-locking approaches (Cabral et al., 2017b) to Hidden Markov Model representations (Baker et al., 2014; Vidaurre et al., 2017) (see also Introduction 1.1.2). Furthermore, to understand the underlying mechanisms maintaining and driving brain states transitions, it is important to move beyond the mere correlative picture of neuroimaging data. In this direction, whole-brain models have emerged as a powerful and useful tool for clinical diagnosis and prediction in various brain diseases (Kringelbach and Deco, 2020). Yet, going back to the need of an adequate brain state description, the models predictive power is only as good as the summary of th experimental data (Cabral et al., 2017a) (see also Introduction 1.1.3). Here, I build on the PL substates of the previous Chapter 2 and on the "Awakening" paradigm proposed by (Deco et al., 2019), whereby the persistent brain states of responders and non-responders before and after treatment with the psychedelic drug psilocybin are defined in terms of Probabilistic Metastable Substates. Assuming temporal

stationarity, these recurrent phase-locking or metastable substates can be characterised by their probability of occurrence. Beyond the description of brain states, I wish to understand what are the possible brain regions that allow or prevent the recovery from depression after the treatment with psilocybin. I show that whole-brain models, tuned to the PMS description of spatio-temporal dynamics, can be used to force transitions between the depressive and recovered state and therefore reveal relevant brain regions responsible for an unsuccessful outcome of the treatment.

## 3.2 Methods

### 3.2.1 Experimental Data

I carried out the analysis using a previously published dataset of patients with treatment-resistant depression undergoing treatment with psilocybin at the Hammersmith Hospital in London (Carhart-Harris et al., 2016a). In brief, I investigated 15 patients (without excessive movement and other MRI data artifacts from the original 19 patients) who were diagnosed with treatment resistant depression (TRD). The MRI scanning sessions were completed pre-treatment with psilocybin and one-day post-treatment. The patients were split into responders and non-responders to the treatment based on the Quick Inventory Symptomatology (QIDS) at 5-weeks post-treatment with 6 out of the 15 patients meeting the criteria for a treatment response (Carhart-Harris et al., 2017).

### 3.2.2 Probabilistic Metastable Substates (PMS)

Firstly, I computed the instantaneous phase relationship between individual brain regions by expressing the demeaned regional BOLD signal $x(t)$ as an analyt-

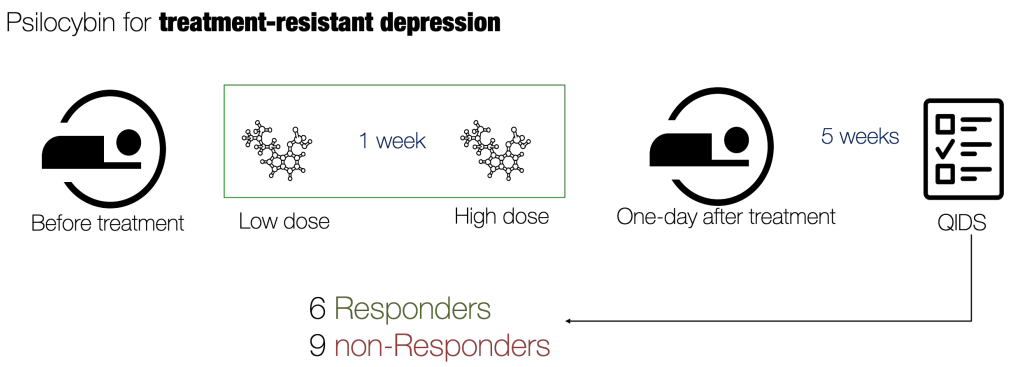



Figure 3.1: ***Experimental Design:*** *Fifteen treatment-resistant patients were scanned before and one day after the psilocybin intervention. Furthermore, patients were split into responders (6 patients) and non-responders (9 patients) according to their QIDS score five weeks after the treatment.*

ical signal i.e. in terms of its time-varying phase $\theta(t)$ and amplitude $A(t)$ as $x(t) = A(t) \cdot cos(\theta(t))$ (Glerean et al., 2012). I excluded the first and last three timepoints to account for the boundary artefacts introduced by the Hilbert transform. Hence for every time point $t$ and pair of brain regions $n$ and $m$, I obtain the phase coherence matrix $dPC$ as follows:

$$dPC(n, m, t) = cos(\theta(n, t) - \theta(m, t)) \tag{3.1}$$

By decomposing the signal in this way, I can identify when the brain regions $n$ and $m$ are aligned with similar angles, $cos(0) = 1$ , orthogonal to each other $cos(\pi/2) = 0$ or anti-aligned $cos(\pi) = -1$. As the phase coherence is a measure of undirected connectivity, the phase coherence matrix $dPC$ is symmetric and all meaningful information is captured in its upper-triangular part.

For further analysis, I used only the $1 \times N$ leading eigenvector $V_1(t)$ of the $dPC$ matrix as described in the Leading Eigenvector Dynamics Analysis (Cabral et al., 2017b). In detail, at every timepoint $t$ of the $dPC(t)$, I performed the eigende-

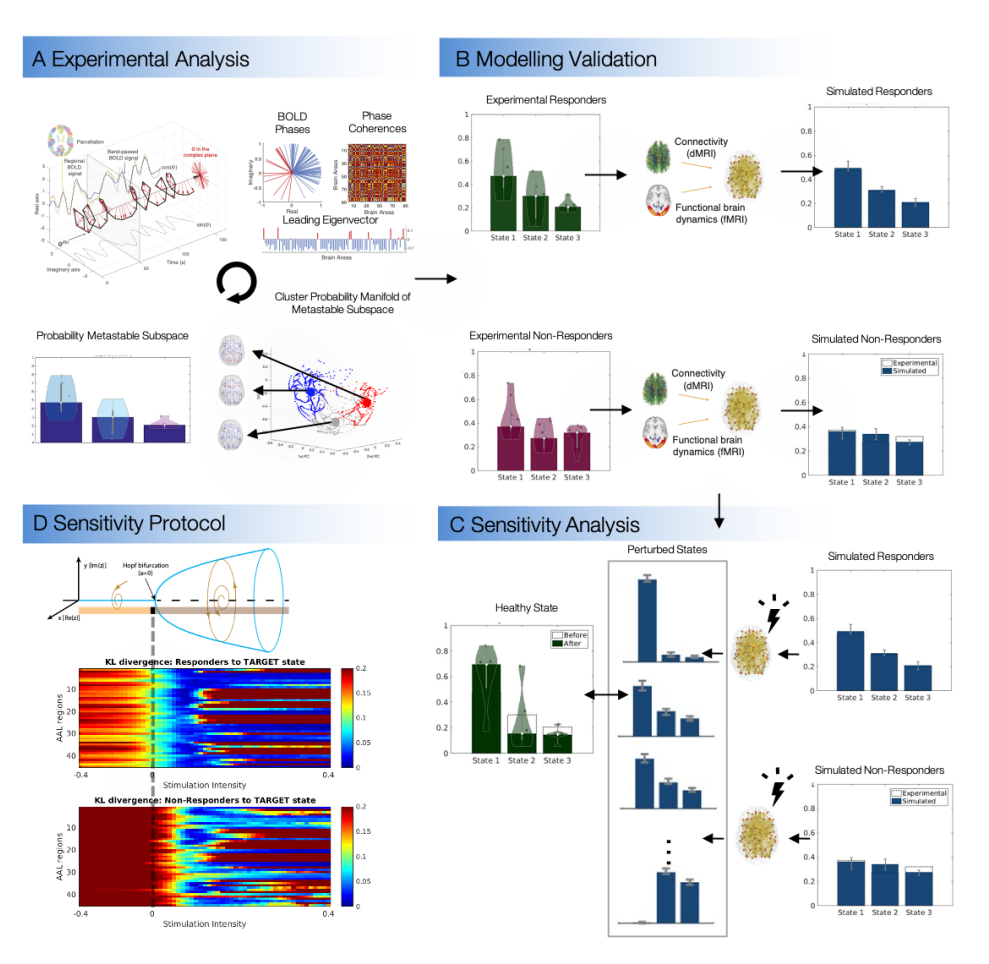



Figure 3.2: ***Study Overview: A) Experimental Analysis***. *Probabilistic Metastable Substates were computed for each condition. In brief, regional fMRI timeseries were first converted to analytical signal, followed by computation of the leading eigenvector of the phase coherence matrix at every timepoint, before the unsupervised k-means algorithm was finally deployed to cluster the timepoints into a three substate solution, yielding the PMS for each condition.* ***B) Modelling Validation***. *Whole-brain models for responders and non-responders before treatment were optimised.* ***C) Sensitivity Analysis***. *Bilateral brain region perturbations were performed to find optimal transition to the healthy brain state.* ***D) Sensitivity Protocol***. *Such perturbations were computed for varying intensities as defined by the bifurcation parameter* $a$.

composition taking the first (most dominant) eigenvector to describe the $dPC(t)$ pattern. The $dPC(t)$ is decomposed as $dPC(t) = V(t)D(t)V^{-1}(t)$ where $D$ is a diagonal matrix carrying the real-valued eigenvalues and $V_1(t)$ and $V_1^{-1}(t)$ are the left and right corresponding orthogonal eigenvectors respectively. The dominant connectivity pattern can be simply reconstructed by the following matrix multiplication $V_1(t) \cdot V_1^T(t)$.

To identify and describe the discrete PL substates of the recurrent phase coherence matrix, I clustered the $1 \times N$ leading eigenvector on the concatenated $dPC$ matrix for the two populations of responders and non-responders. I used the unsupervised k-means algorithm, of varying cluster number $k$ from 2 to 10 clusters, to iteratively converge to a predefined number of clusters with 20 random cluster initialization to ensure stability in the clustering. Again, by computing the matrix multiplication of the $1 \times N$ cluster centroids $V_{c\alpha}$ as $V_{c\alpha}(t) \cdot V_{c\alpha}^T(t)$ I obtain the dominant connectivity pattern of each cluster. In the current analysis, I considered the cluster solution $k = 3$ as an optimal choice between the quality measures such as the Silhouette Value as well as statistical significance given by the p-values. After calculating the PL substates, I defined the Fractional Occupancy of the individual states by calculating their occurrence across the pre- and post-treatment recording sessions for individual subjects, normalised by the lengths (in TRs) of the recordings (all recordings had the same number of TRs; for the mathematical definition of Fractional Occupancy, see previous Chapter 2, Equation 2.1).

### 3.2.3 Whole-brain Computational Model

In order to simulate the spatio-temporal dynamics, I used the canonical form of the Stuart-Landau oscillator model, describing second-order (continuous) bifurcation from noisy to oscillatory dynamics (Kuznetsov, 1996). This so-called supercritical Hopf-bifurcation model was used locally at every brain region of interest (node)

to simulate local dynamics (Deco et al., 2019). To achieve a whole-brain level description of dynamics, the regional Hopf models were coupled in a structural connectivity (SC) network, describing the large-scale white-matter map of the human brain (Deco et al., 2017b; Hagmann et al., 2008). The emerging and complex interactions in the whole-brain network of coupled Hopf-bifurcation models have been shown to describe many aspects of human neurophysiology known from experimental recordings of EEG (Freyer et al., 2011)(Freyer et al., 2012), MEG (Deco et al., 2017a) and fMRI data (Deco et al., 2019; Deco and Kringelbach, 2016; Deco et al., 2017b; Kringelbach et al., 2015).

Formally, the normal form of the supercritical Hopf-bifurcation model for a single uncoupled region of interest ($n$) in Cartesian coordinates is described by the following set of coupled equations:

$$\frac{dx_n}{dt} = (a_n - x_n^2 - y_n^2)x_n - \omega_n y_n + \beta\eta_n(t) \tag{3.2}$$

$$\frac{dy_n}{dt} = (a_n - x_n^2 - y_n^2)y_n - \omega_n x_n + \beta\eta_n(t) \tag{3.3}$$

with $\beta\eta_n(t)$ being Gaussian noise with standard deviation of $\beta = 0.02$. The bifurcation parameter $a$ positions the system at the supercritical bifurcation point when $a = 0$. The noisy activity regime is governed by $\beta\eta_n(t)$ when $a < 0$, and the stable limit cycle regime with oscillatory behaviour of frequency $f$ is defined by $f_n = \omega_n/2\pi$ when $a > 0$. The values of the intrinsic frequency $\omega$ were computed from the experimental data series in the $0.04 - 0.07$ Hz band by taking the peak frequency of the Gaussian-smoothed power spectrum of the individual nodes.

To describe the coupled whole-brain computational model, I introduced the coupling term (modelled as the common difference coupling i.e. describing the linear term of a general coupling function) between the individual nodes weighted by

the corresponding values of the SC matrix. To be noted, I do not consider the next nonlinear coupling term following Taylor expansion of the full coupling in cases where the linear coupling term is non-existent (Kuramoto, 1984; Pikovsky et al., 2002). Equations 3.2 and 3.3 can be hence expanded as follows:

$$\frac{dx_n}{dt} = (a_n - x_n^2 - y_n^2)x_n - \omega_n y_n + G\sum_{p=1}^{N} C_{np}(x_p - x_n) + \beta\eta_n(t) \tag{3.4}$$

$$\frac{dy_n}{dt} = (a_n - x_n^2 - y_n^2)y_n - \omega_n x_n + G\sum_{p=1}^{N} C_{np}(y_p - y_n) + \beta\eta_n(t) \tag{3.5}$$

where $C_{np}$ is the SC weight between node $n$ and $p$, and $G$ is the global coupling weight with equal contribution between all nodal pairs. The SC matrix was rescaled to have mean value $\langle C \rangle = 0.2$ in order to be consistent with previous literature's range of parameters (Deco et al., 2019). The simulated BOLD signal is described by the $x_n$ equation for every node $n$. The variables $G$ and $a$ are the control parameters used respectively for model validation (to experimental data) and the stimulation protocol (Deco et al., 2019)

### 3.2.4 Objective Function

Different realisations of experimental data can be used to validate the simulated signal (Cabral et al., 2017a). For a comparison along the spatial dimension, grand-averaged sFC, as computed by Pearson correlation and Global Brain Connectivity (GBC) are usually considered (Deco and Jirsa, 2012; Honey et al., 2009). To account for the temporally varying nature of the fMRI signal, recent literature has focused on the comparison between the simulated and empirical measures of metastability (standard deviation of the Kuramoto Order Parameter) and FCD

spectrum (quantified by Kolmogorov-Smirnov distance) i.e. the distributions of the cosine distance between consecutive timepoints as described by the leading eigenvector (Deco et al., 2018). However, as alluded to in the previous Chapter 2, the fMRI signal can be described not only as varying in time but also as organising into spatially meaningful PL substates. Here, I compare simulated data to the Fractional Occupancies of the PL substates found in experimental recordings (Deco et al., 2019). I used the symmetrised Kullback-Leibler Divergence (KL divergence) of the simulated and empirical fractional occupancies, to minimise their difference, as follows:

$$KL(P_{emp}, P_{sim}) = 0.5(\sum_i P_{emp}(i) \ln \frac{P_{emp}(i)}{P_{sim}(i)} + \sum_i P_{sim}(i) \ln \frac{P_{sim}(i)}{P_{emp}(i)}) \quad (3.6)$$

where $P_{emp}$ and $P_{sim}$ are the Fractional Occupancies of the same spatial brain substates for empirical and simulated timeseries respectively. To be noted, I chose the symmetrised KL divergence for its simplicity but other objective functions can be used to measure the difference between Fractional Occupancy distributions, for example the Jensen-Shannon divergence.

## 3.3 Results

To obtain an appropriate representation of the spatio-temporal dynamics, I first analysed the experimental findings with regards to their spatial and temporal characteristics. As argued in my Thesis, the temporal fluctuations are relevant for the description of the brain dynamics and as such I used the Probabilistic Metastable Substates (PMS) space to quantitatively characterise the fMRI recordings in space and time. Then, I constructed two whole-brain models of responders and non-

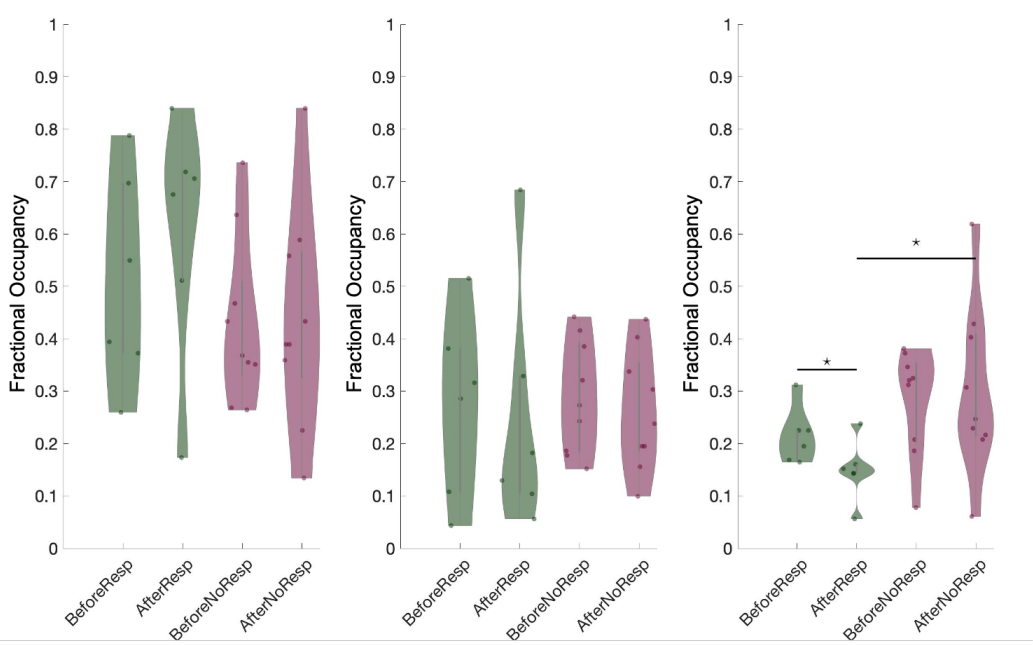



Figure 3.3: ***PMS in Treatment-resistant Depression with Psilocybin Intervention:*** *Experimental results of the Probabilistic Metastable Substates for the three-substate clustering solution. Significant differences were observed in the third substate between responders before and after treatment ($p = 0.0258$, signed rank-sum permutation test) and responders and non-responders after treatment ($p = 0.0141$, rank-sum permutation test).*

responders to psilocybin treatment by fitting their PMS descriptions to that of the experimental data. Finally, I used a perturbation protocol to force a transition to the healthy PMS (responders after psilocybin treatment) and identify regions between responders and non-responders that are less conducive to such rebalancing.

### 3.3.1 Experimental Analysis

As described in Section 3.2, I computed the PMS for responders and non-responders pre- and post-treatment with psilocybin. Here, I focused on the three-substate solution as it already allowed to differentiate the two groups, with substate 3 being statistically significant between pre- and post-treatment responder cohorts (p

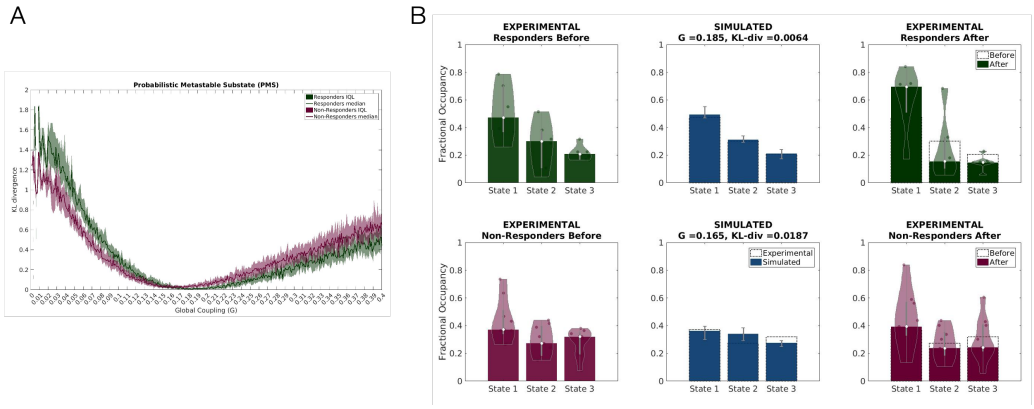



Figure 3.4: ***Model Validation: A)*** *Validation of the responder and non-responder models as a function of the global coupling parameter G, with optimal fits at G = 0.185 (KL-divergence = 0.0064) and G = 0.165 (KL-divergence = 0.0187) respectively.* ***B)*** *Experimental PMS for responders and non-responders before treatment (left), their simulated counterparts at optimal G (middle), and experimental PMS for responders and non-responders after treatment (right).*

= 0.0258, signed rank-sum test) as well as post-treatment responders and non-responders (p = 0.0141, rank-sum test; Figure 3.3). In SI Figure A.3, I reported quality measures across clustering solutions. Furthermore, I also computed the GBC, metastability and FCD measures (see SI Figure A.4). These results clearly indicated the necessity of considering both spatial and temporal dimensions to differentiate between conditions as GBC, synchrony and metastability show non-significant results. Conversely, the FCD measure showed significant differences between the mean histogram values of pre- and post-treatment responders (p = 0.0163, signed rank-sum permutation test), and pre- and post-treatment non-responders with post-treatment responders respectively (p = 0.0183 and p = 0.0273, rank-sum permutation test), further supporting the use of spatio-temporal measures to accurately describe whole-brain dynamics.

### 3.3.2 Optimization of the Whole-brain Model to PMS Space

To obtain the whole-brain computational model for both groups (responders and non-responders) before treatment, I used the Stuart-Landau oscillator (normal form of a supercritical Hopf bifurcation) at every region of the AAL atlas (Tzourio-Mazoyer et al., 2002). I used a structural connectivity in the AAL parcellation to describe the network topology between regions. Each regional intrinsic frequency was defined by the group average of maximum frequency (see Section 3.2). I used the global coupling parameter, $G$, to optimize each model to its appropriate working point. This was achieved by finding the minimum between the experimental and simulated PMS space as defined by the KL Divergence - see Figure 3.3, A, (in SI Figure A.5, I reported optimisation curves for other observables such as the static FC, metastability and FCD). For the responders and non-responders before treatment, I found $G = 0.185$ (KL divergence = 0.0064) and $G = 0.165$ (KL divergence = 0.0187) respectively to minimise the difference. Figure 3.4, B, shows on the left the experimental results for both groups before treatment, in the middle the optimal simulated fits for both groups, and on the right the experimental results after treatment (with the results of responders after treatment serving as the target PMS for rebalancing).

### 3.3.3 Perturbation Protocol

In the previous section, I showed how to successfully create whole-brain models for both responders and non-responders before treatment when focusing on the spatio-temporal dynamics as described by the PMS space. Here, I considered a perturbation protocol to determine whether there is a subset of regions that might be hindering the treatment rebalancing to the healthy state (as defined by the PMS space of responders after treatment). Figure 3.5 illustrates the perturbation proto-

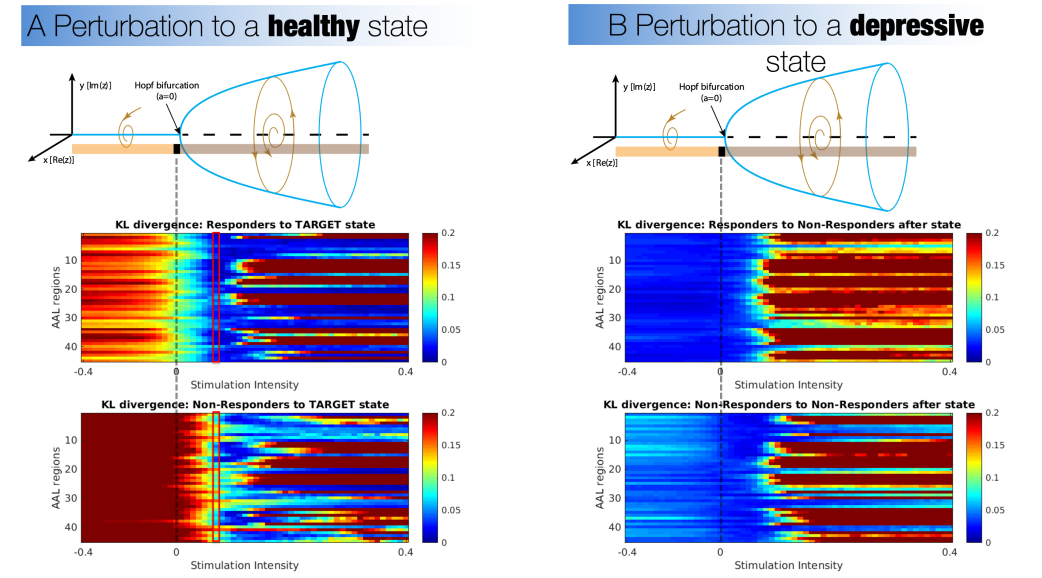



Figure 3.5: ***Perturbation Protocol: A) Perturbation to a healthy state***. *Each homological site was perturbed with varying intensity (magnitude of bifurcation parameter $a$) and type (negative or positive bifurcation parameter $a$) to force transition to the healthy state. Optimal intensity of $a = 0.07$ was achieved for the responder group.* ***B) Perturbation to a depressive state***. *A forced transition to the depressive state showed worse or no effect at varying values of the bifurcation parameter $a$.*

col, whereby the bifurcation parameter $a$ is used to change the strength of nodal dynamics either to a more noisy regime or to an oscillatory regime (as defined by the intrinsic nodal frequencies; see Section 3.2). I focused on homological nodal perturbation of the whole-brain model, meaning that homological regions are perturbed equally, resulting in 45 runs at varying values of $a$. Figure 3.5, Left, shows the perturbation protocol of forcing a transition to the healthy state for models of both responders and non-responders before treatment. Again, an average of the symmetrised KL divergence between either the perturbed responders pre-treatment or non-responder models before treatment and the healthy PMS space was shown. In the noisy regime ($a < 0$), a deterioration of the fit was observed for both groups, while in the synchronous regime ($a > 0$), an initial improvement across all 45 runs was depicted, before subsequent deterioration away from the optimal fit for both groups. Conversely, a forced transition to the depressive state (as described by the non-responder group after treatment) showed a worse fit for both groups in the synchronous state and no effect of the noisy perturbation (Figure 3.5, Right). To compare which regions were less likely to force transition to a healthy state, I first defined the optimal perturbation strength as the minimum of the averaged KL divergence (across the 45 runs) of the responder group to the treatment. This stimulation intensity was found at $a = 0.07$. Then, I inspected the difference between the responders and non-responders at that given value of $a$ to assess what nodal perturbations were less likely to force a transition to the healthy state.

Figure 3.7, Left, shows the rank ordered regional differences in KL divergence between perturbations of the responder and non-responder models before treatment at a stimulation intensity of $a = 0.07$. I highlighted the regions with the largest KL divergence with inability to force a transition to the healthy state. These regions are the Temporal Superior pole, Rolandic operculum, Fusiform gyrus, Sup-

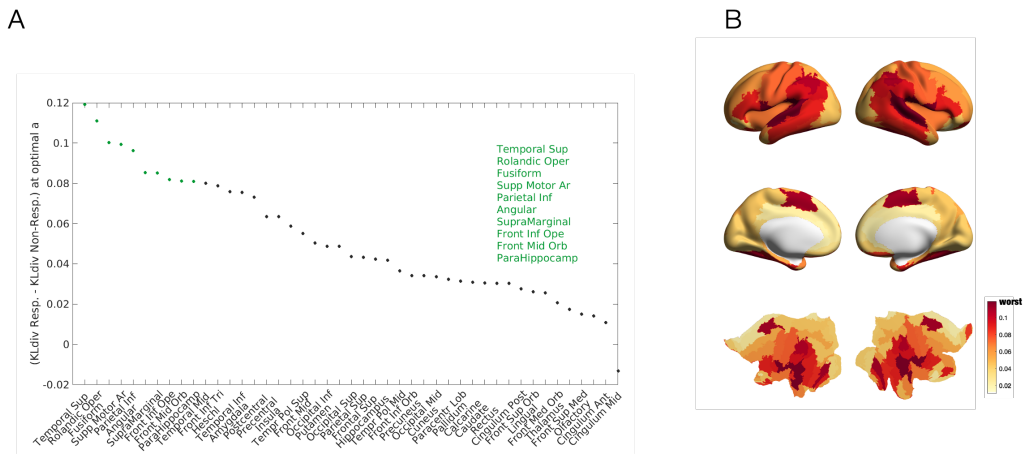



Figure 3.6: ***Inability of Nodes to Force a Transition to the Healthy State : A)*** *Rank ordered difference of KL divergence between perturbations of the responder and non-responder models before treatment at a stimulation intensity of* $a = 0.07$. **B)** Cortical rendering of the KL divergence differences.

plementary Motor Area, Parietal Inferior gyrus, Angular gyrus, Supramarginal gyrus, Frontal Inferior gyrus (opercular), Frontal Middle gyrus (orbital) and the Parahippocampal gyrus. Figure 3.7, Right, shows the cortical rendering of these differences.

### 3.3.4 Correlation with 5HT Maps

Given the unique neuropharmacology of the psychedelic-induced state through serotonergic receptors, I explored whether the regions with less likely perturbation to the healthy state show similarities with the 5HT map densities as collected by PET. Figure 3.7 A shows correlations between the $5HT_{2a}$ and $5HT_{1a}$ receptor density maps and the KL divergence differences for the two groups at optimal $a = 0.07$ (Spearman $\rho = 0.227$, p = 0.032 and Spearman $\rho = 0.284$, p = 0.007 respectively). Figure 3.7 B, shows non-significant correlations to the other three 5HT receptors - namely $5HT_{2b}$ (Spearman $\rho = 0.064$, p = 0.055), $5HT_4$ (Spearman $\rho = 0.055$, p = 0.607) and 5HTT (Spearman $\rho = -0.172$, p = 0.106).

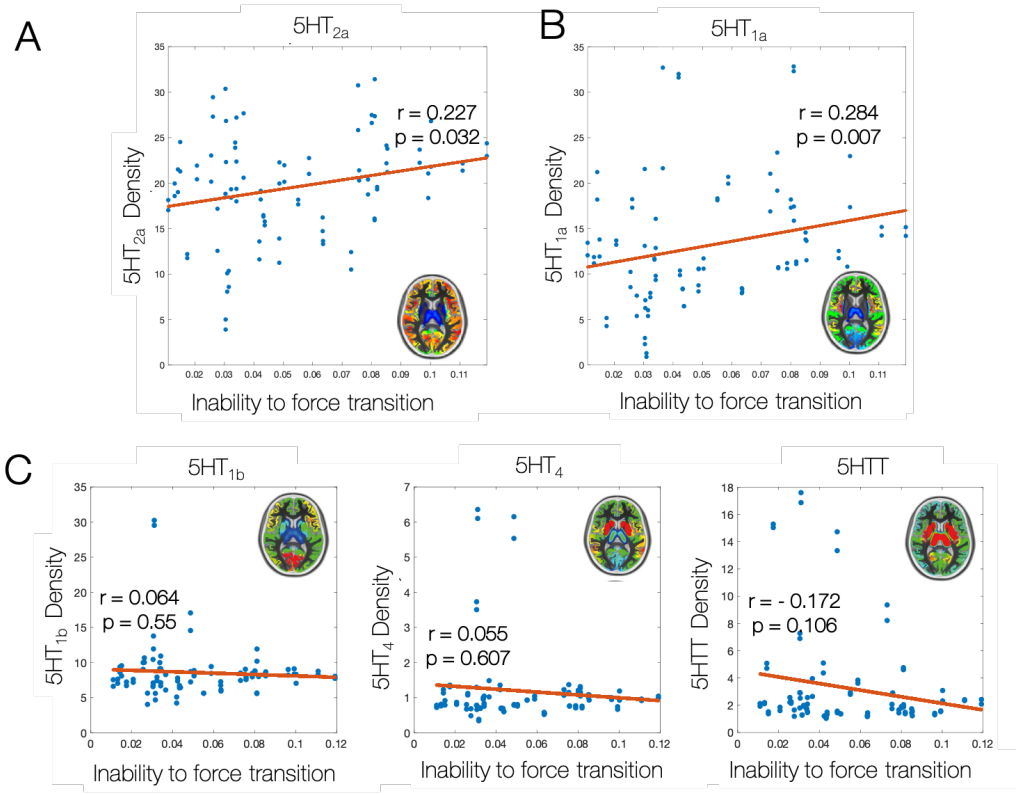



Figure 3.7: ***Correlations with Serotonergic Receptors:*** **A)** Correlation maps of the Inability to force transition (KL divergence differences) and $5HT_{2a}$ map densities (Spearman $\rho$ = 0.227, p = 0.032). **B)** Correlation maps of the Inability to force transition (KL-divergence differences) and $5HT_{1a}$ map densities (Spearman $\rho$ = 0.284, p = 0.007). **C)** Other 5HT receptors with non-significant results: $5HT_{2b}$ (Spearman $\rho$ = 0.064, p = 0.055), $5HT_4$ (Spearman $\rho$ = 0.055, p = 0.607) and 5HTT (Spearman $\rho$ = -0.172, p = 0.106).

## 3.4 Discussion

In this Chapter, I described spatio-temporal dynamics in terms of the Probabilistic Metastable Substates space of depressive patients undergoing treatment with psilocybin. Moreover, I created two whole-brain models fitted to the PMS space of responders and non-responders before treatment and by exhaustive stimulation demonstrated how to force transition to the healthy state (as defined by the responders after treatment). The results showed a subset of regions that are less likely to allow transition to the healthy state. Furthermore, these regions correlated with the density maps of the $5HT_{2a}$ and $5HT_1a$ neuroreceptors known to be mediators of the psychedelic neuropharmacology.

A summary of complex spatio-temporal dynamics in terms of brain substates and their transitions has drawn a lot of attention in systems neuroscience due to its utility in pharmacological and electromagnetic interventions for the rebalancing of brain activity in disease. Brain substates have been characterised in different ways; by minimal energy (Gu et al., 2018), as attractor landscapes (Deco and Jirsa, 2012) and more heuristically through sliding-window analysis and unsupervised clustering (Hutchison et al., 2013; Allen et al., 2014). However, it has been challenging to extrapolate many approaches to the full extent of the richness across temporal and spatial hierarchies. Here, PMS build on a description of the data in terms of a probabilistic "cloud" in substate space and as such can be extended to different neuroimaging modalities with higher temporal resolution, such as EEG and MEG, or potentially to more fine-grained spatial resolutions (Deco et al., 2019; Kringelbach et al., 2020).

Cutting-edge non-invasive brain stimulation techniques such as Transcranial Magnetic Stimulation (TMS) and Direct Electrical Stimulation (DES), and new neu-

ropsychopharmacological drugs for treatment of psychiatric disorders have heralded an era of both external and endogenous brain perturbations. For example, TMS has been considered for treatment of many psychiatric disorders such as depression, schizophrenia and addiction (Ridding and Rothwell, 2007). Furthermore, the renaissance of psychedelic drugs for clinical applications has promised to revolutionise psychiatry when administering drugs for patients with treatment-resistant depression, OCD or anxiety disorders (Carhart-Harris and Goodwin, 2017). However, due to the brain's complexity across hierarchies of time and space, a mere empirical "trial and effect" approach might not bring advancements any further than the initial success in neurology and neuropsychology, where localised damage of a particular brain area informed diagnoses of cognitive and perceptual disorders (Turkheimer et al., 2021). For example how DES-induced signal propagates within the neuronal microcircuits remains unclear and often paradoxical. Recent studies point to the disruption of cortico-cortical signal propagation by inhibiting neocortex with afferent fibers that are electrically stimulated (Logothetis et al., 2010). Such indirect and often non-intuitive explanations motivate theoretical neuroscience studies and in-silico perturbation protocols where both interactions within neuronal populations in mesoscopic microcircuits and system-wide changes to localised external stimulation can be explored.

Beyond in-silico perturbations, the exhaustive stimulation protocol can also be used as a sensitivity analysis tool from the complex systems perspective. Traditionally, statistical differences in measures summarising spatio-temporal dynamics are obtained using signal detection theory. Such approaches can be enhanced by considering whole-brain models and their structural differences between conditions, for example as described by the $G$ parameter. Moreover, rather than describing and assessing expressions of spatio-temporal dynamics, an exhaustive protocol allows to shift the focus onto transitions to a target state and thus

draw differences between groups. Here, the example of the responder and non-responder groups and their transition to the healthy state serves to demonstrate the differential relevance of brain regions for healthy brain rebalancing.

Forcing transitions in large-scale brain networks has also been investigated through the prism of control network theory. In such scenarios, control strategies are deployed to navigate complex systems from a source (initial) state to a target (final) state (Srivastava et al., 2020). This approach has obtained a lot of attention due to its wide-ranging engineering applicability in technological, social and cyberphysical systems across various experimental scenarios (Gu et al., 2015; Lynn et al., 2020). However, the conceptual understanding of controlling neuronal signals from source to target states might be problematic as the Shannonian idea of information transmission might be ill-posed in the context of complex systems such as the brain (Tognoli and Kelso, 2013). On the contrary, the approach considered in this Chapter attempts to describe spatio-temporal dynamics in terms of Probabilistic Metastable Substates and through systematic perturbation to rebalance the spatio-temporal dynamics between two PMS spaces. Through this approach the brain is not "forced" to a specific configuration but rather rebalanced to its healthy working point, without specific instructions of what the relevant pathway might be.

To obtain a PMS approximation of the brain substate of interest, several methodological choices are made which inevitably introduce several caveats. Firstly, a regional parcellation has to be chosen, which might introduce artificial spatial boundaries especially when dealing with dynamics. Secondly, the choice of clustering algorithm defines the type of substates that can be obtained. Here, I use unsupervised k-means clustering which has been shown to adequately represent functionally meaningful brain substates (as described in previous Chapter 2), but other algorithms could be used as well (e.g. k-medoids). Lastly, the whole-brain

models constructed are based on group approximations of the underlying structural and functional information. For clinical relevance, further research will be needed to create individual-based whole-brain models that might allow for future in-silico assisted personalised psychiatry (Deco and Kringelbach, 2014).

## 3.5 Summary

Taken together, in this Chapter I have demonstrated how whole-brain models, validated to the spatio-temporal description of brain substates as described in Chapter 2, can aid in understanding intervention with psychedelics for treatment-resistant depression. Using a PMS space description of spatio-temporal dynamics, I created and validated two whole-brain models for responders and non-responders before treatment. Furthermore, through an exhaustive stimulation protocol, I demonstrated relevant brain regions that might hinder the successful recovery from depression of the non-responders in comparison to the responders to treatment (as defined by the QIDS score five weeks after treatment). Intriguingly, these regions correlate with the density maps of the $5HT_{2a}$ and $5HT_{1a}$ receptors and thus hint at the potential mechanisms preventing patients from successful recovery.

# 4 | DMT Psychedelic State Revealed by Connectome Harmonics Decomposition

> If the doors of perception were cleansed every thing would appear to man as it is, infinite. For man has closed himself up, till he sees all things thro' narrow chinks of his cavern
>
> — W. Blake, The Marriage of Heaven and Hell

> The perusal of a page from even the most beautiful written cookbook is no substitute for the eating of dinner
>
> — Aldous Huxley, Moksha

## 4.1 Introduction

One of the most potent mind-manifesting experiences is induced by the N,N - Dimethyltryptamine (DMT) - a naturally occurring serotonergic psychedelic (Nichols, 2016). Unlike psilocybin and LSD, its expression is marked by a short duration of the psychedelic experience. It is often associated with alterations in visual and somatic effects. At high doses, a complete dissociation from the external environment marks an immersion into worlds or dimensions described by being in "other" but not less "real" worlds to that of normal waking consciousness. Such experiences correlate with subjective reports such as "I experienced a different reality or dimension", "I saw geometric patterns" and "I felt unusual bodily sensations" (Timmermann et al., 2019). It is these qualities of one's conscious experience that motivate the renewed interest in DMT to inform on phenomena such as the near-death experience (NDE) and dreams (Timmermann et al., 2018).

Furthermore, like other psychedelics, DMT has the potential of clinical relevance in treating depressive symptoms (Davis et al., 2019). Studies with Ayahuasca, containing DMT itself as well as monoamine oxidase inhibitors (MAOIs), have shown promising results in patients with depression (Barker, 2018). However, it is still unclear whether the anti-depressive effects can be associated solely to DMT itself or as a complex interaction with the MAOIs. Therefore, future clinical studies with DMT are warranted to disentangle such interactions (Barker, 2018).

As discussed in the Introduction 1.3.1, psychedelics enhance the richness of spatio-temporal dynamics along both the temporal and spatial dimensions. This has been corroborated by repertoire broadening of functional states and increases in temporal complexity as well as shifting of the brain to a more integrated state with the subversion of substate specific segregative tendencies (Tagliazucchi et al., 2014; Atasoy et al., 2018). To this date, DMT has not been studied using fMRI neuroimaging and therefore this dataset presents a unique opportunity to explore the DMT-induced state and its place amongst other psychedelics (Timmermann et al., 2019). It is to be noted that Timmermann and colleagues analysed the EEG part of this dataset, demonstrating increases in temporal complexity and theta and delta power, as well as decreases in alpha and beta power, consistent with previous findings on other psychedelics (Timmermann et al., 2019). Taken all together, the current findings and subjective reports are in line with the entropic brain hypothesis where an increase in entropy of spontaneous brain activity results in an enhanced informational richness of brain states.

Here, I apply Connectome Harmonic Decomposition (CHD) as discussed in the Introduction 1.2, whereby spatio-temporal dynamics are described as a decomposition of fundamental building blocks of brain activity, derived from the Laplacian of the structural connectivity matrix (Atasoy et al., 2016). This allows to then define the changes in the contributions of individual harmonics to the DMT-induced

state. I hypothesised changes in CHD characteristics of other psychedelics with connectome harmonic repertoire broadening and enhancement of signatures of criticality (Atasoy et al., 2018). It is to be noted that I also used other previously published data on psychedelics, psilocybin and LSD, to analyse CHD across different psychedelic substances. Furthermore, given the experiential intensity of the DMT-induced state, I expected potentially stronger differences in spatio-temporal dynamics than induced by other psychedelics (Carhart-Harris et al., 2014; Carhart-Harris, 2018).

## 4.2 Methods

### 4.2.1 DMT dataset

The complete description of the participants, experimental design and acquisitions parameters can be found in (Timmermann et al., 2019). Here, I report a succinct summary of this information.

#### Participants

A group of 25 participants was recruited in a single-blind, placebo-controlled and counter-balanced design. Subjects were considered for the study unless they were younger than 18 year of age, lacked experience with a psychedelic, had a previous negative response to a psychedelic and/or currently suffered from or had a history of psychiatric or physical illness. Out of the 25 participants, 20 completed the whole study (7 female, mean age = 33.5 years, SD = 7.9). A further 3 subjects were excluded due to excessive motion during the 8 minutes DMT recording (more than 15% of volumes scrubbed with framewise displacement (FD) of 0.4 mm).

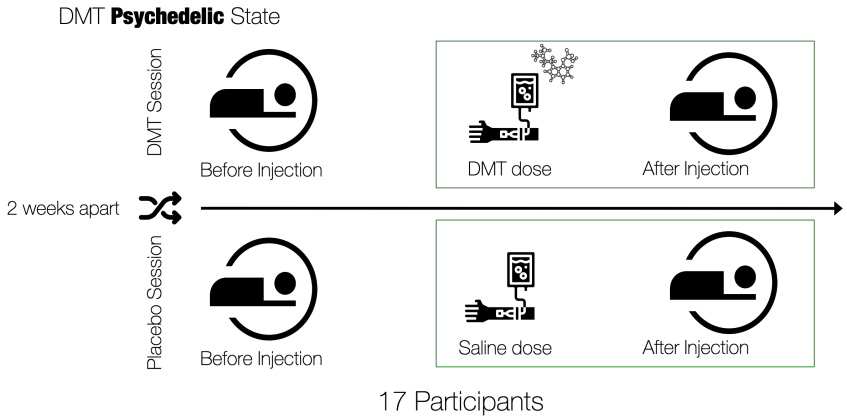



Figure 4.1: ***Experimental Design:*** Seventeen subjects were considered in the connectome harmonics analysis. From a single-blind, placebo-controlled and counter-balanced design, four scans for each subject were obtained (before/after the DMT-induced state and before/after the placebo condition).

### Experimental Paradigm

In total, all subjects were scanned on two days, two weeks apart, each consisting of two scanning sessions. The initial scan lasted 28 minutes with the 8th minute marking the intravenous administration of either DMT or placebo (saline) (50/50 DMT/placebo). Subjects were asked to lay in the scanner with their eyes closed (wearing an eye-mask). After the recording, assessment of subjective effects was carried out. The second session was identical to the first except for the assessment of subjective intensity scores at every minute of the recording. The experimental design also included simultaneous EEG recording during the sessions (see Figure 4.1).

### fMRI Acquisition Parameters

The experiment was performed on a 3T scanner (Siemens Magnetom Verio syngo MR 12) with compatibility for EEG recording. A T2$^*$-weighted echo planar sequence was used. In brief, the parameters were as follows: TR/TE = 2000ms/30ms,

acquisition time = 28.06 minutes, flip angle = $80^o$, voxel size = 3x3x3 $mm^3$ and 35 slices with 0 mm interslice distance. T1-weighted structural scans of the brain were also acquired.

#### FMRI Pre-processing

For fMRI pre-processing, a pipeline previously developed for an LSD experiment was used, which can be accessed in the supplementary information of (Carhart-Harris et al., 2016a). Briefly, the following steps were applied 1) despiking, 2) slice-timing correction, 3) motion correction, 4) brain extraction, 5) rigid body registration to structural scans, 6) non-linear registration to 2mm MNI brain, 7) motion-correction scrubbing, 8) spatial-smoothing (FWHM) of 6 mm, 9) band-pass filtering into the frequency range 0.01-0.08 Hz, 10) linear and quadratic de-trending, 11) regression of 9 nuisance regressors (3 translations, 3 rotations and 3 anatomical signals).

### 4.2.2 Psilocybin Dataset

A complete description of the psilocybin study protocol can be found in the original paper (Carhart-Harris et al., 2012). In brief, nine participants were considered for this analysis following rigorous exclusion criteria; no younger than 21 year of age, pregnancy, history of psychiatric disorders, cardiovascular disease, substance dependence, claustrophobia, blood or needle phobia or adverse response to hallucinogenics. Furthermore, participants were excluded if their mean framewise displacement (FD) exceeded 0.4 mm. Two eye-closed scans, separated by seven days, were performed for each participant. In a counterbalanced design each participant was given intravenously either psilocybin (2 mg dissolved in 10 ml saline, 60 s) or saline (10 ml saline, 60 s). The recording session lasted 12 minutes with the 6th minute marking the solution infusion. For the study last five minutes

(post the 60 s infusion) were analysed and a control pre-injection recording was matched accordingly to be 5 minutes as done in the original study (Carhart-Harris et al., 2012). I analysed segments of 100 timepoints pre- and post-psilocybin injection (TR = 3 seconds).

### 4.2.3 LSD Dataset

A complete description of the LSD study protocol can be found in the original paper (Carhart-Harris et al., 2016b). Briefly, twelve subjects were considered for this analysis with key exclusion criteria; no younger than 21 year of age, pregnancy, history of psychiatric disorders, cardiovascular disease, substance dependence, claustrophobia, blood or needle phobia or adverse response to hallucinogenics, previous experience with serotonergic psychedelics or use within 6 weeks of first scanning. Furthermore participants were excluded if their mean framewise displacement (FD) exceeded 0.4 mm. In a counter-balanced design each participant was given intravenously either LSD (75 $\mu$ g in 10 ml saline, 120 s) or saline (10 ml saline, 120 s). After 60 minutes acclimatisation in the scanner, there were three resting-state recording sessions; one with music interleaved in-between two standard resting-state sessions. Only results of the first resting-state recording session are considered here as done in the original study Carhart-Harris et al. (2016a). The scan lasted 7.23 minutes with a TR of 2 seconds, resulting in 217 timepoints pre- and post-LSD injection.

### 4.2.4 Structural Connectome Construction

For the construction of group connectome harmonics, an independent cohort of 10 participants (6 female, 22-35 years) was used from the Human Connectome Project, WU-Minn Consortium (Principal Investigators: David Van Essen and Kamil Ugurbil: 1U54MH091657). This project was made possible by funding

from the sixteen NIH Institutes and Centres supporting the NIH Blueprint for Neuroscience Research; and by the McDonell Centre for Systems Neuroscience at Washington University. Both structural and Diffusion Tractography Imaging (DTI) data was used for the construction of connectomes with pre-processing according to the minimal pre-processing guidelines of the HCP protocol (Glasser et al., 2013).

For the estimation of the connectome harmonics, I used the identical workflow as in (Atasoy et al., 2018). In general, this consisted of combining local, surface based, and long-range white-matter connectivity in a sparse vertex-based representation. In brief, cortical surface reconstruction from high-resolution T1-weighted MRI of individual participants was carried out with Freesurfer software. Then, each participant's cortical surface was registered to the 1000-subject group template yielding a common-space mesh of 10,242 vertices in each hemisphere. For the white-matter cortico-cortical and thalamo-cortical fibers, deterministic tractography was applied to the DTI data of individual subjects (resolution 1.25 mm) with Matlab implementation of Vista Lab, Stanford University. For the tractography itself, eight seeds were initialised in each vertex (total of 20,484) with the termination criteria being either fractional anisotropy (FA) below 0.3, minimum track length of 20 mm and a maximum angle of 30$^{o}$ between two adjacent tracking steps.

### 4.2.5 Derivation of Connectome Harmonics

Connectome Harmonics were computed from the structural connectome described as a graph, $\Re = (\nu, \varepsilon)$, of vertices $\nu = \{v_i | \in 1, ..., n\}$ and edges $\varepsilon = \{e_{ij} | \in \nu \times \nu\}$. The graph's edges represent 1) local connectivity, defined by 6 nearest neighbours of each vertex on the cortical surface, and 2) long-range connectivity as determined by tractography in terms of cortico-cortical and thalamo-cortical

fibres. The graph's edges were further binarised and symmetrised and represented in an unweighted and undirected adjacency matrix, $A$, as follows:

$$A(i,j) = \begin{cases} 1, & \text{if } (i,j) \in \varepsilon \\ 0, & \text{otherwise} \end{cases} \tag{4.1}$$

where $i$,$j$ are the indices of the adjacency matrix $A$ (20,424 $\times$ 20,424). In order to obtain a group adjacency matrix $\bar{A}$, the individual adjacency matrices of the 10 subjects were averaged. Furthermore, the discrete counterpart of the Laplace operator $\Delta$, applied to the structural connectivity (local and long-range) of the human brain $\bar{A}$, is estimated by computing the symmetric Laplacian $\Delta_{\bar{A}}$ in the following manner:

$$\Delta_{\bar{A}} = D^{-1/2}\, L\, D^{-1/2}, \text{ where } L = D - \bar{A} \tag{4.2}$$

where the $D$ is the diagonal degree matrix, $D = \sum_{i=1}^{n} \bar{A}(i,j)$. Lastly, the connectome harmonics,$\psi_k$, $k \in 1, ..., n$ were defined and computed as the eigenvectors of the following eigenvalue problem,

$$\Delta_{\bar{A}} \psi_{k(v_i)} = \lambda \psi_{k(v_i)}, \forall\, v_i \ \in \nu \tag{4.3}$$

where $\lambda, k \in 1, ..., n$ are the associated eigenvalues of $\Delta_{\bar{A}}$.

### 4.2.6 Connectome Harmonic Decomposition of Resting-state fMRI

The derived connectome harmonics can be used to represent resting-state fMRI in each of the DMT conditions. First, resting-state fMRI is projected from its MNI voxel-space to the Freesurfer surface vertex-space using the HCP command - *volume-to-surface-mapping*. The resulting timecourse can be represented as $\mathcal{F}(v,t)$ for every vertex $v \in \nu$. Once in the same space, the fMRI activity $\mathcal{F}(v,t)$ at every time step $t \in [1,...,T]$ can be described as a sum of weighted contributions $\alpha_k$ of individual connectome harmonics $k$. This fMRI decomposition can be described in the following format,

$$\mathcal{F}(t_i) = \sum_{k=1}^{n} \alpha_k(t_i)\psi_k = \alpha_1(t_i)\psi_1 + \alpha_2(t_i)\psi_2 + ... + \alpha_n(t_i)\psi_n \tag{4.4}$$

with $\alpha_k$ being the contribution of $k$ connectome harmonic $\psi_k$ to the fMRI activity $\mathcal{F}(t_i)$ at time $t_i$. Formally, the connectome harmonic contributions are described as $\alpha_k(t) = \langle \mathcal{F}(t), \psi_k \rangle$.

### 4.2.7 Measures

Further analysis describes several measures which summarise different aspects of the decomposed fMRI timecourses in terms of the contributions of the connectome harmonic spectrum.

#### Power and Energy

The connectome harmonic weight $\alpha_k$ at each time $t$ represents the strength of a given connectome harmonic $\psi_k$ of that particular fMRI pattern $\mathcal{F}(v,t)$ at the same time $t$ and its absolute value can be defined as power, $P(\psi_t, t) = |\alpha_k(t)|$. To

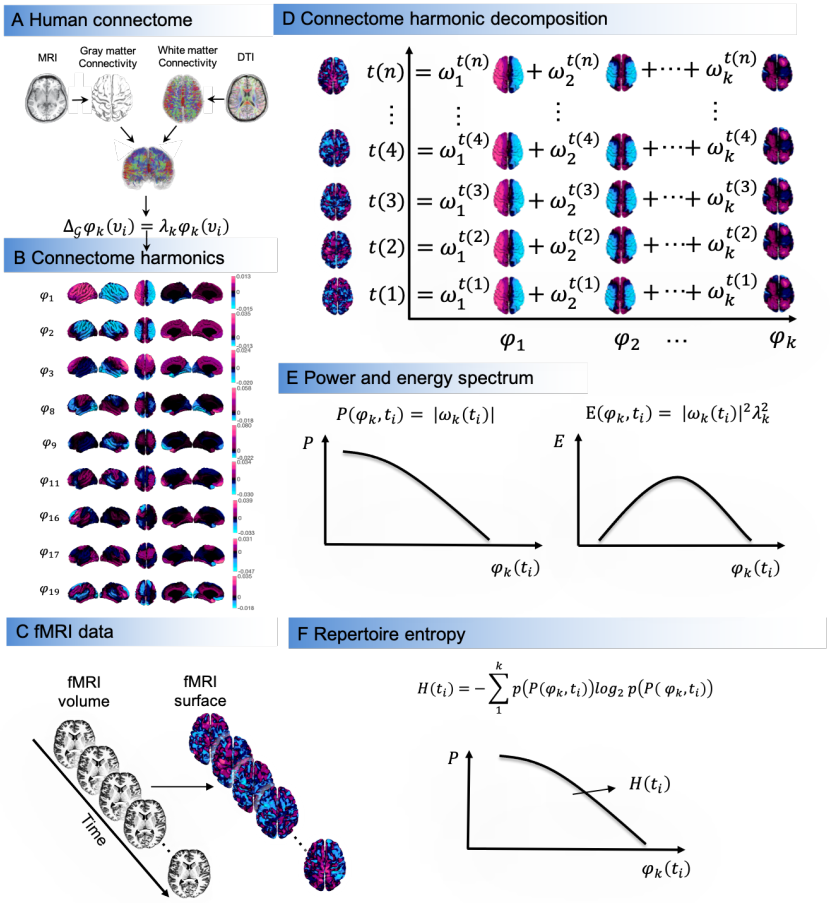



Figure 4.2: ***Study Overview:*** **A)** Human Connectome constructed from structural and diffusion MRI. **B)** Connectome Harmonics computed from the eigendecomposition of Laplacian operator applied to the human connectome. **C)** Functional MRI projected from MNI volumetric space to Freesurfer surface space. **D)** Connectome Harmonic Decomposition summarising fMRI timeseries as a linear summation of individual harmonics and their weights. **E)** Power and Energy spectrum. **F)** Repertoire entropy of CH.

further estimate the connectome harmonic contribution $\alpha_k$ in relation to its eigenvalue $\lambda_k$, a measure of energy, $E$, is defined as the square of connectome harmonic contribution and its intrinsic energy,($\lambda$), in the following way $E(\psi_k, t) = |\alpha_k(t)|^2\lambda_k^2$. Note that both Power and Energy are computed for every connectome $\psi_k$ at every timepoint $t$ across the fMRI timecourse $\mathcal{F}(v, t)$. Moreover, total power and energy at every timepoint $t$ can be defined as $P_{total}(t) = \sum_{k=1}^{N} |\alpha_k(t)|$ and $E_{total}(t) = \sum_{k=1}^{N} |\alpha_k(t)|^2\lambda_k^2$ respectively.

**Repertoire of Connectome Harmonics and Repertoire Entropy**

To estimate the repertoire of connectome harmonics, in other words, the probability of occurrence of recruited connectome harmonics, I computed the projection value $\alpha$ of each harmonic bin (200 bins) and normalised each harmonic bin's projection value $\alpha$ by the maximum $\alpha$ of the placebo (baseline) condition. Similarly, the repertoire entropy, $H$, was defined as the time-averaged histogram entropy of the binned (15 logarithmic bins) power distribution, $P$, at each condition i.e. $H(t_i) = -\sum_1^k p(P(\psi_k, t_i))log_2p(P(\psi_k, t_i))$. The bin choice for both measures was chosen historically as a common frame of reference for comparison with previous literature (Atasoy et al., 2018).

**Power Laws**

To evaluate the power-law relationship between several power signatures as a function of connectome harmonic wavenumber $k$, the time-averaged power, maximum power as well as fluctuations of power were plotted in a log-log plot against the connectome harmonic wavenumber $k$. Prior to the goodness-of-fit estimation, the curve was binned into 100 logarithmic bins. Then, the power-law critical exponent $\beta$ and goodness-of-fit $\epsilon$ were estimated for each of the three measures. The goodness-of-fit was computed as the root mean square error of the line fit in

log-log space.

## 4.3 Results

Connectome Harmonic Decomposition is a powerful analysis of the spatio-temporal dynamics in psychedelic-induced state such as DMT. Using connectome harmonics as the spatial basis of brain activity, it is possible to describe the temporal evolution of these harmonics in terms of their contribution. Here, I use CHD to describe the spatio-temporal changes of the DMT-induced state in terms of its connectome harmonic spectrum and repertoire, power-laws as a function of connectome harmonic wavenumber and repertoire entropy as its signatures of criticality.

### 4.3.1 The DMT-induced State Suppresses Low-level Harmonics and Increases High-level Harmonics

I first estimated the power and energy spectrum of each condition (DMT pre/post and PCB pre/post) across all timepoints and subjects. After time-averaging the power and energy timeseries, I then binned the connectome harmonic spectrum into 15 logarithmically spaced bins and obtained the harmonic profiles (see Subsection 4.2.7).

For the DMT-induced state, a range of low frequency harmonic bins ($k \in [1,...,10^2]$) were found significantly suppressed as opposed to the pre-DMT condition (p-value < 0.05, Bonferonni corrected Monte-Carlo Simulation). No significant differences were observed in the placebo condition. A mirror opposite change was observed in the high frequency harmonic bins whereby a range of $k \in [10^3,...,10^4]$ was found significantly increased (p-value < 0.05, Bonferonni corrected Monte-

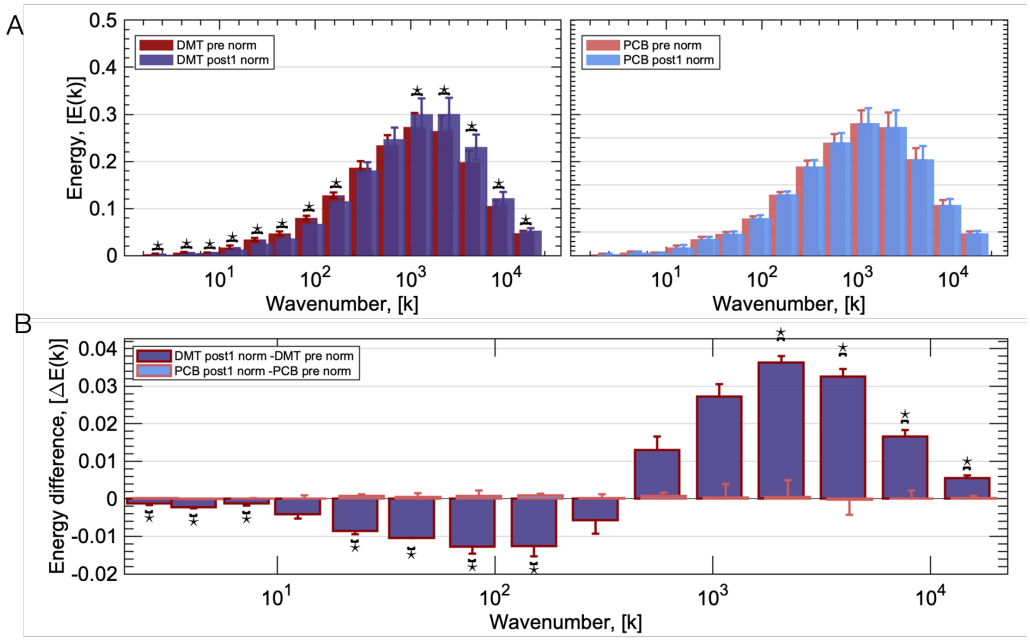



Figure 4.3: ***DMT-induced Energy Changes in the Connectome Harmonic Spectrum:*** **A)** A decrease of energy for low-frequency harmonics $k \in [1,...,10^2]$ (p-value < 0.01, Bonferonni corrected Monte-Carlo Simulation) and an increase of energy for high-frequency harmonics $k \in [10^3,...,10^4]$ (p-value < 0.01, Bonferonni corrected Monte-Carlo Simulation) were observed. No significant changes was observed in the placebo conditions. **B)** Furthermore, energy differences between the DMT and placebo conditions were observed with decreases in low-frequency harmonics $k \in [1,...,10^2]$ (p-value < 0.01, Bonferonni corrected Monte-Carlo Simulation) and increases in high-frequency harmonics $k \in [10^3,...,10^4]$ (p-value < 0.01, Bonferonni corrected Monte-Carlo Simulation). No significant differences were observed at the inflexion point $[10^2,...,10^3]$

Carlo Simulation). Again, no significant differences were observed for the placebo condition (Figure 4.3, A). This profile change across quantized harmonic bins can be further explored by looking at the energy differences across the DMT conditions of each subject while comparing it to the placebo condition difference. Remarkably, a similar suppression of the lower-harmonics $k \in [1,...,10^2]$ (p-value < 0.05, Bonferonni corrected Monte-Carlo Simulation) and increase of the higher harmonics $k \in [10^3,...,10^4]$ (p-value < 0.05, Bonferonni corrected paired t-test) are observed with non-significant results for bins at the inflexion point $[10^2,...,10^3]$ (Figure 4.3, B). To this date, this is the first psychedelic dataset where the connectome harmonic decomposition can be statistically tested with a placebo condition.

### 4.3.2 DMT-induced State Enhances Signatures of Criticality

As discussed in the Introduction (Section 1.1), the brain is thought to operate at a working point demonstrating near-critical dynamics. In such regimes, long-range spatial and temporal correlations are made possible (Tagliazucchi et al., 2012). Here, I explore several signatures of critical dynamics and argue that the DMT-induced state enhances the brain's criticality and corroborates the entropic brain hypothesis whereby the richness of spatio-temporal dynamics is expanded (Carhart-Harris et al., 2014; Carhart-Harris, 2018).

First, I look at how the repertoire of active harmonics changes in the DMT-induced state. As in Figure 1.5, I argue here that a spatial signature of enhanced near-criticality, as during the psychedelic-induced experience, will result in a broadening of the repertoire of active harmonics. Intuitively, this reflects the idea of the flattening of the dynamical landscape. To do so, I computed the normalised repertoire entropy for each condition (pre/post DMT and pre/post placebo). The results showed significant differences between the repertoire of connectome harmonics between pre/post DMT (two-sample ks-test, p-value < $10^{-5}$) but not for

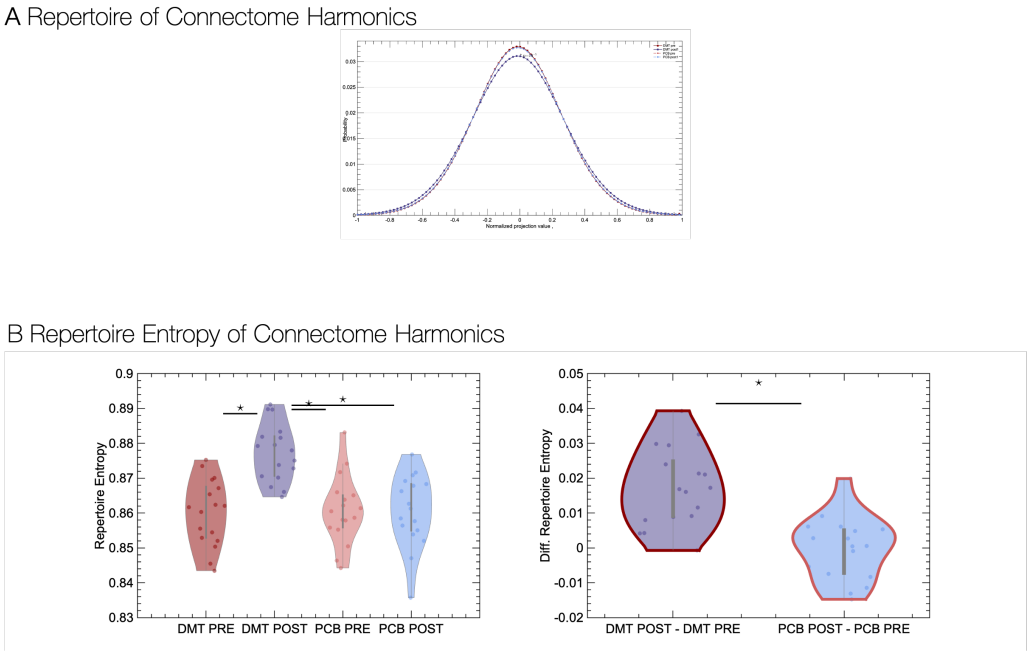



Figure 4.4: ***Repertoire of CH and Repertoire Entropy:*** **A)** Repertoire of connectome harmonics (pre/post DMT two-sample ks-test, p-value < $10^{-5}$). **B)** Repertoire Entropy (Pre/Post DMT: p-value < $10^{-4}$, Pre PCB/Post DMT: p-value < $10^{-4}$, Post PCB/Post DMT: p-value < $10^{-4}$, paired t-test). Repertoire Entropy Difference (Diff. in Pre-Post DMT and Pre-Post PCB: p-value < $10^{-5}$, paired t-test).

the placebo condition. Similarly, it is possible to look at the repertoire of harmonics from the perspective of histogram entropy. Repertoire entropy increased in the DMT-induced state compared to the other three conditions (Pre/Post DMT: p-value < $10^{-4}$, Pre PCB/Post DMT:-value < $10^{-4}$, Post PCB/Post DMT: p-value < $10^{-4}$, paired t-test). Furthermore, the result was strengthened by comparing the repertoire entropy difference between post/pre DMT and post/pre placebo where an increase was observed as well (Diff. in Pre-Post DMT and Pre-Post PCB: p-value < $10^{-5}$, paired t-test).

Another signature of criticality are the distinct power-law distributions. Power-laws describe scale-invariance across space and time and are abundant in natural

complex systems. In the brain, they have been demonstrated in fMRI recordings (Tagliazucchi et al., 2012; Kitzbichler et al., 2009), MEG (Muthukumaraswamy et al., 2013) as well as in cortical slices (Beggs and Plenz, 2003) (see Section 1.1.1). Hence, it is pertinent to look at the changes in brain dynamics induced by DMT as described through power-laws. Here, I looked at the mean, maximum and fluctuations of power across the range of connectome harmonics (see Section 4.2.7). Importantly, all three observables across the wavenumber range followed power-law distributions (Figure 4.5). To assess the goodness-of-fit of experimental distributions to the power-law fit, I computed the root-mean squared error, $\epsilon$. The root-mean squared error decreased for mean power (p-value < $10^{-1}$, paired t-test), maximum power (p-value < $10^{-3}$, paired t-test) and power fluctuations (p-value < $10^{-3}$, paired t-test). Importantly, no change was significant in the placebo condition. The goodness-of-fit, $\epsilon$, signifies a closer alignment with the power-law distribution under the DMT-induced state. Furthermore, the power-law exponent, $\beta$, was found to decrease significantly for all three measures; mean power (p-value < $10^{6}$, paired t-test), maximum power (p-value < $10^{5}$, paired t-test) and power fluctuations (p-value < $10^{-5}$, paired t-test) with no significance for the placebo condition except for power fluctuations (p-value < $10^{-1}$, paired t-test). The $\beta$ exponent signifies the slope of the power-law in the log-log scale, indicating increased power and fluctuations of higher frequency harmonics, and in reverse, decreased power and fluctuations of lower frequency harmonics.

Taken all together, the shift towards higher frequency harmonics in terms of their power and fluctuations as described by the decreased $\beta$ exponent corroborates previous findings of the energy spectrum where enhancement of high frequency harmonics was observed. Furthermore, as described by the power-law goodness-of-fit $\epsilon$ of the power and fluctuations of the harmonic spectrum, the brain was suggested to tune more towards criticality in the DMT-induced state, and this

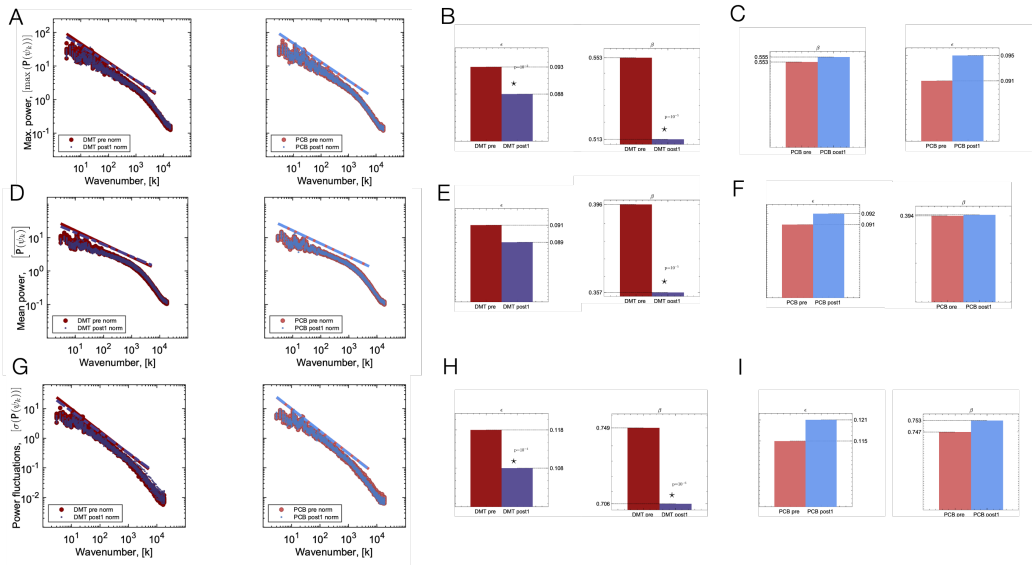



Figure 4.5: ***Power-laws of Connectome Harmonics in the DMT-induced State:*** **A)** Power-law distribution of maximum power across the connectome harmonic spectrum with significant decreases **B)** in both goodness-of-fit $\epsilon$ (p-value < $10^{-3}$, paired t-test) and slope $\beta$ (p-value < $10^{-5}$, paired t-test), and **C)** no significant difference in the placebo condition . **D)** Power-law distribution of mean power across the connectome harmonic spectrum with significant decreases **E)** in slope $\beta$ (p-value < $10^{6}$, paired t-test) and in goodness-of-fit $\epsilon$ (p-value < $10^{-1}$, paired t-test), and **F)** no significant difference in the placebo condition. **G)** Power-law distribution of power fluctuations across the connectome harmonic spectrum with significant decreases both **H)** in goodness-of-fit $\epsilon$ (p-value < $10^{-3}$, paired t-test) and slope $\beta$ (p-value < $10^{-5}$, paired t-test), and **I)** no significant differences in the placebo condition except for power fluctuations (p-value < $10^{-1}$, paired t-test).

was indeed reinforced by the increase in repertoire entropy and broadening of the repertoire spectrum.

### 4.3.3 DMT-induced Changes in CHD Compare to LSD and Psilocybin

DMT is a classical serotonin-mediated psychedelic alongside substances such as psilocybin and LSD. As argued in the Introduction, psychedelic-induced states

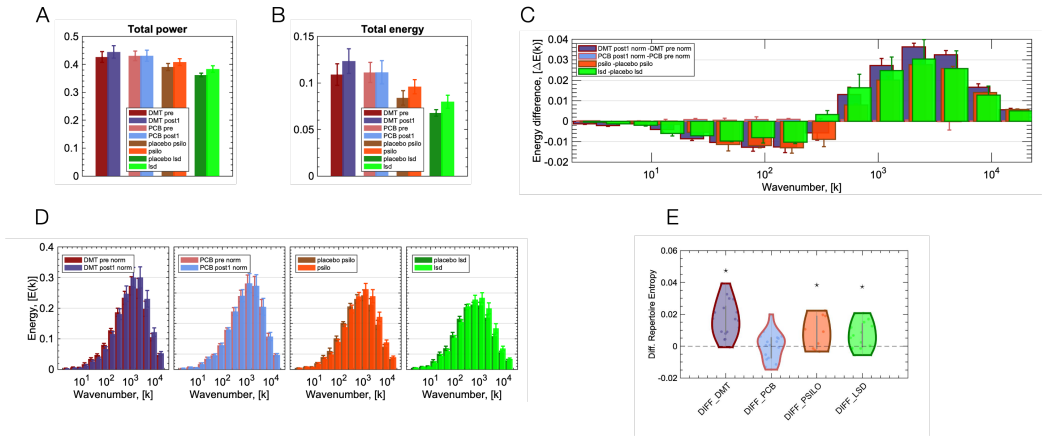



Figure 4.6: ***Connectome Harmonic Decomposition across Psychedelic-induced States:*** **A), B)** Total power and energy of DMT, psilocybin and LSD-induced states, and a control placebo condition. **C)** Energy Difference Connectome Harmonic Spectrum of DMT, psilocybin and LSD-induced states, and a control placebo condition. **D)** Energy Connectome Harmonic Spectrum of DMT, psilocybin and LSD-induced states, and a control placebo condition. **E)** Repertoire entropy difference of DMT, psilocybin and LSD-induced states, and a control placebo condition (DMT to $PCB_{DMT}$: p-value < 0.05, paired t-test, psilocybin to $PCB_{DMT}$: p-value < 0.05, t-test, LSD to $PCB_{DMT}$: p-value < 0.05, t-test).

manifest enhanced spatio-temporal brain dynamics. In the previous Results Section, I demonstrated such tendencies in the DMT-induced state from the Connectome Harmonic Decomposition perspective. Here, I generalise these findings across other psychedelics, namely psilocybin and LSD, in terms of previously reported results on power and energy of connectome harmonics and newly in terms of repertoire entropy (Atasoy et al., 2018). To be noted, there is a current pre-print with collaborators where repertoire entropy of the LSD-induced state is considered as one end of a spectrum of states of consciousness (Luppi et al., 2020).

For all three psychedelics, DMT, psilocybin and LSD, a consistent decrease of total power and energy was observed (Figure 4.6, **A, B**). Similarly, the energy and energy difference profiles of connectome harmonics were shown to follow the same suppression of low-frequency harmonics and enhancement of high-frequency

harmonics for all three psychedelics (Figure 4.6, **C** and **D**). The DMT-induced state exhibited a slightly greater increase in high-frequency harmonics compared to psilocybin and LSD. This was perhaps linked to the intensity of the psychedelic experience under DMT. However, this was not supported by statistical tests. Lastly, the repertoire entropy difference increased in all psychedelics, with greatest increases observed in the DMT-induced state compare to the placebo condition (DMT to $PCB_{DMT}$: p-value $< 0.05$, paired t-test, psilocybin to $PCB_{DMT}$: p-value $< 0.05$, t-test, LSD to $PCB_{DMT}$: p-value $< 0.05$, t-test) (Figure 4.6, **E**).

## 4.4 Discussion

In this Chapter, I described the psychedelic-induced state, as defined by DMT, in terms of Connectome Harmonic Decomposition. From this perspective, the spatio-temporal dynamics have been modelled in terms of the temporal contribution of a set of spatial frequencies realised on the structural connectivity of the brain - the connectome. The results demonstrate full harmonic spectrum changes under the influence of DMT, with a suppression of low-frequency harmonics and an increase of high frequency harmonics. Furthermore, signatures of criticality have been observed with a broadening of the harmonic repertoire, increase in repertoire entropy and tuning towards power-law distributions for observables such as maximum and mean power, and power-fluctuations. Taken all together, these results have been shown to generalise across other psychedelic-induced states such as psilocybin and LSD.

As discussed in the Introduction 1.1 and throughout this Chapter, near-critical behaviour has been hypothesised to give rise to complex spatio-temporal dynamics in the brain. In this regime, tendencies of stability (order) are balanced with flexibility (disorder) to exhibit novel patterns of activity. Often, these properties are

manifested in terms of scale invariance across space and time (Expert et al., 2011), long-range spatial and temporal correlations (Tagliazucchi et al., 2014) as well as sensitivity and fast dissipation through the system to incoming signal (Deco et al., 2017b). In the psychedelic-induced state, such dynamics have been hypothesised to tune the brain closer to criticality, resulting in repertoire broadening of brain substates (Tagliazucchi et al., 2014), an increase in global integration (Tagliazucchi et al., 2016c) and closer correspondence to power-law distributions (Atasoy et al., 2018). Here, for the first time, fMRI recordings of participants under the influence of the psychedelic N,N-Dimethyltryptamine (DMT) were analysed, revealing dynamic changes including repertoire broadening of connectome harmonics and increased fits to the power-law distributions for maximum and mean power, and power fluctuations, thus corroborating previous findings.

The entropic brain hypothesis has been proposed to index the richness of the spatio-temporal dynamics along the entropy continuum. Furthermore, the psychedelic-induced state is considered to increase the level of entropy within the brain (Carhart-Harris et al., 2014; Carhart-Harris, 2018). Cognitively, the psychedelic experience has been hypothesised to undermine the integrity of large-scale networks which constrain the susceptibility of any incoming signal. It is a state of inducing novelty in thinking, as bottom-up signals are put on the same footing with high-level priors; in other words, the functional hierarchy is lost, resulting in the anarchic brain (Carhart-Harris and Friston, 2019). Here, I have shown for the first time the effect of DMT on repertoire entropy as defined by the connectome harmonic power spectrum. This is supported by an increase in the high-frequency energy spectrum of localised but decoupled harmonic contributions and at the same time a suppression of the low frequency energy spectrum representative of global and coupled harmonic contributions.

How structure shapes function has been at the forefront of contemporary neuro-

science (Hagmann et al., 2008; Honey et al., 2009) with many approaches considered (Griffa et al., 2017; Gilson et al., 2018; Avena-Koenigsberger et al., 2018). Recent advances have considered diffusion process to describe the unfolding brain activity on the structural connectome, of which connectome harmonics are the representative example (Atasoy et al., 2016), but also considered elsewhere (Tewarie et al., 2019; Huang et al., 2018). In graph signal theory, it is well known that the low eigenvalues associated eigenvectors of the Laplacian approximate the global structural topology of the underlying graph, while higher eigenvalues capturing localised representations are more decoupled from global structure. Thus the harmonic spectrum can be considered in terms of the level of decoupling from structure. Indeed, the level of structural decoupling has been shown to correlate with the gradient of low- to high-level cognitive functions (Preti and Van De Ville, 2017). In general terms, the correlation strength of structure-function relationships has been indicative of the level of consciousness - a stronger relationship has signified a loss of consciousnesses, for example in anesthesia (Barttfeld et al., 2015). This is relevant as the corresponding opposite effect is observed here, with a suppression of lower frequency harmonics and an increase of high frequency harmonics suggesting an opposite trend towards a more structurally decoupled brain state.

This leads to the following question - Could the harmonic spectrum be used as a signature of the different brain states of consciousness? This is motivated by results presented in the aforementioned paragraph as well as the fact that connectome harmonics are hypothesised to arise from the same structural connectivity template, independent of the associated brain state. This has been explored in a recent study where high generalisibility of the connectome harmonic decomposition spectrum was shown across minimal conscious, anesthetic, and ketamine and LSD-induced psychedelic states (Luppi et al., 2020).

To represent fMRI activity in different brain states, it is possible to use different bases on which the activity is projected. In this sense, connectome harmonics are considered as an extension of spherical harmonics - similarly derived as the eigenfunctions of the Laplace operator applied to the sphere (Jirsa et al., 2002; Robinson et al., 2016). Hence, when considering only local grey-matter connectivity, connectome harmonics equal to spherical harmonics represented on the cortical surface. However, I argue here that long-range connectivity is a necessary feature for an accurate representation of brain states (Naze et al., 2021). Therefore, connectome harmonics are extending spherical harmonics approaches by embedding both local grey matter and long-range white matter connectivity of the human brain. Moreover, when the associated spatial information of connectome harmonics is shuffled or the underlying graph is randomised with a degree-preserving algorithm, the ability to distinguish brain states is lost (Luppi et al., 2020). One limitation of the current approach lies in the binarization of the connectivity matrix whereby connectivity between distant regions is weighted the same way as connectivity between proximal regions. This might for example explain the two different slopes of the power spectrum in Figure 4.5. At the lower spatial frequencies the representation might be describing global anisotropy while at the higher spatial frequencies local isotropy.

To represent fMRI activity in different brain states, it is possible to use different bases on which the activity is projected, including for example the spherical harmonics basis (Robinson et al., 2016). However, I argue here that structural information, surface cortical folding, local cortical and long-range connectivity, are all necessary to accurately represent appropriate features of the emergent dynamics (Naze et al., 2021). Moreover, when the associated spatial information is shuffled or the underlying graph is randomised with a degree-preserving algorithm, the ability to distinguish brain states is lost (Luppi et al., 2020).

Experimentally, the DMT dataset is a single-blind and counter-control placebo design and, unlike previous experiments with psilocybin (Carhart-Harris et al., 2012) and LSD (Carhart-Harris et al., 2016b), contains a control group that is important to differentiate the changes in the connectome harmonic decomposition under the influence of DMT from its baseline. Moving forward, future work might further differentiate the level of vigilance that comes with the psychedelic experience by considering additional control groups under the influence of stimulants such as Modafinil and caffeine.

In general, caution must be exercised when analysing and interpreting power-law distributions. Fitting of the data is often performed with least-square linear regression on the log-log scale (as done in this Chapter). This approach is problematic, creating issues about the assumptions of the standard error on the slope, $R^2$ validation and probability assumptions of the regression lines (Clauset et al., 2009; Deluca and Corral, 2013). Future work should focus on the analysis of power-law distributions with maximum-likelihood estimations (MLE) as for example implemented in the Python package *powerlaw* (Alstott et al., 2014). Importantly, I have considered other signatures of criticality such as the broadening of the spatial repertoire or increases in repertoire entropy, alongside power-law distributions.

## 4.5 Summary

To summarise this Chapter, I have analysed the DMT-induced state, through the lens of Connectome Harmonic Decomposition. Importantly, this description allows to represent the spatio-temporal dynamics and its associated psychedelic-induced state as a contribution of fundamental building blocks of brain activity varying in time. The results show that a suppression of low-frequency harmonics and an increase of high frequency harmonics is observed in the DMT-induced

state. Furthermore, a broadening of the harmonic repertoire, increase in repertoire entropy and proximity of power-law distributions for observables such as maximum and mean power as well as power-fluctuations, have been indicative of the brain becoming more critical under the influence of DMT. Lastly, these results are consistent across other psychedelic-induced states such as psilocybin and LSD.

# 5 | HArmonic DEcomposition of Spacetime (HADES)

> The later Greeks read 'Cronus' as *Chronos*, 'Father Time' with his relentless sickle. (6.2)
>
> Rhea's name is probably a variant of *Era*, 'Earth'; her chief bird was the dove, her chief beast the mountain-lion. (7.8)
>
> Cronus married his sister Rhea, to whom the oak is sacred. But it was prophesied by Mother Earth, and by his dying father Uranus, that one of his own sons would dethrone him. Every year, therefore, he swallowed the children whom Rhea bore him: first Hestia, then Demeter and Hera, then Hades, then Poseidon. (7.a)
>
> — Robert Graves, The Greek Myths

## 5.1 Introduction

As argued throughout my Thesis, the brain's complex dynamics can be perceived along spatial and temporal dimensions. Traditionally, neuroscience has focused on delineating and studying localised cortical regions in order to map brain function in a temporarily static fashion (Felleman and Van Essen, 1991). However, recent developments in neuroscience have started to indicate more spatially continuous representations of functional topography (Margulies et al., 2016; Glomb et al., 2019), and at the same time to stress the importance of temporally varying brain dynamics (Preti et al., 2016). Despite such progress, it remains unknown

what underlying mechanisms drive, on one hand, the gradient-like organisation of cortical topography, and on the other, the waning and waxing of the brain's temporal activity. Here, I propose Harmonic Decomposition of Spacetime as a new model of hierarchical processing across both spatial and temporal dimensions.

Historically, Brodmann's interactive atlas of cellular morphology and organisation has given rise to the view of functional specialisation of individual brain areas. Spatially, this suggests a sharp delineation between cortical areas in terms of their anatomy and function. However, supported by evolutionary and developmental neuroscience (Cahalane et al., 2014; Charvet et al., 2015), cortical gradients have challenged this view by suggesting gradually varying boundaries between and within brain regions, both in terms of function and anatomy (Margulies et al., 2016; Burt et al., 2018; Glomb et al., 2019). Functionally, gradient-like organisation proposes an intrinsic coordinate system of human brain organisation continuously varying from unimodal to transmodal cortical areas (Margulies et al., 2016; Huntenburg et al., 2018). Similarly, topographical maps of retinotopy, somatotopy and tonotopy have shown smooth variation of anatomy and function within brain areas (Sereno et al., 2001; Perrone-Capano et al., 2017; Kaufman, 1951; Haak et al., 2018). Furthermore along the temporal dimension, as argued in Chapter 1, studies of FCD in fMRI have revealed the importance of characterising the temporal features of brain activity as opposed to the static picture as described by known resting-state networks (Fox et al., 2005; Preti et al., 2016).

The motivation for HADES methods is two-fold, conceptual and methodological. To find an appropriate representation of brain activity in space and time has been a prominent topic of contemporary neuroscience. On one hand the, the picture has to account for increasing spatial scale from neuronal circuits to large-scale brain networks, and on the other, for its temporal evolution. Here, HADES builds on previous work of Functional Harmonics whereby patterns of correlated neural

activity emerge from dense functional connectivity of the human brain (Glomb et al., 2019). Furthermore, these patterns explain the temporal evolution of brain activity (as described here by fMRI data). Methodologically, studies of FCD in fMRI have revealed the importance of investigating the temporal features of brain activity over the grand-average picture as described by sFC (Preti et al., 2016). Furthermore, dFC has been proposed to further constrain whole-brain models in order to arrive at a more precise description of experimentally derived spatio-temporal dynamics. However, current techniques suffer from several limitations such as ill-defined temporal evolution, modelling feasibility or spatial interpretation (Cabral et al., 2017b; Atasoy et al., 2016). HADES attempts to improve on the earlier limitations demonstrating spatial interpretability, modelling feasibility and analysis flexibility.

Building on previous methods across space and time as considered in the earlier Chapters, I derive Functional Harmonics (FH) from communication structure of the brain and decompose brain's functional activity as a temporal evolution of the contribution of individual FHs. Firstly, I assess the relevance of FHs, and then for the first time, I use fMRI data from the DMT-induced state to describe HADES's multifaceted applications. Empirically, based on REBUS and the anarchic brain model discussed in Chapter 1, as well as findings of enhanced signatures of criticality described in Chapter 4, I hypothesised an undermined hierarchy of cortical functional organisation with enhanced integrative properties across cortex (Carhart-Harris, 2018; Atasoy et al., 2017b).

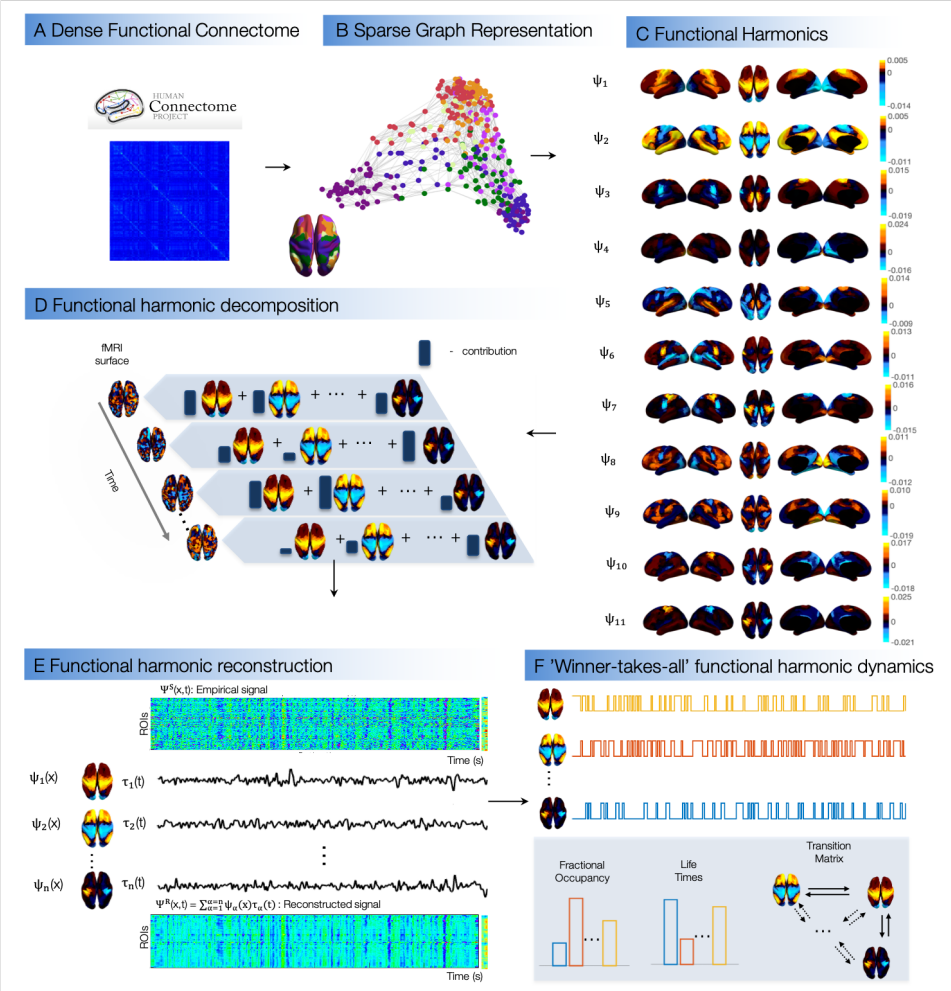



Figure 5.1: ***Overview of HADES:*** **A)** Dense Functional Connectome constructed from the HCP S1200 release of 812 subjects. **B)** A graph representation is constructed as a sparse, symmetric and binary adjacency matrix of the dense functional connectome. **C)** First, Functional Harmonics $(\Psi_k(x))$ are obtained from the Laplacian decomposition of the sparse adjacency matrix. **D)** Functional harmonic decomposition is computed by projecting individual harmonics on the fMRI time-series (surface representation) and calculating their contributions. **E)** Empirical signal reconstructed with only the first 12 Functional Harmonics. **F)** Functional Harmonic Dynamics in terms of a 'Winner-takes-all' approach.

## 5.2 Methods

### 5.2.1 Data

The dataset used for the analysis was made publicly available by the Human Connectome Project, WU-Minn Consortium (Principal Investigators: David Van Essen and Kamil Ugurbil: 1U54MH091657). This project was made possible by funding from the sixteen NIH Institutes and Centres supporting the NIH Blueprint for Neuroscience Research; and by the McDonell Centre for Systems Neuroscience at Washington University.

### 5.2.2 Dense Functional Connectome

To define the appropriate functional basis, I used the dense functional connectome as part of the HCP 1200 Subject Release. The data is freely downloadable (with a connectomeDB account) at https://db.humanconnectome.org/data/projects/HCP_1200 under the zip-file called 812 Subjects, recon r227, Dense Connectome. Details about the dense functional connectome pipeline can be found on the same website under the following pdf 'HCP1200-DenseConnectome +PTN+Appendix-July2017.pdf'. In brief, out of the 1200 HCP subjects, 1003 have undergone four rsfMRI runs (total of 4800 timepoints). An improved reconstruction software ('recon2') was used on a further subset of 812 participants, whom I use in this part of my analysis. Timeseries were minimally processed, had artefacts removed with ICA+FIX and were inter-subject registered. Further group-PCA was performed on the temporally demeaned and variance normalised timeseries. The outputs of the group-PCA are used to create the dense connectome. This can be thought of as a low-noise regularised equivalent of concatenating individual subject's gray-ordinate timeseries and calculating

the correlation between all the individual grey-ordinate timeseries, in order to create dense functional connectome (Figure 5.1, A).

### 5.2.3 Resting-state fMRI Timeseries and DMT

I used the same DMT dataset as described in Chapter 4 Section 4.2 for the application of HADES. Similarly, as in Chapter 4 Section 4.2, the timeseries were projected from MNI voxel-space to the HCP surface vertex-space using the HCP command *-volume-to-surface-mapping*.

### 5.2.4 Functional Harmonics

As described previously in (Glomb et al., 2019), Functional Harmonics describe the eigenfunctions of the Laplacian applied to the graph representation of the human brain's communication structure. The graph representation of the human brain's communication structure, $\Re = (\nu, \varepsilon)$, is represented by nodes, $\nu = \{x_i| \in 1, ..., n\}$, and edges, $\varepsilon = \{e_{i,j}| \in \nu \times \nu\}$, derived from the dense functional connectome. In other words, from the nodes as parcels of the vertex-based dense connectome n = 59, 412 and edges as connections between the vertices. The graph is constructed as a sparse, symmetric and binary adjacency matrix where each node is connected to its 300 k-nearest neighbours according to the correlation values from the original dense functional connectome (Figure 5.1, B and C) as follows,

$$A(i,j) = \begin{cases} 1, & \text{if } (i,j) \in \varepsilon \\ 0, & \text{otherwise} \end{cases} \tag{5.1}$$

where $i, j$ are the indices of the adjacency matrix $A(59412 \times 59412)$. Then, the discrete counterpart of the Laplace operator $\Delta$ is applied to the adjacency matrix $A$ in the following manner,

$$\Delta_A = D^{-1/2}\, L\, D^{-1/2}, \text{ with } L = D - A \tag{5.2}$$

where $D$ is the diagonal degree matrix, $D = \sum_{i=1}^{n} A(i,j)$. Lastly, Functional Harmonics, $\Psi_k(x_i)$, $k \in 1, ..., n$ were defined and computed as eigenvectors of the following eigenvalue problem,

$$\Delta_A \Psi_k(x_i) = \lambda \Psi_k(x_i)\,,\ \forall x_i\ \in \nu \tag{5.3}$$

where $\lambda_k,\ \ k \in 1, ..., n$ are the associated eigenvalues of $\Delta_A$.

### 5.2.5 Functional Harmonic Decomposition

To describe how Functional Harmonics evolve in time, I weighted their contribution, $\tau$, for each participant at every timepoint, $t$, of the recording $\mathcal{F}^S(x,t)$, and thus retrieved timecourses of individual harmonic contributions (Figure 5.1, D) in the following format,

$$\mathcal{F}^S(x,t_i) = \sum_{k=1}^{n} \tau_k(t_i)\Psi_k(x) = \tau_1(t_i)\Psi_1(x) + \tau_2(t_i)\Psi_2(x) + ... + \tau_n(t_i)\Psi_n(x) \tag{5.4}$$

where $\tau_k$ is the contribution of $k^{th}$ Functional Harmonic $\Psi_k(x)$ to the fMRI recording $\mathcal{F}^S(x,t_i)$ at time $t_i$. Formally, the Functional Harmonic contributions are described as $\tau_k(t) = \langle \mathcal{F}^S(x,t), \Psi_k \rangle$. The reconstructed signal can be further defined as follows

$$\mathcal{F}^R(x,t_i) = \sum_{k=1}^{n} \Psi_k(x)\tau_k(t_i) \tag{5.5}$$

where $\mathcal{F}^R(x,t_i)$ is the reconstructed signal obtained from spatial components (Functional Harmonics), $\Psi_k(x)$, and temporal components (contributions of Func-

tional Harmonics), $\tau_k(t_i)$, at every timepoint $t_i$ (Figure 5.1 E).

### 5.2.6 Parcellation and Reference Functional Networks

Functional Harmonics in vertex dimensions (n = 59, 412) were reduced to the Schaefer multiscale atlas of varying numbers of brain regions. Schaefer400 was applied in the main text to compare FH with the known canonical networks (7 and 17 Yeo resting-state networks (Yeo et al., 2011)) but other scales were also considered (Schaefer100, 200, 300, 500 and 1000). The parcellated data was obtained by averaging vertices belonging to a given brain region as defined by the Schaefer parcellation. Unlike standard volumetric fMRI to atlas registration, the parcellated data were obtained in the surface space of 59, 412 vertices. I used the following Schaefer HCP surface templates `www.github.com/ThomasYeoLab`.

### 5.2.7 Power

Similar to Chapter 4 Section 4.2, a Functional Harmonic contribution $\tau_k(t)$ at each timepoint $t$ represents the strength of a given Functional Harmonic $\Psi_k(x)$ at that particular fMRI timepoint, $\mathcal{F}^R(x, t_i)$. Its absolute value can be defined as the power as follows: $P(\Psi(x), t) = |\tau_k(t)|$. Here, I further define the absolute and normalised power as the time-averaged overall power of each harmonic, and as the time-averaged power normalised by the sum of all the Functional Harmonic powers of each participant and condition, respectively. In other words, absolute power describes the overall state of each Functional Harmonic for every participant and condition, and relative power depicts how power becomes redistributed for a given Functional Harmonic relative to the rest.

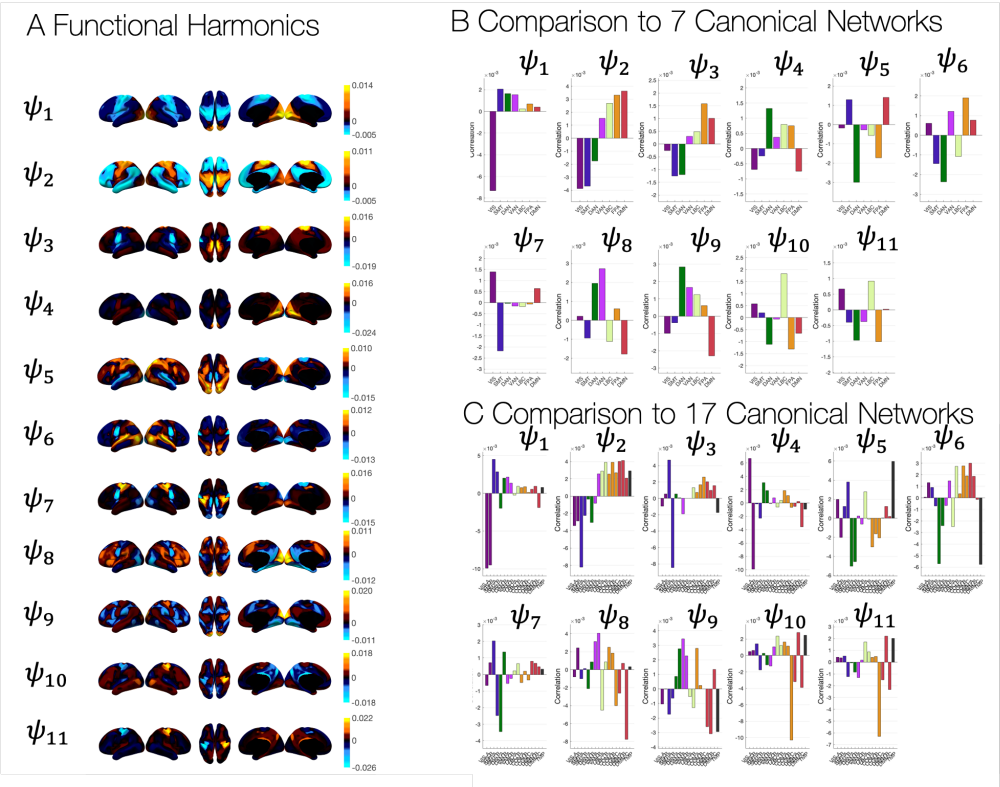



Figure 5.2: ***Functional Harmonics:*** **A)** The first 11 Functional Harmonics as obtained from the Laplacian eigendecomposition of the dense functional connectome. **B)** Comparison with 7 canonical resting-state networks. **C)** Comparison with 17 canonical resting-state networks (Yeo et al., 2011). Different Functional Harmonics indicate separation into various weighted combinations of resting state networks.

### 5.2.8 Dynamic Measures

To summarise dynamics of Functional Harmonics, I chose to describe each timepoint by its dominant Functional Harmonics, i.e. a Functional Harmonic with the largest contribution at a given timepoint. As such, I was able to depict the individual timeseries as a sequence of dominant Functional Harmonic contributions. I further defined Fractional Occupancy and Life Times as the probability of a given Functional Harmonic being active during the duration of the recording, and the averaged consecutive period a given Functional Harmonic was on respectively (see Section 2.2).

## 5.3 Results

By leveraging benefits from previously considered methods, HArmonic DEcomposition of Spacetime (HADES) describes the spatio-temporal dynamics in terms of spatial bases (defined from the brain's communication structure) and the spatial bases functional contributions to the fMRI recording evolving in time. Here, I apply HADES to show its viability in researching rich and complex brain dynamics in different brain states, and illustrate this in the context of the DMT-induced state.

### 5.3.1 Functional Relevance

Firstly, I compute and verify the overlap of Functional Harmonics with the canonical networks - specifically the 7 and 17 resting-state networks as described in the following study (Yeo et al., 2011). Previously, Glomb et al. have demonstrated the neurophysiological relevance of Functional Harmonics (Glomb et al., 2019). In the Supplementary Information (Section A.8), I display Functional Harmonics

as computed both by HADES and by (Glomb et al., 2019) for visual inspection. Apart from the Functional Harmonic $\psi_{10}$, the patterns are consistent across the two datasets. As the calculation steps were kept identical, a possible discrepancy might have arisen from the dense functional connectome itself where an improved reconstruction software was used for the HADES dataset (in HADES: S1200 release of HCP subjects, in (Glomb et al., 2019) S900 release of HCP subjects).

Strikingly, the first two Functional Harmonics $\psi_{1,2}$ reflect the principal gradients of human cortex delineating unimodal and transmodal networks of the brain (Margulies et al., 2016) both in the 7 and 17 RSN implementation (Yeo et al., 2011). In the 17 RSN implementation, FHs $\psi_{3,4}$ demonstrate separation of SMN and VIS. Moreover, FH $\psi_5$ places in opposite polarities the SMN and DMN (mainly its temporal parietal part) networks on one side, and DAN and FPN on the other. FH $\psi_6$ separates SMN and the temporal parietal part of the DMN from the rest of the DMN and FPN. FH $\psi_7$ further differentiates the VIS and SM. FH $\psi_8$ splits attention networks (mainly VAN) and DMN. FH$\psi_9$ demonstrates gradient-like separation between DMN and other higher-order cognitive networks (DAN, VAN, LN and FPN). FHs $\psi_{10,11}$ represent strongly part of the FPN (and LN in the 7 RSNs representation).

### 5.3.2 Signal Reconstruction

By projecting Functional Harmonics onto the timeseries, it is possible to obtain the contribution of each FH evolving in time (Figure 5.1, D). Henceforth, the underlying spatio-temporal activity is described in terms of its spatial (FH) and temporal (signal of FH contributions) dimensions and can be reconstructed back by linear summation (Figure 5.3,A and Equation 5.3). For a template (DMT pre-treatment) condition, I show that reconstruction with 100 FHs achieves a correlation of 0.5, and 0.6 when the $0^{th}$ global FH is considered, with the original signal. Further-

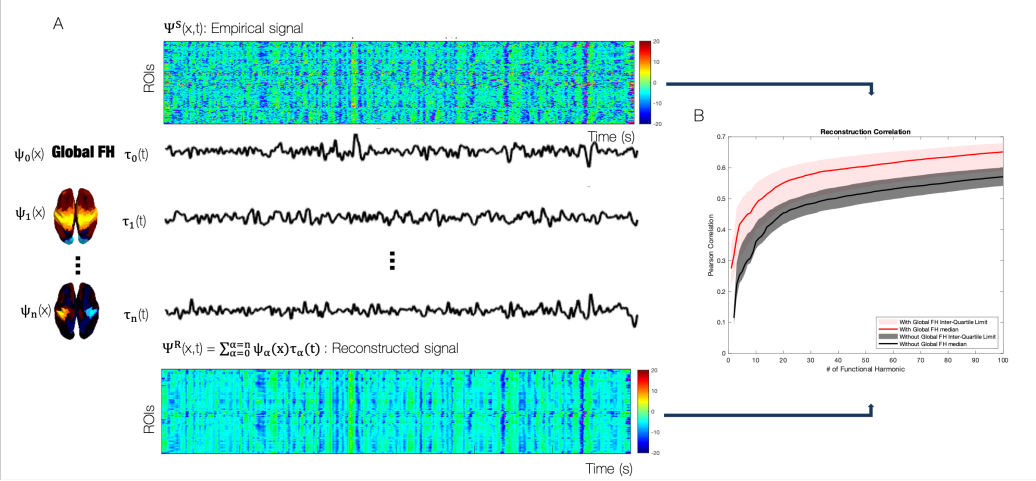



Figure 5.3: ***Signal Reconstruction:*** **A)** After the Functional Harmonic Decomposition as in Figure 5.1, a signal can be reconstructed back by combining the spatial component (FHs) and temporal component (FH contribution). Furthermore, a good portion of the signal can be reconstructed with only a fraction of the FHs. **B)** Correlation of reconstruction between the empirical signal of DMT before injection and its reconstructed counterpart with varying number of FHs. The reconstruction with 100 FHs achieves a correlation of 0.5, and 0.6 with the $0^{th}$ global FH. Furthermore, only when considering the first 11 FHs, they correlate 0.4 and when the $0^{th}$ global FH is included 0.5.

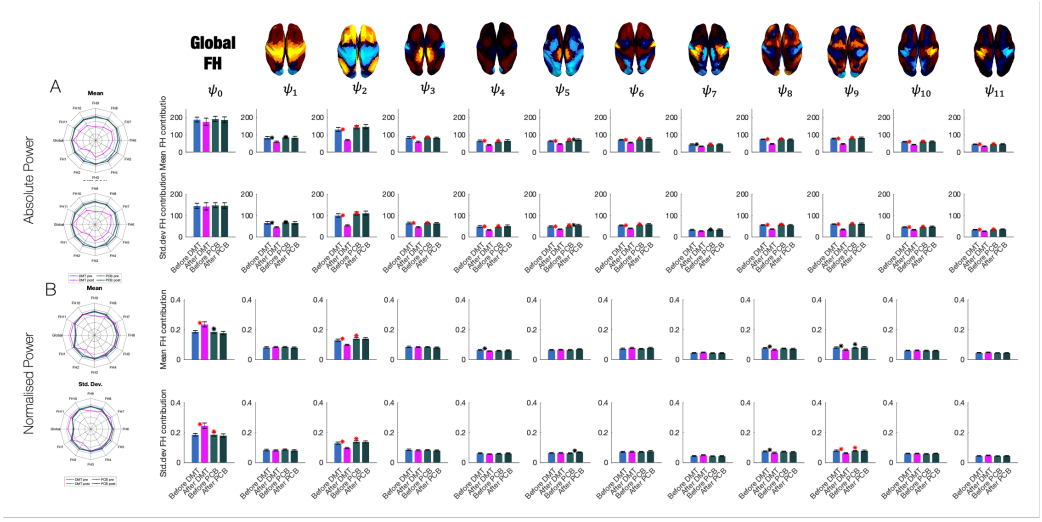



Figure 5.4: ***Power Results:*** **A)** Absolute power across the first 11 FHs represented both visually on a spider plot and statistically for individual FH across the four DMT-based conditions. The results show a decrease in the DMT-induced state (compared to DMT before injection and the placebo state) across many of the 11 FHs except FH $\psi_1$ as well as the $0^{th}$ global FH (red star p-value < 0.05 Bonferonni corrected paired t-test, black star p-value < 0.05 not Bonferonni corrected paired t-test). **B)** Relative power across the first 11 FHs represented both visually on a spider plot and statistically for individual FHs across the four DMT-based conditions. The results demonstrate an increase in the global FH and a decrease in FH $\psi_2$ compared to DMT before injection and the placebo state (red star p-value < 0.05 Bonferonni corrected paired t-test, black star p-value < 0.05 not Bonferonni corrected paired t-test).

more, when taking only the first 11 FHs for the reconstruction, the reconstructed signal correlates 0.4 with the original signal and further 0.5 when the $0^{th}$ global FH is considered (Figure 5.3, B).

### 5.3.3 Power across Functional Harmonics

To quantify contributions of individual harmonics in the different conditions, I compute the absolute and relative power of each harmonic (Section 5.2.7). The absolute power results show a decrease in the DMT-induced state (compared to DMT before injection and placebo-induced states) across most of the 11 FHs ex-

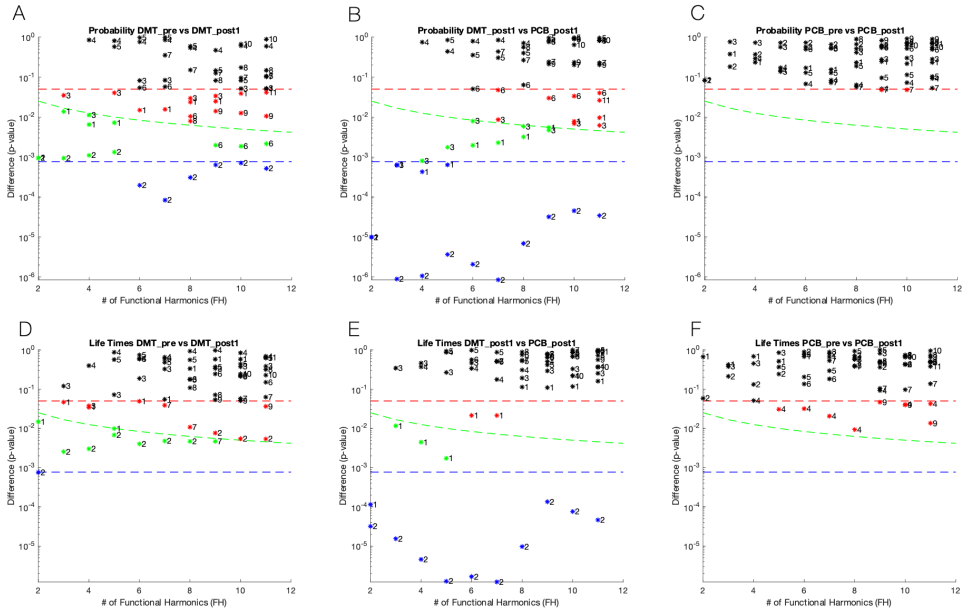



Figure 5.5: ***Dynamic Measures of HADES:*** **A), B) and C)** Fractional Occupancy of FHs across a varying number of harmonics (from 2 to 11). $\psi_2$ consistently decreased in the DMT-induced state versus pre DMT injection and the placebo-induced state. **D), E) and F)** Life Time of FHs across a varying number of harmonics (from 2 to 11). Again, $\psi_2$ consistently decreased in the DMT-induced state versus pre DMT injection and the placebo-induced state. The statistics were performed with paired t-test (blue star: p-value < 0.05/sum(# of FHs across solutions), green star: p-value < 0.05/(# of FH), red star: p-value < 0.05)

cept FH $\psi_1$ as well as the global FH (red star: p-value < 0.05 Bonferonni-corrected paired t-test, black star: p-value < 0.05 uncorrected paired t-test, Figure, 5.5). This is contrasted by the relative power results demonstrating an increase in the global FH and a decrease in FH $\psi_2$ compared to DMT before injection and the placebo-induced state (red star: p-value < 0.05 Bonferonni-corrected paired t-test, black star: p-value < 0.05 uncorrected paired t-test, Figure 5.5). Spider plots in Figure 5.5 represent a visual redistribution of FHs across different conditions.

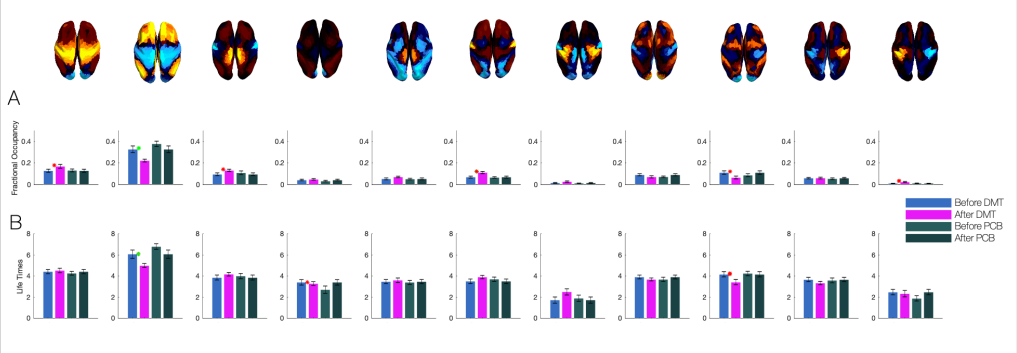



Figure 5.6: ***Fractional Occupancy and Life Times:*** Results of Fractional Occupancy and Life Times for a choice of 11 Functional Harmonics. **A)** Fractional Occupancy decreases for FH $\psi_2$. **B)** Equally, Life Times decrease for FH $\psi_2$. Statistical tests were performed with paired t-test (blue star p-value < 0.05/(# of FH), red star p-value < 0.05)

### 5.3.4 Dynamic Measures of HADES

To assess the temporal evolution of FH weights, I apply a winner-takes-all approach (similar to Chapter 2.2) whereby I take the most prominent FH at every time point and compute Fractional Occupancy (FO) and Life Times (LT) of each FH. In Figure 5.6, I report findings across different number of FHs considered showing a consistent pattern of decreasing FO and LT of $\psi_2$ in the DMT-induced state versus both DMT pre-injection and placebo states (blue star: p-value < 0.05/sum(# of FHs across solutions) paired t-test, green star: p-value < 0.05/(# of FH) paired t-test, red star: p-value < 0.05 uncorrected paired t-test). In Figure 5.6, I show results when choosing all 11 FHs. As before, strongest statistical significance for FO and LT is observed in $\psi_2$ (blue star: p-value < 0.05/(# of FH) paired t-test, red star: p-value < 0.05 uncorrected paired t-test).

## 5.4 Discussion

In this Chapter, I have developed and applied HArmonic DEcomposition of Space-time (HADES) to the DMT-induced brain state as a proof-of-principle. HADES describes the spatial component in terms of Functional Harmonics, computed from the communication structure of the brain, and the time component in terms of temporal contributions of Functional Harmonics derived from Functional Harmonic Decomposition. Consistent with previous literature, I have demonstrated the functional relevance of Functional Harmonics (Glomb et al., 2019). Moreover, I have demonstrated that an experimental signal can be accurately reconstructed with a subset of Functional Harmonics. Applying HADES to the DMT-induced state has shown decreases in power across most FHs, while the global FH has remained unchanged. However, when looking at normalised power in individual subjects, a decrease in FH $\psi_2$ was mirrored by an increase in the global substate. These results motivate a non-trivial reconfiguration whereby the DMT-induced state decreases in overall power with a relative increase towards the global substate and a decrease of FH $\psi_2$ representative of the functional hierarchies of the brain. This was further reinforced by the analysis of Functional Harmonic dynamics with decreases both in fractional occupancy and life times of FH $\psi_2$.

Remarkably, FH $\psi_2$ represents a gradient between unimodal and transmodal regions, which are predominantly situated in visual and somatomotor, and frontoparietal and default mode areas respectively. Such a separation has been proposed to account for a varying level of brain function from low- to high-order cognitive networks (Margulies et al., 2016). Throughout my Thesis, I have argued that psychedelic-induced states result in the undermining of functional systems' hierarchies in the brain as proposed by REBUS and the anarchic brain (Figure 1.7) (Carhart-Harris and Friston, 2019). Furthermore, the relative increase in global

FH speaks to a less functionally defined and more integrated global substate under the influence of DMT. Indeed, on the RSN level, psychedelic-induced states have been shown to subvert within functional network-connectivity while enhancing between-network connectivity and overall global and integrative tendencies (Tagliazucchi et al., 2014).

Traditionally, neuroscience has focused on delineating and studying localised cortical regions in order to map the brain's function. As described in the Introduction 1.1 this approach has been of importance albeit with fragmented insights as to how multiscale brain organisation gives rise to complex spatio-temporal dynamics and ultimately behaviour. A recent development in system neuroscience has been that of cortical gradients (Margulies et al., 2016). This proposes an intrinsic coordinate system of human brain organisation continuously varying from unimodal to transmodal cortical areas (Huntenburg et al., 2018). Indeed, such gradient organisation was for example demonstrated in terms of myelination (Huntenburg et al., 2017), anatomical structure (Burt et al., 2018) or temporal processing (Baldassano et al., 2017). The framework of multidimensional harmonic representation, described here by HADES, attempts to reconcile these views by decomposing brain activity maps into frequency-specific communication channels that unveil dynamic contributions of connectivity gradients and cortical parcellations to brain function - Figure (5.2) (Glomb et al., 2019).

As argued in the Introduction 1.1, the brain as a complex system is hypothesised to manifest hierarchies across time and space. Indeed, such a nested organisation was suggested both in terms of the structural architecture of the brain as well as its temporal frequencies (Betzel et al., 2016; He, 2014). Functional Harmonics are by construction intrinsically ordered according to their spatial frequencies and as such provide a multiscale representation of brain activity across cortical space. Intuitively, spatial frequencies relate to temporal frequencies of oscillations and

therefore further research with modalities such as EEG or MEG will be interesting for drawing a closer relationship between the two (Atasoy et al., 2017a).

Previously and in Chapter 4, connectome harmonics have been used to decompose the brain's spatio-temporal activity into a combination of time-varying contributions (Atasoy et al., 2017b). Using long-range and local connectivity as an underlying structure has been relevant in exploring the structure-function relationship of large-scale brain organisation (Atasoy et al., 2016). However, it seems that structural connectivity alone cannot explain the emergence of rich and spontaneous activity of the human brain (Hagmann et al., 2008; Deco and Jirsa, 2012). Firstly, neocortex is endowed with remarkable heterogeneity in cytoarchitecture. This will result in various computational differentiation across the cortex, for example in terms of temporal processing (Baldassano et al., 2017). Secondly, the neuromodulatory system is known to alter the electrical composition of neurons and thus exercise non-linear effects on the emergent activity of various microcircuits across the brain (Shine, 2019; Kringelbach and Deco, 2020). The hypothesis here is that the communication structure of dense FC has implicitly embedded within it information on anatomical structure, cortical computational heterogeneity as well as neuromodulatory expression and as such serves as a prominent candidate to be used for the derivation of fundamental functional building blocks of spatio-temporal activity.

A limitation of the current approach for describing Functional Harmonics propagating in time is that it might be too reductionist. 'Winner-takes-all' is a powerful technique summarising the brain's dynamics in terms of fractional occupancy and lifetimes of the Functional Harmonics. However, it considers only one FH to be active at a given timepoint and as such might not consider important information. Future work should implement weighted contributions of individual FHs at given timepoints and as such more completely describe the multidimensional represen-

tation of spatio-temporal dynamics.

## 5.5 Summary

Taken all together, in this Chapter I have introduced a new method called Harmonic Decomposition of Spacetime (HADES) to describe spatio-temporal dynamics of the brain. Using Functional Harmonics (FHs) derived from the brain's communication structure, HADES models dynamics as weighted contributions of FHs evolving in time. Firstly, I verified the functional relevance of FHs with known resting-state networks showing both gradient-like and network-based organisation. Then, I reconstructed aspects of the original timeseries with only 100 FHs and their contributions. Furthermore, I applied HADES to the DMT-induced state as in Chapter 4. I showed how normalised and absolute power can be used to demonstrate suppression of functional hierarchy and enhancement of whole-brain integration. Lastly, I demonstrated similar findings of impaired hierarchical organisation in dynamic terms as shown by fractional occupancy and life times of FH $\psi_2$. These findings corroborate the REBUS and anarchic brain model by demonstrating the dynamic changes to the brain functional hierarchy.

# 6 | Discussion

> ...you had not yet been able to acquire the 'Oxford temper' in intellectual matters, never, I mean, been one who could play gracefully with ideas but had arrived at the violence of opinion merely
>
> — Oscar Wilde, Epistola: In Carcere et Vinculis

The brain as a complex system and its associated rich and spontaneous dynamics are at the core of intrinsic human functioning, ultimately giving rise to higher cognition and behaviour. Throughout my doctoral programme, I have focused on describing such dynamics across space and time in altered brain states, especially in psychedelic-induced and depressive states, with a particular focus on the empirical window provided by functional MRI. As the overall picture of spatio-temporal dynamics remains elusive, I have put forward several complementary techniques that all treat brain activity in its entirety (Chapters 2, 3,4 and 5). The findings from psychedelic-induced state corroborate the notion of the dynamical landscape 'flattening', characterised across space and time, and together with whole-brain models suggest clinical interventions for treatment of depression.

In this Chapter I recapitulate the topics I have researched as well as the resulting findings and contributions (Section 6.1). I conclude with a discussion on the implications of these findings and broader relevance to the field of neuroscience as a whole (Section 6.2).

## 6.1 Novel Insights

### 6.1.1 Brain Spatio-temporal Dynamics as a Temporal Trajectory in a Landscape of Phase-locking Substates

In Chapter 2, I mathematically formalised spatio-temporal dynamics as a temporal trajectory through a landscape of phase-locking substates. In this formalism, phase-locking substates are defined by their fractional occupancy, life times and probability of transitions, summarising the dynamics across space and time. To my knowledge, this is the first application of this analysis to a state-of-the-art dataset of resting-state functional MRI, in this case as collected by the Human Connectome Project. I validated the obtained phase-locking substates in terms of their functional relevance, and showed that they are recurrent in time and across scanning recordings. Furthermore, I demonstrated their reliability and thus opened up potential avenues for such analyses to be used in clinical scenarios for diagnosis and prognosis of psychiatric disorders.

### 6.1.2 Rebalancing the Depressive Brain State with Psychedelics

This chapter built upon the spatio-temporal description of Chapter 2 whereby I used Probabilistic Metastable Substates, defined by their Fractional Occupancy, to build a whole-brain model in order to predict a clinical outcome. There has been a growing list of studies on FCD describing brain states in health and disease (Bolton et al., 2020b). However, it is not yet clear how a healthy brain state transits to a diseased brain state and vice versa. Here, as a proof-of-concept, I modelled the treatment-resistant depressive brain state and demonstrated how it can be rebalanced (or not) to a healthy brain state through an intervention with psychedelics. I showed that this can be ascribed to a subset of brain regions un-

able to force the transition from diseased to healthy brain states as obtained from the difference between responders and non-responders to treatment. Furthermore, I demonstrated that the regional inability to promote transition to the healthy state is correlated with $5HT_{1A}$ and $5HT_{2A}$ density maps of the serotonergic system, suggesting a relationship between depression and recovery on the neuropharmacological level.

### 6.1.3 DMT-induced Psychedelic State Revealed by Connectome Harmonic Decomposition

In Chapter 4, I applied Connectome Harmonic Decomposition for the first time to the DMT-induced state in order to characterise spatio-temporal dynamics emergent from the structural scaffold of the human brain - the connectome. As such, I showed full-range reorganisation of the energy harmonic spectrum under the DMT-induced state, with a suppression of the low-harmonic range and an increase in the high-harmonic range respectively. Indeed these findings were found consistent with the known psychedelic profile of the energy harmonic spectrum (Atasoy et al., 2018). Uniquely, I applied several signatures of criticality to demonstrate the broadening of the repertoire of connectome harmonics as described by repertoire entropy, and more prominent power-law statistics as described by the goodness-of-fit to the observable distributions such as mean and maximum power, and power fluctuations. Taken together these results provide further evidence of the tuning of brain dynamics closer to the critical point under the psychedelic-induced state.

### 6.1.4 HArmonic DEcomposition of Spacetime (HADES)

In this Chapter, building on approaches from previous Chapters 2, 3 and 4, I introduced a new method called Harmonic Decomposition of Spacetime (HADES), to define space in terms of Functional Harmonics derived from the communication structure of the brain, and time in terms of temporal contributions of Functional Harmonics obtained by Functional Harmonic decomposition. By applying HADES, I showed that Functional Harmonics and their temporal contributions can be used as a compressed version of the underlying spatio-temporal dynamics. Furthermore, analysis of the Functional Harmonics in terms of their similarity to resting-state networks showed a unique combination of gradient-like and functionally segregated harmonics, building on previous literature unifying gradients and localised brain function (Glomb et al., 2020). This perspective led to new and exciting findings when applying HADES to the DMT-induced state, where a known unimodal to transmodal gradient was shown to decrease in power and fractional occupancy, with the global Functional Harmonic power becoming more prominent in relation to the other harmonics. These results corroborate previously proposed perspectives on the undermining of functional hierarchies and enhancements of integrative functioning under the psychedelic-induced state (Carhart-Harris, 2018; Tagliazucchi et al., 2014).

## 6.2 Perspective

Throughout my thesis, I have introduced and applied several methods in describing spatio-temporal brain dynamics as obtained from fMRI recordings. In Figure 6.1, I list advantages and disadvantages of the different methods. Due to their theoretical underpinning in dynamic system theory and functional interpretability, PL substates of Chapter 2 and 3 have found use in many clinical and modelling

applications Figueroa et al. (2019); Deco et al. (2019). However, the method only partially describes the temporal evolution of PL substates and only considers one PL substate at a given time. On the other hand, Connectome Harmonic Decomposition introduces temporal evolution as a weighted combination of Connectome Harmonics. While Connectome Harmonics address the structure-function relationship their individual functional relevance is less clear and modelling more challenging to implement.

The motivation for HADES was to build on previous chapters of this Thesis in several conceptual ways. While the structural connectome has been shown to constrain the emerging function of the human brain, it cannot account alone for heterogeneities of brain anatomy and tonic neuromodulatory effects on neuronal processing (Huntenburg et al., 2018; Shine et al., 2019). To address these limitations, I used the communication structure of the human brain that implicitly represents the neuromodulatory effects and cytoarchitectural heterogeneities in intrinsic brain activity. Furthermore, Functional Harmonics are orthogonal bases and as such can be used to reconstruct any given signal. This is important as timeseries can be represented as a weighted combination of individual Functional Harmonics without an information loss. Moreover, the perceived dichotomy of gradient-like versus locally specialised brain function can be synthesised into a unique framework whereby the multiscale and multidimensional nature of Functional Harmonics accounts for both continuous and localised brain function within the brain. Lastly, to be mechanistically relevant, future work should combine whole-brain models with HADES.

Importantly, all aforementioned approaches are consistent with the notion of a dynamical landscape whereby brain states can be represented as a time-evolving trajectory through a terrain of spatial patterns considered as attractors (Turkheimer et al., 2021). By regarding different brain states from a single unified frame of ref-

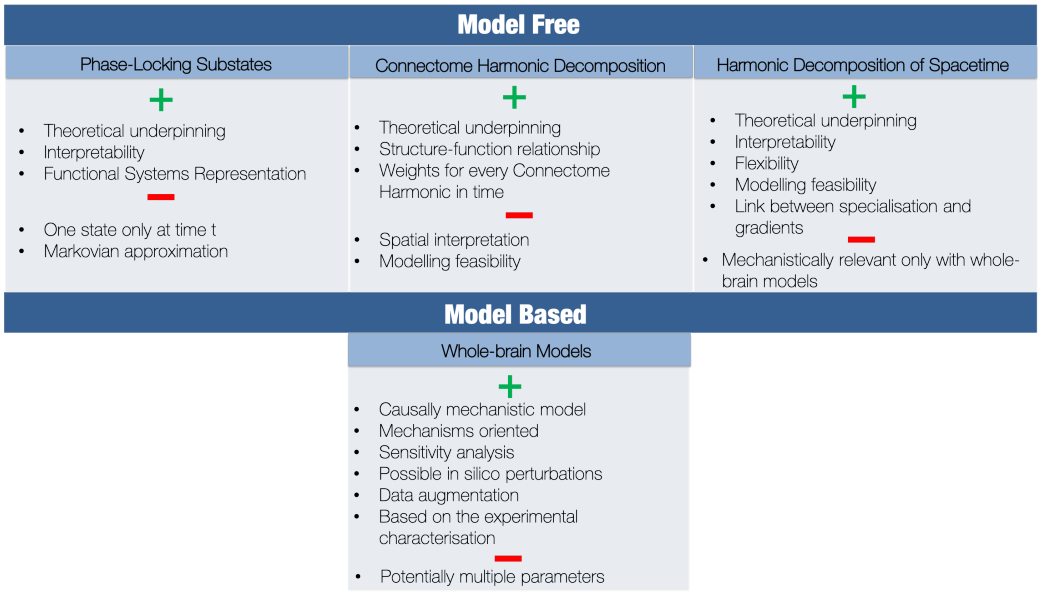



Figure 6.1: ***Summary of Methods:*** **Phase-Locking Substates** of Chapter 2, **Connectome Harmonic Decomposition** of Chapter 4, **Harmonic Decomposition of Spacetime (HADES)** (Chapter 5), **Whole-brain Models** based on Probabilistic Metastable Substates (PMS; Chapter 3).

erence as described by a set of spatial substates, it becomes possible to compare these landscapes across different conditions (see Figure 2.5 and (Atasoy et al., 2018)). In my Thesis, I have shown how psychedelic-induced states flatten the dynamical landscape, in terms of a broadening of the repertoire of active substates and a suppression of functional hierarchies. Furthermore, this intuition informed the use of psychedelics to rebalance the dynamical landscape of the depressive state, which was shown to operate in ruminative states corresponding to less flexible brain functioning (see Figure 1.9).

Experimentally, results presented in this Thesis reinforce the view of compromised functional hierarchies with decreased localised specialisation under the DMT-induced state as motivated by REBUS and the anarchic brain (see Figure 1.7 and (Carhart-Harris and Friston, 2019)). This serves as a breakdown of sum-

mary models represented in large-scale associated networks resulting in richer realisations of incoming signal, both in terms of spatial and temporal extent, as hypothesised by the entropic brain (see Figure 1.6 and (Carhart-Harris et al., 2014; Carhart-Harris, 2018)). This was shown in Chapter 3 and 4 with the observation of a suppression of the uni- to trans-modal functional systems gradient, an increase in prominence of the global integrative substate as well as richer repertoire entropy. Conversely, under the depressive state the functional hierarchies are even more pronounced (possibly spearheaded by the default-mode network) and thus entrap brain functioning into a more consistent and predictable pattern of intrinsic activity. This was demonstrated in Chapter 2 where regions unable to mediate transition to a healthy state were those correlated with $5HT_{2a}$ and $5HT_{1a}$ receptor distributions.

An open question in systems neuroscience is how best to describe the spatial composition of brain states. As described in Figure 6.1 this is an important concern as whole-brain models are only as accurate as the concise representation of experimental data itself (Cabral et al., 2017a). A common approach to describe spatial composition has been a mere correlation-based relationship between regional timeseries with the retrieval of resting-state networks (Damoiseaux et al., 2006). Moving beyond grand-averaged representations, a standard derivation of substates has been that of clustered windows of signal correlation (Allen et al., 2014; Hutchison et al., 2013). Other methods also relying on clustering have successfully derived substates from point-process analysis (considering substates as binary activation across regions) (Tagliazucchi et al., 2012) and Phase-Locking substates (Cabral et al., 2017b); Chapter 2 and 3 are examples of such approaches. Another way is to describe spatial substates realised on the structural scaffold of the brain and thus obtain spatial frequency-dependent building blocks of resting-state activity (Chapter 4 and (Atasoy et al., 2017b; Preti and Van De Ville, 2019)).

Lastly, one can describe brain activity as lying on a low-dimensional manifold embedded in a high-dimensional space. The dimensions of the manifold can then be used as the spatial substates of various brain states. The most commonly used spatial embeddings are linear approaches such as PCA and non-linear approaches such as Diffusion Mappings and Laplacian Eigenmaps (Vos de Wael et al., 2020). To my knowledge, HADES described in Chapter 5 is the first approach to combine Laplacian Eigenmaps and their temporal unfolding to describe brain states.

Another relevant aspect of spontaneous brain activity is that of energy constraints. It is well known that the brain weighs about 2% of total human body mass despite of consuming about 20% of the overall body energy (Tozzi et al., 2016; Bullmore and Sporns, 2012; Laughlin and Sejnowski, 2003). Moreover, an astounding 60 to 80% of energy is devoted solely to the maintenance of intrinsic activity, in contrast to the 0.5 to 1% of energy used in evoked brain activity. Unsurprisingly, this phenomenon has been dubbed "the brain's dark energy" (Raichle, 2006). Traditionally, energy consumption is perceived at the level of ATP usage for neuronal signalling (Laughlin and Sejnowski, 2003) but recently energy constraints have also been proposed to tune large-scale cortical networks (Roberts et al., 2014). Broadly, these constraints relate to the free energy principle whereby brain activity evolves to a substate which minimises its free energy (Friston, 2010). Recent work on maximum entropy models has hypothesised that within an energy landscape, substates with minimal energy are the most functionally co-activated substates. A further postulate was that the default mode network is more frequently activated as it is mainly related to intrinsic brain activity, and lastly that between-system interactions are more energetically costly compared to within-network interactions (Gu et al., 2018). In the presented work, local minima in the dynamic landscape pertain to either phase-locking (Chapter 2 and 3) or spatial frequency dependent substates (Chapter 4 and 5), consistent with the notion of minimally energetic sub-

states. Going forward it will be interesting to obtain a formal definition of such a dynamical landscape where the ability to sustain proximity to a substate and transitions between various substates are quantifiable in terms of their energetic costs.

Another popular idea has become that of control theory where a complex system such as the brain is navigated from its source to final state by targeted stimulations (Srivastava et al., 2020; Gu et al., 2015; Lynn et al., 2020). However, from a complexity perspective this might be problematic as the Shannonian idea of information flow might be ill-defined in the context of the waning and waxing of spontaneous brain activity (Tognoli and Kelso, 2013). Here, I have considered Probabilistic Metastable Substates that imply a sense of uncertainty as to the evolution of the system. By systematic perturbations, independent of the notion of what the specific dynamical pathway might be, it is possible to find a scenario where the brain rebalances itself to a healthy working point, rather than being forced to a preconceived terminus along a certain pathway (Deco et al., 2019).

As argued throughout my thesis, an accurate description of brain states and corresponding whole-brain models will serve to inform future clinical diagnosis and prognosis. Indeed, in Chapters 2, 4 and 5, I respectively created, formalised and used frameworks to help achieve this goal. Furthermore, in Chapter 3 I presented a proof-of-concept demonstration of how whole-brain modelling enriched with a description of brain states can be used to force transitions from diseased to healthy states. Beyond a good approximation of brain states in terms of their spatio-temporal dynamics, recent developments have introduced cortical heterogeneity (Deco et al., 2021a; Demirtas et al., 2019) as well as non-linear neuromodulatory effects (Kringelbach and Deco, 2020; Deco et al., 2018) to further constrain and personalise whole-brain models. This is a hopeful ambition that these advances might bring to fulfil the transnational promise of computational neuroimaging.

One of the ultimate frontiers of neuroscience is that of consciousness. Anil Seth in his recent book 'Being You' argues that the progress will come from tackling what he calls the 'real problem' - an ability to explain, predict and control the phenomenological properties of consciousness. He further argues that this comes about by addressing relatable but distinguishable processes of consciousness, namely conscious level, content and self (Seth, 2021). A profound insight to what all conscious experiences should have in common was put forward in a seminal paper by Giulio Tononi and Gerald Edelman, where the authors argued that all conscious experiences are both informative and integrated (Tononi and Edelman, 1998). This simple yet profound observation has been behind many theoretical and practical developments in consciousness science, with scales of awareness being measured by its informational richness, or clinical applications using Perturbation Complexity Index to distinguish between vegetative-state and locked-in patients (Laureys, 2005; Casali et al., 2013). While successful, these approaches often take into consideration only aspects of the integration and information propositions, and it is yet to be seen what the suitable explanation is. The dominant thread of my Thesis has been of brain states; an idea which is intimately linked to thinking of conscious levels. I predominantly focused on addressing both spatial and temporal dimensions that are at the heart of fully comprehending what integration across space and information across time really mean. HADES, as a spatio-temporal description of brain activity, is a prime candidate to tackle these question both on the theoretical level of parsing different levels/states of consciousness, and also as a candidate for clinical prognosis as argued earlier. Together with whole-brain models and their causal implications to the workings of the brain, it might be possible to glimpse at what makes us, humans.

# Bibliography

Allen, E. A., Damaraju, E., Plis, S. M., Erhardt, E. B., Eichele, T., and Calhoun, V. D. (2014). Tracking whole-brain connectivity dynamics in the resting state. *Cerebral Cortex*, 24(3):663–676.

Alstott, J., Bullmore, E., and Plenz, D. (2014). Powerlaw: A python package for analysis of heavy-tailed distributions. *PLoS ONE*, 9(1).

Andrade, R. (2011). Serotonergic regulation of neuronal excitability in the prefrontal cortex. *Neuropharmacology*, 61(3):382–386.

Aqil, M., Atasoy, S., Kringelbach, M. L., and Hindriks, R. (2021). Graph neural fields: A framework for spatiotemporal dynamical models on the human connectome. *PLoS Computational Biology*, 17(1):e1008310.

Atasoy, S., Deco, G., Kringelbach, M. L., and Pearson, J. (2017a). Harmonic brain modes: a unifying framework for linking space and time in brain dynamics. *The Neuroscientist*, pages 25–27.

Atasoy, S., Donnelly, I., and Pearson, J. (2016). Human brain networks function in connectome-specific harmonic waves. *Nature Communications*, 7:1–10.

Atasoy, S., Roseman, L., Kaelen, M., Kringelbach, M. L., Deco, G., and Carhart-Harris, R. L. (2017b). Connectome-harmonic decomposition of human brain activity reveals dynamical repertoire re-organization under LSD. *Scientific Reports*, 7(1):17661.

Atasoy, S., Vohryzek, J., Deco, G., Carhart-Harris, R. L., and Kringelbach, M. L. (2018). Common neural signatures of psychedelics: Frequency-specific energy changes and repertoire expansion revealed using connectome-harmonic decom-

position. In *Progress in Brain Research*, volume 242, pages 97–120. Elsevier B.V.

Avena-Koenigsberger, A., Misic, B., and Sporns, O. (2018). Communication dynamics in complex brain networks.

Bak, P. and Paczuski, M. (1995). Complexity, contingency, and criticality. *Proceedings of the National Academy of Sciences of the United States of America*, 92(15):6689–6696.

Baker, A. P., Brookes, M. J., Rezek, I. A., Smith, S. M., Behrens, T., Smith, P. J. P., and Woolrich, M. (2014). Fast transient networks in spontaneous human brain activity. *eLife*, 2014(3):1–18.

Baldassano, C., Chen, J., Zadbood, A., Pillow, J. W., Hasson, U., and Norman, K. A. (2017). Discovering Event Structure in Continuous Narrative Perception and Memory. *Neuron*, 95(3):709–721.e5.

Barker, S. A. (2018). N, N-Dimethyltryptamine (DMT), an Endogenous Hallucinogen: Past, Present, and Future Research to Determine Its Role and Function. *Frontiers in Neuroscience*, 12(AUG):536.

Barttfeld, P., Uhrig, L., Sitt, J. D., Sigman, M., and Jarraya, B. (2015). Erratum: Signature of consciousness in the dynamics of resting-state brain activity (Proceedings of the National Academy of Sciences of the United States of America (2015) 112 (887-892)). *Proceedings of the National Academy of Sciences of the United States of America*, 112(37):E5219–E5220.

Bassett, D. S. and Bullmore, E. (2006). Small-world brain networks. *Neuroscientist*, 12(6):512–523.

Bassett, D. S. and Sporns, O. (2017). Network neuroscience.

Bayne, T., Hohwy, J., and Owen, A. M. (2016). Are There Levels of Consciousness? *Trends in Cognitive Sciences*, 20(6):405–413.

Beckmann, C. and Smith, S. (2004). Probabilistic Independent Component Analysis for Functional Magnetic Resonance Imaging. *IEEE Transactions on Medical Imaging*, 23(2):137–152.

Beckmann, C. F., DeLuca, M., Devlin, J. T., and Smith, S. M. (2005). Investigations into resting-state connectivity using independent component analysis. *Philosophical Transactions of the Royal Society B: Biological Sciences*, 360(1457):1001–1013.

Beggs, J. M. and Plenz, D. (2003). Neuronal Avalanches in Neocortical Circuits. *The Journal of Neuroscience*, 23(35):11167–11177.

Beliveau, V., Ganz, M., Feng, L., Ozenne, B., Højgaard, L., Fisher, P. M., Svarer, C., Greve, D. N., and Knudsen, G. M. (2017). A high-resolution in vivo atlas of the human brain's serotonin system. *Journal of Neuroscience*, 37(1):120–128.

Betzel, R. F., Fukushima, M., He, Y., Zuo, X. N., and Sporns, O. (2016). Dynamic fluctuations coincide with periods of high and low modularity in resting-state functional brain networks. *NeuroImage*, 127:287–297.

Bolton, T. A., Kebets, V., Glerean, E., Zöller, D., Li, J., Yeo, B. T., Caballero-Gaudes, C., and Van De Ville, D. (2020a). Agito ergo sum: Correlates of spatio-temporal motion characteristics during fMRI. *NeuroImage*, 209(December 2019).

Bolton, T. A., Morgenroth, E., Preti, M. G., and Van De Ville, D. (2020b). Tapping into Multi-Faceted Human Behavior and Psychopathology Using fMRI Brain Dynamics.

Bressler, S. L. and Tognoli, E. (2006). Operational principles of neurocognitive networks. *International Journal of Psychophysiology*, 60(2):139–148.

Bullmore, E. and Sporns, O. (2009). Complex brain networks: Graph theoretical analysis of structural and functional systems.

Bullmore, E. and Sporns, O. (2012). The economy of brain network organization.

Burt, J. B., Demirtas, M., Eckner, W. J., Navejar, N. M., Ji, J. L., Martin, W. J., Bernacchia, A., Anticevic, A., and Murray, J. D. (2018). Hierarchy of transcriptomic specialization across human cortex captured by structural neuroimaging topography. *Nature Neuroscience*, 21(9):1251–1259.

Burt, J. B., Helmer, M., Shinn, M., Anticevic, A., and Murray, J. D. (2020). Generative modeling of brain maps with spatial autocorrelation. *NeuroImage*, 220:117038.

Cabral, J., Hugues, E., Sporns, O., and Deco, G. (2011). Role of local network oscillations in resting-state functional connectivity. *NeuroImage*, 57(1):130–139.

Cabral, J., Kringelbach, M. L., and Deco, G. (2017a). Functional connectivity dynamically evolves on multiple time-scales over a static structural connectome: Models and mechanisms. *NeuroImage*, 160(March):84–96.

Cabral, J., Vidaurre, D., Marques, P., Magalhães, R., Silva Moreira, P., Miguel Soares, J., Deco, G., Sousa, N., and Kringelbach, M. L. (2017b). Cognitive performance in healthy older adults relates to spontaneous switching between states of functional connectivity during rest. *Scientific Reports*, 7(1):5135.

Cahalane, D. J., Charvet, C. J., and Finlay, B. L. (2014). Modeling local and cross-species neuron number variations in the cerebral cortex as arising from a

common mechanism. *Proceedings of the National Academy of Sciences of the United States of America*, 111(49):17642–17647.

Cammoun, L., Gigandet, X., Meskaldji, D., Thiran, J. P., Sporns, O., Do, K. Q., Maeder, P., Meuli, R., and Hagmann, P. (2012). Mapping the human connectome at multiple scales with diffusion spectrum MRI. *Journal of Neuroscience Methods*, 203(2):386–397.

Carhart-Harris, R. L. (2018). The entropic brain - revisited. *Neuropharmacology*, 142:167–178.

Carhart-Harris, R. L., Bolstridge, M., Rucker, J., Day, C. M., Erritzoe, D., Kaelen, M., Bloomfield, M., Rickard, J. A., Forbes, B., Feilding, A., Taylor, D., Pilling, S., Curran, V. H., and Nutt, D. J. (2016a). Psilocybin with psychological support for treatment-resistant depression: an open-label feasibility study. *The Lancet Psychiatry*, 3(7):619–627.

Carhart-Harris, R. L., Erritzoe, D., Williams, T., Stone, J. M., Reed, L. J., Colasanti, A., Tyacke, R. J., Leech, R., Malizia, A. L., Murphy, K., Hobden, P., Evans, J., Feilding, A., Wise, R. G., and Nutt, D. J. (2012). Neural correlates of the psychedelic state as determined by fMRI studies with psilocybin. *Proceedings of the National Academy of Sciences of the United States of America*, 109(6):2138–43.

Carhart-Harris, R. L. and Friston, K. J. (2019). REBUS and the Anarchic Brain: Toward a Unified Model of the Brain Action of Psychedelics. *Pharmacological reviews*, 71(3):316–344.

Carhart-Harris, R. L., Giribaldi, B., Watts, R., Baker-Jones, M., Murphy-Beiner, A., Murphy, R., Martell, J., Blemings, A., Erritzoe, D., and Nutt, D. J. (2021).

Trial of Psilocybin versus Escitalopram for Depression. *New England Journal of Medicine*, 384(15):1402–1411.

Carhart-Harris, R. L. and Goodwin, G. M. (2017). The Therapeutic Potential of Psychedelic Drugs: Past, Present, and Future. *Neuropsychopharmacology*, 42(11):2105–2113.

Carhart-Harris, R. L., Leech, R., Hellyer, P. J., Shanahan, M., Feilding, A., Tagliazucchi, E., Chialvo, D. R., and Nutt, D. (2014). The entropic brain: a theory of conscious states informed by neuroimaging research with psychedelic drugs. *Frontiers in human neuroscience*, 8(February):20.

Carhart-Harris, R. L., Muthukumaraswamy, S., Roseman, L., Kaelen, M., Droog, W., Murphy, K., Tagliazucchi, E., Schenberg, E. E., Nest, T., Orban, C., Leech, R., Williams, L. T., Williams, T. M., Bolstridge, M., Sessa, B., McGonigle, J., Sereno, M. I., Nichols, D., Hellyer, P. J., Hobden, P., Evans, J., Singh, K. D., Wise, R. G., Curran, H. V., Feilding, A., and Nutt, D. J. (2016b). Neural correlates of the LSD experience revealed by multimodal neuroimaging. *Proceedings of the National Academy of Sciences*, 113(17):4853–4858.

Carhart-Harris, R. L. and Nutt, D. J. (2017). Serotonin and brain function: A tale of two receptors. *Journal of Psychopharmacology*, 31(9):1091–1120.

Carhart-Harris, R. L., Roseman, L., Bolstridge, M., Demetriou, L., Pannekoek, J. N., Wall, M. B., Tanner, M., Kaelen, M., McGonigle, J., Murphy, K., Leech, R., Curran, H. V., and Nutt, D. J. (2017). Psilocybin for treatment-resistant depression: FMRI-measured brain mechanisms. *Scientific Reports*, 7(1):1–11.

Casali, A. G., Gosseries, O., Rosanova, M., Boly, M., Sarasso, S., Casali, K. R., Casarotto, S., Bruno, M. A., Laureys, S., Tononi, G., and Massimini, M. (2013).

A theoretically based index of consciousness independent of sensory processing and behavior.

Chang, C. and Glover, G. H. (2010). Time-frequency dynamics of resting-state brain connectivity measured with fMRI. *NeuroImage*, 50(1):81–98.

Charvet, C. J., Cahalane, D. J., and Finlay, B. L. (2015). Systematic, cross-cortex variation in neuron numbers in rodents and primates. *Cerebral Cortex*, 25(1):147–160.

Chialvo, D. R. (2004). Critical brain networks. *Physica A: Statistical Mechanics and its Applications*, 340(4 SPEC. ISS.):756–765.

Chialvo, D. R. (2010). Emergent complex neural dynamics. *Nature Physics*, 6(10):744–750.

Clauset, A., Shalizi, C. R., and Newman, M. E. (2009). Power-law distributions in empirical data.

Cocchi, L., Gollo, L. L., Zalesky, A., and Breakspear, M. (2017). Criticality in the brain: A synthesis of neurobiology, models and cognition. *Progress in Neurobiology*, 158:132–152.

Cocchi, L., Harding, I. H., Lord, A., Pantelis, C., Yucel, M., and Zalesky, A. (2014). Disruption of structure-function coupling in the schizophrenia connectome. *NeuroImage: Clinical*, 4:779–787.

Cowen, P. J. and Browning, M. (2015). What has serotonin to do with depression?

Crick, F. and Clark, J. (1994). The astonishing hypothesis. *Journal of Consciousness Studies*, 1(1):10–16.

Daducci, A., Gerhard, S., Griffa, A., Lemkaddem, A., Cammoun, L., Gigandet, X., Meuli, R., Hagmann, P., and Thiran, J. P. (2012). The Connectome Mapper:

An Open-Source Processing Pipeline to Map Connectomes with MRI. *PLoS ONE*, 7(12):e48121.

Damoiseaux, J. S., Rombouts, S. A. R. B., Barkhof, F., Scheltens, P., Stam, C. J., Smith, S. M., and Beckmann, C. F. (2006). Consistent resting-state networks across healthy subjects. *Proceedings of the National Academy of Sciences*, 103(37):13848–13853.

Davis, Z., Muller, L., Trujillo, J.-M., Sejnowski, T., and Reynolds, J. (2019). Spontaneous Traveling Cortical Waves Gate Perception in Awake Behaving Primates. *Nature*, 20(February 2019).

Dayan, P. and Huys, Q. J. M. (2008). Serotonin, inhibition, and negative mood. *PLoS Computational Biology*, 4(2).

Deco, G., Aquino, K. M., Arnatkeviciute, A., Oldham, S., Sabaroedin, K., Rogasch, N. C., Kringelbach, M. L., and Fornito, A. (2021a). Dynamical consequences of regional heterogeneity in the brains transcriptional landscape. *bioRxiv*, page 2020.10.28.359943.

Deco, G., Cabral, J., Woolrich, M. W., Stevner, A. B., van Hartevelt, T. J., and Kringelbach, M. L. (2017a). Single or multiple frequency generators in on-going brain activity: A mechanistic whole-brain model of empirical MEG data. *NeuroImage*, 152(November 2016):538–550.

Deco, G., Cruzat, J., Cabral, J., Knudsen, G. M., Carhart-Harris, R. L., Whybrow, P. C., Logothetis, N. K., and Kringelbach, M. L. (2018). Whole-Brain Multimodal Neuroimaging Model Using Serotonin Receptor Maps Explains Non-linear Functional Effects of LSD. *Current Biology*, 28(19):3065–3074.e6.

Deco, G., Cruzat, J., Cabral, J., Tagliazucchi, E., Laufs, H., Logothetis, N. K., and Kringelbach, M. L. (2019). Awakening: Predicting external stimulation

to force transitions between different brain states. *Proceedings of the National Academy of Sciences*, page 201905534.

Deco, G., Jirs, V., McIntosh, A. R., Sporns, O., and Kötter, R. (2009a). Key role of coupling, delay, and noise in resting brain fluctuations. *Proceedings of the National Academy of Sciences of the United States of America*, 106(25):10302–10307.

Deco, G. and Jirsa, V. K. (2012). Ongoing cortical activity at rest: Criticality, multistability, and ghost attractors. *J Neurosci*, 32(10):3366–3375.

Deco, G., Jirsa, V. K., and McIntosh, A. R. (2011). Emerging concepts for the dynamical organization of resting-state activity in the brain. *Nature reviews. Neuroscience*, 12(1):43–56.

Deco, G. and Kringelbach, M. L. (2014). Great expectations: Using whole-brain computational connectomics for understanding neuropsychiatric disorders.

Deco, G. and Kringelbach, M. L. (2016). Metastability and Coherence: Extending the Communication through Coherence Hypothesis Using A Whole-Brain Computational Perspective.

Deco, G. and Kringelbach, M. L. (2020). Turbulent-like Dynamics in the Human Brain. *Cell Reports*, 33(10):108471.

Deco, G., Kringelbach, M. L., Jirsa, V. K., and Ritter, P. (2017b). The dynamics of resting fluctuations in the brain: Metastability and its dynamical cortical core. *Scientific Reports*, 7(1):1–14.

Deco, G., Perl, Y. S., Sitt, J. D., Tagliazucchi, E., and Kringelbach, M. L. (2021b). Deep learning the arrow of time in brain activity: characterising brain-environment behavioural interactions in health and disease. *bioRxiv*, page 2021.07.02.450899.

Deco, G., Ponce-Alvarez, A., Hagmann, P., Romani, G. ., Mantini, D., and Corbetta, M. (2014). How local excitation-inhibition ratio impacts the whole brain dynamics. *The Journal of neuroscience*, 34(23):7886–98.

Deco, G., Ponce-Alvarez, A., Mantini, D., Romani, G. L., Hagmann, P., and Corbetta, M. (2013). Resting-state functional connectivity emerges from structurally and dynamically shaped slow linear fluctuations. *Journal of Neuroscience*, 33(27):11239–11252.

Deco, G., Rolls, E. T., and Romo, R. (2009b). Stochastic dynamics as a principle of brain function.

Deco, G., Tononi, G., Boly, M., and Kringelbach, M. L. (2015). Rethinking segregation and integration: contributions of whole-brain modelling. *Nature reviews. Neuroscience*, 16(7):430–439.

Deluca, A. and Corral, Á. (2013). Fitting and goodness-of-fit test of non-truncated and truncated power-law distributions. *Acta Geophysica*, 61(6):1351–1394.

Demertzi, A., Tagliazucchi, E., Dehaene, S., Deco, G., Barttfeld, P., Raimondo, F., Martial, C., Fernández-Espejo, D., Rohaut, B., Voss, H. U., Schiff, N. D., Owen, A. M., Laureys, S., Naccache, L., and Sitt, J. D. (2019). Human consciousness is supported by dynamic complex patterns of brain signal coordination. *Science Advances*, 5(2):eaat7603.

Demirtas, M., Burt, J. B., Helmer, M., Ji, J. L., Adkinson, B. D., Glasser, M. F., Van Essen, D. C., Sotiropoulos, S. N., Anticevic, A., and Murray, J. D. (2019). Hierarchical Heterogeneity across Human Cortex Shapes Large-Scale Neural Dynamics. *Neuron*, 101(6):1181–1194.e13.

Demirtas, M., Tornador, C., Falcón, C., López-Solà, M., Hernández-Ribas, R., Pujol, J., Menchón, J. M., Ritter, P., Cardoner, N., Soriano-Mas, C., and Deco,

G. (2016). Dynamic functional connectivity reveals altered variability in functional connectivity among patients with major depressive disorder. *Human Brain Mapping*, 37(8):2918–2930.

Eguíluz, V. M., Chialvo, D. R., Cecchi, G. A., Baliki, M., and Apkarian, A. V. (2005). Scale-free brain functional networks. *Physical Review Letters*, 94(1).

Esteban, O., Markiewicz, C. J., Blair, R. W., Moodie, C. A., Isik, A. I., Erramuzpe, A., Kent, J. D., Goncalves, M., DuPre, E., Snyder, M., Oya, H., Ghosh, S. S., Wright, J., Durnez, J., Poldrack, R. A., and Gorgolewski, K. J. (2019). fMRIPrep: a robust preprocessing pipeline for functional MRI. *Nature Methods*, 16(1):111–116.

Expert, P., Lambiotte, R., Chialvo, D. R., Christensen, K., Jensen, H. J., Sharp, D. J., and Turkheimer, F. (2011). Self-similar correlation function in brain resting-state functional magnetic resonance imaging. *Journal of the Royal Society Interface*, 8(57):472–479.

Felleman, D. J. and Van Essen, D. C. (1991). Distributed hierarchical processing in the primate cerebral cortex. *Cerebral Cortex*, 1(1):1–47.

Figueroa, C. A., Cabral, J., Mocking, R. J., Rapuano, K. M., van Hartevelt, T. J., Deco, G., Expert, P., Schene, A. H., Kringelbach, M. L., and Ruhé, H. G. (2019). Altered ability to access a clinically relevant control network in patients remitted from major depressive disorder. *Human Brain Mapping*, 40(9):2771–2786.

Fox, M. D. and Greicius, M. (2010). Clinical applications of resting state functional connectivity. *Frontiers in systems neuroscience*, 4(June):19.

Fox, M. D., Snyder, A. Z., Vincent, J. L., Corbetta, M., Van Essen, D. C., and Raichle, M. E. (2005). The human brain is intrinsically organized into dynamic,

anticorrelated functional networks. *Proceedings of the National Academy of Sciences of the United States of America*, 102(27):9673–8.

Freyer, F., Roberts, J. A., Becker, R., Robinson, P. A., Ritter, P., and Breakspear, M. (2011). Biophysical mechanisms of multistability in resting-state cortical rhythms. *Journal of Neuroscience*, 31(17):6353–6361.

Freyer, F., Roberts, J. A., Ritter, P., and Breakspear, M. (2012). A Canonical Model of Multistability and Scale-Invariance in Biological Systems. *PLoS Computational Biology*, 8(8):e1002634.

Friston, K. (2010). The free-energy principle: A unified brain theory? *Nature Reviews Neuroscience*, 11(2):127–138.

Fu, X., Liu, F., Cui, Z., and Guo, W. (2020). Editorial: Dynamic Functional Connectivity in Neuropsychiatric Disorders: Methods and Applications. *Frontiers in Neuroscience*, 14.

Gaynes, B. N. (2009). Identifying difficult-to-treat depression: Differential diagnosis, subtypes, and comorbidities. *Journal of Clinical Psychiatry*, 70(SUPPL. 6):10–15.

Ghosh, A., Rho, Y., McIntosh, A. R., Kötter, R., and Jirsa, V. K. (2008). Cortical network dynamics with time delays reveals functional connectivity in the resting brain. *Cognitive Neurodynamics*, 2(2):115–120.

Gilson, M., Kouvaris, N. E., Deco, G., and Zamora-López, G. (2018). Framework based on communicability and flow to analyze complex network dynamics. *Physical Review E*, 97(5).

Glasser, M. F., Smith, S. M., Marcus, D. S., Andersson, J. L., Auerbach, E. J., Behrens, T. E., Coalson, T. S., Harms, M. P., Jenkinson, M., Moeller, S., Robinson, E. C., Sotiropoulos, S. N., Xu, J., Yacoub, E., Ugurbil, K., and Van Essen,

D. C. (2016). The Human Connectome Project's neuroimaging approach. *Nature Neuroscience*, 19(9):1175–1187.

Glasser, M. F., Sotiropoulos, S. N., Wilson, J. A., Coalson, T. S., Fischl, B., Andersson, J. L., Xu, J., Jbabdi, S., Webster, M., Polimeni, J. R., Van Essen, D. C., and Jenkinson, M. (2013). The minimal preprocessing pipelines for the Human Connectome Project. *NeuroImage*, 80:105–124.

Glennon, R. A., Titeler, M., and McKenney, J. D. (1984). Evidence for 5-HT2 involvement in the mechanism of action of hallucinogenic agents. *Life Sciences*, 35(25):2505–2511.

Glerean, E., Salmi, J., Lahnakoski, J. M., Jääskeläinen, I. P., and Sams, M. (2012). Functional Magnetic Resonance Imaging Phase Synchronization as a Measure of Dynamic Functional Connectivity. *Brain Connectivity*, 2(2):91–101.

Glomb, K., Mullier, E., Carboni, M., Rubega, M., Iannotti, G., Tourbier, S., Seeber, M., Vulliemoz, S., and Hagmann, P. (2019). Using structural connectivity to augment community structure in EEG functional connectivity. *bioRxiv*, page 831743.

Glomb, K., Rué Queralt, J., Pascucci, D., Defferrard, M., Tourbier, S., Carboni, M., Rubega, M., Vulliémoz, S., Plomp, G., and Hagmann, P. (2020). Connectome spectral analysis to track EEG task dynamics on a subsecond scale. *NeuroImage*, 221(June).

Greicius, M. (2008). Resting-state functional connectivity in neuropsychiatric disorders. *Curr Opin Neurol*, 21(4):424–430.

Griffa, A., Baumann, P. S., Thiran, J. P., and Hagmann, P. (2013). Structural connectomics in brain diseases. *NeuroImage*, 80:515–526.

Griffa, A., Ricaud, B., Benzi, K., Bresson, X., Daducci, A., Vandergheynst, P.,

Thiran, J. P., and Hagmann, P. (2017). Transient networks of spatio-temporal connectivity map communication pathways in brain functional systems. *NeuroImage*, 155(April):490–502.

Griffiths, R. R., Johnson, M. W., Carducci, M. A., Umbricht, A., Richards, W. A., Richards, B. D., Cosimano, M. P., and Klinedinst, M. A. (2016). Psilocybin produces substantial and sustained decreases in depression and anxiety in patients with life-threatening cancer: A randomized double-blind trial. *Journal of Psychopharmacology*, 30(12):1181–1197.

Gu, S., Cieslak, M., Baird, B., Muldoon, S. F., Grafton, S. T., Pasqualetti, F., and Bassett, D. S. (2018). The Energy Landscape of Neurophysiological Activity Implicit in Brain Network Structure. *Scientific Reports*, 8(1):2507.

Gu, S., Pasqualetti, F., Cieslak, M., Telesford, Q. K., Yu, A. B., Kahn, A. E., Medaglia, J. D., Vettel, J. M., Miller, M. B., Grafton, S. T., and Bassett, D. S. (2015). Controllability of structural brain networks. *Nature Communications*, 6:1–10.

Haak, K. V., Marquand, A. F., and Beckmann, C. F. (2018). Connectopic mapping with resting-state fMRI. *NeuroImage*, 170:83–94.

Hagmann, P., Cammoun, L., Gigandet, X., Meuli, R., Honey, C. J., Van Wedeen, J., and Sporns, O. (2008). Mapping the structural core of human cerebral cortex. *PLoS Biology*, 6(7):1479–1493.

Hagmann, P., Sporns, O., Madan, N., Cammoun, L., Pienaar, R., Wedeen, V. J., Meuli, R., Thiran, J.-P., and Grant, P. E. (2010). White matter maturation reshapes structural connectivity in the late developing human brain. *Proceedings of the National Academy of Sciences*, 107(44):19067–19072.

Haimovici, A., Tagliazucchi, E., Balenzuela, P., and Chialvo, D. R. (2013). Brain

organization into resting state networks emerges at criticality on a model of the human connectome. *Physical Review Letters*, 110(17).

Halberstadt, A. L. (2015). Recent advances in the neuropsychopharmacology of serotonergic hallucinogens. *Behavioural Brain Research*, 277:99–120.

Hansen, E. C., Battaglia, D., Spiegler, A., Deco, G., and Jirsa, V. K. (2015). Functional connectivity dynamics: Modeling the switching behavior of the resting state. *NeuroImage*, 105:525–535.

Harmer, C. J., Goodwin, G. M., and Cowen, P. J. (2009). Why do antidepressants take so long to work? A cognitive neuropsychological model of antidepressant drug action. *British Journal of Psychiatry*, 195(2):102–108.

Hawrylycz, M. J., Lein, E. S., Guillozet-Bongaarts, A. L., Shen, E. H., Ng, L., Miller, J. A., Van De Lagemaat, L. N., Smith, K. A., Ebbert, A., Riley, Z. L., Abajian, C., Beckmann, C. F., Bernard, A., Bertagnolli, D., Boe, A. F., Cartagena, P. M., Mallar Chakravarty, M., Chapin, M., Chong, J., Dalley, R. A., Daly, B. D., Dang, C., Datta, S., Dee, N., Dolbeare, T. A., Faber, V., Feng, D., Fowler, D. R., Goldy, J., Gregor, B. W., Haradon, Z., Haynor, D. R., Hohmann, J. G., Horvath, S., Howard, R. E., Jeromin, A., Jochim, J. M., Kinnunen, M., Lau, C., Lazarz, E. T., Lee, C., Lemon, T. A., Li, L., Li, Y., Morris, J. A., Overly, C. C., Parker, P. D., Parry, S. E., Reding, M., Royall, J. J., Schulkin, J., Sequeira, P. A., Slaughterbeck, C. R., Smith, S. C., Sodt, A. J., Sunkin, S. M., Swanson, B. E., Vawter, M. P., Williams, D., Wohnoutka, P., Ronald Zielke, H., Geschwind, D. H., Hof, P. R., Smith, S. M., Koch, C., Grant, S. G., and Jones, A. R. (2012). An anatomically comprehensive atlas of the adult human brain transcriptome. *Nature*, 489(7416):391–399.

He, B. J. (2014). Scale-free brain activity: Past, present, and future. *Trends in Cognitive Sciences*, 18(9):480–487.

Hlinka, J., Paluš, M., Vejmelka, M., Mantini, D., and Corbetta, M. (2011). Functional connectivity in resting-state fMRI: Is linear correlation sufficient? *NeuroImage*, 54(3):2218–2225.

Honey, C. J., Kötter, R., Breakspear, M., and Sporns, O. (2007). Network structure of cerebral cortex shapes functional connectivity on multiple time scales. *Proceedings of the National Academy of Sciences of the United States of America*, 104(24):10240–10245.

Honey, C. J., Sporns, O., Cammoun, L., Gigandet, X., Thiran, J.-P., Meuli, R., and Hagmann, P. (2009). Predicting human resting-state functional connectivity from structural connectivity. *Proceedings of the National Academy of Sciences of the United States of America*, 106(6):2035–40.

Huang, W., Bolton, T. A., Medaglia, J. D., Bassett, D. S., Ribeiro, A., and Van De Ville, D. (2018). Graph Signal Processing of Human Brain Imaging Data. *ICASSP, IEEE International Conference on Acoustics, Speech and Signal Processing - Proceedings*, 2018-April:980–984.

Huntenburg, J. M., Bazin, P. L., Goulas, A., Tardif, C. L., Villringer, A., and Margulies, D. S. (2017). A Systematic Relationship Between Functional Connectivity and Intracortical Myelin in the Human Cerebral Cortex. *Cerebral cortex (New York, N.Y. : 1991)*, 27(2):981–997.

Huntenburg, J. M., Bazin, P. L., and Margulies, D. S. (2018). Large-Scale Gradients in Human Cortical Organization.

Hutchison, R. M., Womelsdorf, T., Allen, E. A., Bandettini, P. A., Calhoun, V. D., Corbetta, M., Della Penna, S., Duyn, J. H., Glover, G. H., Gonzalez-Castillo, J., Handwerker, D. A., Keilholz, S., Kiviniemi, V., Leopold, D. A., de Pasquale,

F., Sporns, O., Walter, M., and Chang, C. (2013). Dynamic functional connectivity: Promise, issues, and interpretations. *NeuroImage*, 80:360–378.

Huxley, A. (1977). *Moksha: Classic Writings on Psychedelics and the Visionary experience*. Stonehill Pub. Co.

Jbabdi, S. and Johansen-Berg, H. (2011). Tractography: Where Do We Go from Here?

Jirsa, V. K., Jantzen, K. J., Fuchs, A., and Kelso, J. A. (2002). Spatiotemporal forward solution of the EEG and MEG using network modeling. *IEEE Transactions on Medical Imaging*, 21(5):493–504.

Johnson, M. W., Garcia-Romeu, A., and Griffiths, R. R. (2017). Long-term follow-up of psilocybin-facilitated smoking cessation. *The American Journal of Drug and Alcohol Abuse*, 43(1):55–60.

Josephs, O. and Henson, R. N. (1999). Event-related functional magnetic resonance imaging: Modelling, inference and optimization. *Philosophical Transactions of the Royal Society B: Biological Sciences*, 354(1387):1215–1228.

Kaiser, M. (2017). Mechanisms of Connectome Development.

Kaiser, R. H., Andrews-Hanna, J. R., Wager, T. D., and Pizzagalli, D. A. (2015). Large-Scale Network Dysfunction in Major Depressive Disorder. *JAMA Psychiatry*, 72(6):603.

Karahanoglu, F. I. and Van De Ville, D. (2015). Transient brain activity disentangles fMRI resting-state dynamics in terms of spatially and temporally overlapping networks. *Nature Communications*, 6:7751.

Kaufman, I. C. (1951). The Cerebral Cortex of Man: A Clinical Study of Localization of Function. *American Journal of Psychiatry*, 108(2):153–153.

Kelso, J. A. (1995). Dynamic patterns: The self-organization of brain and behavior. *Complexity*, 2(3):45–46.

Kitzbichler, M. G., Smith, M. L., Christensen, S. R., and Bullmore, E. (2009). Broadband criticality of human brain network synchronization. *PLoS Computational Biology*, 5(3):e1000314.

Koch, C., Massimini, M., Boly, M., and Tononi, G. (2016). Neural correlates of consciousness: Progress and problems.

Kometer, M., Schmidt, A., Jancke, L., and Vollenweider, F. X. (2013). Activation of Serotonin 2A Receptors Underlies the Psilocybin-Induced Effects on Oscillations, N170 Visual-Evoked Potentials, and Visual Hallucinations. *Journal of Neuroscience*, 33(25):10544–10551.

Kraehenmann, R., Pokorny, D., Aicher, H., Preller, K. H., Pokorny, T., Bosch, O. G., Seifritz, E., and Vollenweider, F. X. (2017). LSD increases primary process thinking via serotonin 2A receptor activation. *Frontiers in Pharmacology*, 8(NOV):1–9.

Kringelbach, M. L., Cruzat, J., Cabral, J., Knudsen, G. M., Carhart-Harris, R., Whybrow, P. C., Logothetis, N. K., and Deco, G. (2020). Dynamic coupling of whole-brain neuronal and neurotransmitter systems. *Proceedings of the National Academy of Sciences of the United States of America*, 117(17):9566–9576.

Kringelbach, M. L. and Deco, G. (2020). Brain States and Transitions: Insights from Computational Neuroscience.

Kringelbach, M. L., McIntosh, A. R., Ritter, P., Jirsa, V. K., and Deco, G. (2015). The Rediscovery of Slowness: Exploring the Timing of Cognition.

Kuramoto, Y. (1984). Chemical oscillations, waves, and turbulence. *Springer Science & Business Media*, 19.

Kuznetsov, Y. a. (1996). Elements of applied bifurcation theory. *Choice Reviews Online*, 33(06):33–3370–33–3370.

Landis, J. R. and Koch, G. G. (1977). The Measurement of Observer Agreement for Categorical Data. *Biometrics*, 33(1):159.

Laughlin, S. B. and Sejnowski, T. J. (2003). Communication in neuronal networks.

Laureys, S. (2005). The neural correlate of (un)awareness: Lessons from the vegetative state. *Trends in Cognitive Sciences*, 9(12):556–559.

Liégeois, R., Laumann, T. O., Snyder, A. Z., Zhou, J., and Yeo, B. T. (2017). Interpreting temporal fluctuations in resting-state functional connectivity MRI.

Liégeois, R., Li, J., Kong, R., Orban, C., Van De Ville, D., Ge, T., Sabuncu, M. R., and Yeo, B. T. (2019). Resting brain dynamics at different timescales capture distinct aspects of human behavior. *Nature Communications*, 10(1).

Loggia, M. L., Edwards, R. R., Kim, J., Vangel, M. G., Wasan, A. D., Gollub, R. L., Harris, R. E., Park, K., and Napadow, V. (2012). Disentangling linear and nonlinear brain responses to evoked deep tissue pain. *Pain*, 153(10):2140–2151.

Logothetis, N. K. (2002). The neural basis of the blood-oxygen-level-dependent functional magnetic resonance imaging signal. *Philosophical Transactions of the Royal Society B: Biological Sciences*, 357(1424):1003–1037.

Logothetis, N. K., Augath, M., Murayama, Y., Rauch, A., Sultan, F., Goense, J.,

Oeltermann, A., and Merkle, H. (2010). The effects of electrical microstimulation on cortical signal propagation. *Nature Neuroscience*, 13(10):1283–1291.

Logothetis, N. K. and Wandell, B. A. (2004). Interpreting the BOLD signal.

Lord, L. D., Expert, P., Atasoy, S., Roseman, L., Rapuano, K., Lambiotte, R., Nutt, D. J., Deco, G., Carhart-Harris, R. L., Kringelbach, M. L., and Cabral, J. (2019). Dynamical exploration of the repertoire of brain networks at rest is modulated by psilocybin. *NeuroImage*, 199:127–142.

Lord, L. D., Stevner, A. B., Deco, G., and Kringelbach, M. L. (2017). Understanding principles of integration and segregation using whole-brain computational connectomics: Implications for neuropsychiatric disorders. *Philosophical Transactions of the Royal Society A: Mathematical, Physical and Engineering Sciences*, 375(2096):20160283.

Luppi, A. I., Vohryzek, J., Kringelbach, M. L., Mediano, P. A., Craig, M. M., Adapa, R., Carhart-Harris, R. L., Roseman, L., Pappas, I., Finoia, P., Williams, G. B., Allanson, J., Pickard, J. D., Menon, D. K., Atasoy, S., and Stamatakis, E. A. (2020). Connectome harmonic decomposition of human brain dynamics reveals a landscape of consciousness. *bioRxiv*, page 2020.08.10.244459.

Lynn, C. W., Kahn, A. E., Nyema, N., and Bassett, D. S. (2020). Abstract representations of events arise from mental errors in learning and memory. *Nature Communications*, 11(1):1–12.

Malhi, G. S. and Mann, J. J. (2018). Depression. *The Lancet*, 392(10161):2299–2312.

Margulies, D. S., Ghosh, S. S., Goulas, A., Falkiewicz, M., Huntenburg, J. M., Langs, G., Bezgin, G., Eickhoff, S. B., Castellanos, F. X., Petrides, M., Jefferies, E., and Smallwood, J. (2016). Situating the default-mode network along

a principal gradient of macroscale cortical organization. *Proceedings of the National Academy of Sciences of the United States of America*, 113(44):12574–12579.

Menon, V. (2011). Large-scale brain networks and psychopathology: A unifying triple network model. *Trends in Cognitive Sciences*, 15(10):483–506.

Messé, A., Rudrauf, D., Benali, H., and Marrelec, G. (2014). Relating Structure and Function in the Human Brain: Relative Contributions of Anatomy, Stationary Dynamics, and Non-stationarities. *PLoS Computational Biology*, 10(3).

Moreno, F. A., Wiegand, C. B., Taitano, E. K., and Delgado, P. L. (2006). Safety, tolerability, and efficacy of psilocybin in 9 patients with obsessive-compulsive disorder. *Journal of Clinical Psychiatry*, 67(11):1735–1740.

Morgan, C., McAndrew, A., Stevens, T., Nutt, D., and Lawn, W. (2017). Tripping up addiction: the use of psychedelic drugs in the treatment of problematic drug and alcohol use. *Current Opinion in Behavioral Sciences*, 13:71–76.

Murphy, K., Birn, R. M., Handwerker, D. A., Jones, T. B., and Bandettini, P. A. (2009). The impact of global signal regression on resting state correlations: Are anti-correlated networks introduced? *NeuroImage*, 44(3):893–905.

Murphy, K. and Fox, M. D. (2017). Towards a consensus regarding global signal regression for resting state functional connectivity MRI. *NeuroImage*, 154:169–173.

Muthukumaraswamy, S. D., Carhart-Harris, R. L., Moran, R. J., Brookes, M. J., Williams, T. M., Errtizoe, D., Sessa, B., Papadopoulos, A., Bolstridge, M., Singh, K. D., Feilding, A., Friston, K. J., and Nutt, D. J. (2013). Broadband Cortical Desynchronization Underlies the Human Psychedelic State. *Journal of Neuroscience*, 33(38):15171–15183.

Naze, S., Proix, T., Atasoy, S., and Kozloski, J. R. (2021). Robustness of connectome harmonics to local gray matter and long-range white matter connectivity changes: Sensitivity analysis of Connectome Harmonics. *NeuroImage*, 224(August 2020).

Nichols, D. E. (2016). Psychedelics. *Pharmacological Reviews*, 68(April):264–355.

Nutt, D. J., King, L. a., and Nichols, D. E. (2013). Effects of Schedule I drug laws on neuroscience research and treatment innovation. *Nature Reviews Neuroscience*, 14(August):577–585.

Palhano-Fontes, F., Andrade, K. C., Tofoli, L. F., Santos, A. C., Crippa, J. A. S., Hallak, J. E. C., Ribeiro, S., and de Araujo, D. B. (2015). The psychedelic state induced by ayahuasca modulates the activity and connectivity of the default mode network. *PloS one*, 10(2):e0118143.

Perl, Y. S., Pallavicini, C., Ipiña, I. P., Kringelbach, M., Deco, G., Laufs, H., and Tagliazucchi, E. (2020). Data augmentation based on dynamical systems for the classification of brain states. *Chaos, Solitons and Fractals*, 139:1–22.

Perrone-Capano, C., Volpicelli, F., and Di Porzio, U. (2017). Biological bases of human musicality. *Reviews in the Neurosciences*, 28(3):235–245.

Petri, G., Expert, P., Turkheimer, F., Carhart-Harris, R., Nutt, D., Hellyer, P. J., and Vaccarino, F. (2014). Homological scaffolds of brain functional networks. *Journal of The Royal Society Interface*, 11(101):20140873–20140873.

Pikovsky, A., Rosenblum, M., Kurths, J., and Hilborn, R. C. (2002). Synchronization: A Universal Concept in Nonlinear Science. *American Journal of Physics*, 70(6):655–655.

Plenz, D. (2013). The Critical Brain. *Physics*, 6.

Poldrack, R. A. and Gorgolewski, K. J. (2014). Making big data open: Data sharing in neuroimaging.

Pollan, M. (2019). *How to change your mind: What the new science of psychedelics teaches us about consciousness, dying, addiction, depression, and transcendence*. Penguin Books.

Ponce-Alvarez, A., Uhrig, L., Deco, N., Signorelli, C. M., Jarraya, B., and Deco, G. (2021). Macroscopic quantities of collective brain activity during wakefulness and anesthesia. *bioRxiv*, page 2021.02.03.429578.

Power, J. D., Plitt, M., Laumann, T. O., and Martin, A. (2017). Sources and implications of whole-brain fMRI signals in humans. *NeuroImage*, 146:609–625.

Preller, K. H., Herdener, M., Pokorny, T., Planzer, A., Kraehenmann, R., Stämpfli, P., Liechti, M. E., Seifritz, E., and Vollenweider, F. X. (2017). The Fabric of Meaning and Subjective Effects in LSD-Induced States Depend on Serotonin 2A Receptor Activation. *Current Biology*, 27(3):451–457.

Preti, M. G., Bolton, T. A., and Ville, D. V. D. (2016). The dynamic functional connectome: State-of-the-art and perspectives. *NeuroImage*.

Preti, M. G. and Van De Ville, D. (2017). Dynamics of functional connectivity at high spatial resolution reveal long-range interactions and fine-scale organization. *Scientific Reports*, 7(1).

Preti, M. G. and Van De Ville, D. (2019). Decoupling of brain function from structure reveals regional behavioral specialization in humans. *Nature Communications*, 10(1).

Raichle, M. E. (2006). The Brain's Dark Energy. *Science*, 314.

Reiche, S., Hermle, L., Gutwinski, S., Jungaberle, H., Gasser, P., and Majić, T. (2018). Serotonergic hallucinogens in the treatment of anxiety and depression in patients suffering from a life-threatening disease: A systematic review. *Progress in Neuro-Psychopharmacology and Biological Psychiatry*, 81(August 2017):1–10.

Ridding, M. C. and Rothwell, J. C. (2007). Is there a future for therapeutic use of transcranial magnetic stimulation?

Roberts, J. A., Gollo, L. L., Abeysuriya, R. G., Roberts, G., Mitchell, P. B., Woolrich, M. W., and Breakspear, M. (2019). Metastable brain waves. *Nature Communications*, 10(1).

Roberts, J. A., Iyer, K. K., Finnigan, S., Vanhatalo, S., and Breakspear, M. (2014). Scale-free bursting in human cortex following hypoxia at birth. *Journal of Neuroscience*, 34(19):6557–6572.

Robinson, P. A., Zhao, X., Aquino, K. M., Griffiths, J. D., Sarkar, S., and Mehta-Pandejee, G. (2016). Eigenmodes of brain activity: Neural field theory predictions and comparison with experiment. *NeuroImage*, 142:79–98.

Rosas, F. E., Mediano, P. A., Jensen, H. J., Seth, A. K., Barrett, A. B., Carhart-Harris, R. L., and Bor, D. (2020). Reconciling emergences: An information-theoretic approach to identify causal emergence in multivariate data. *PLoS Computational Biology*, 16(12 December).

Roseman, L., Leech, R., Feilding, A., Nutt, D. J., and Carhart-Harris, R. L. (2014). The effects of psilocybin and MDMA on between-network resting state functional connectivity in healthy volunteers. *Frontiers in human neuroscience*, 8(May):204.

Saad Al-Harbi, K. (2012). Patient Preference and Adherence Treatment-resistant

depression: therapeutic trends, challenges, and future directions. *Patient Preference and Adherence*, pages 6–369.

Sarwar, T., Ramamohanarao, K., and Zalesky, A. (2019). Mapping connectomes with diffusion MRI: deterministic or probabilistic tractography? *Magnetic Resonance in Medicine*, 81(2):1368–1384.

Schaefer, A., Kong, R., Gordon, E. M., Laumann, T. O., Zuo, X.-N., Holmes, A. J., Eickhoff, S. B., and Yeo, B. T. T. (2018). Local-Global Parcellation of the Human Cerebral Cortex from Intrinsic Functional Connectivity MRI. *Cerebral Cortex*, 28(9):3095–3114.

Schartner, M. M., Carhart-Harris, R. L., Barrett, A. B., Seth, A. K., and Muthukumaraswamy, S. D. (2017). Increased spontaneous MEG signal diversity for psychoactive doses of ketamine, LSD and psilocybin. *Scientific reports*, 7(April):46421.

Schenberg, E. E., Alexandre, J. F. M., Filev, R., Cravo, A. M., Sato, J. R., Muthukumaraswamy, S. D., Yonamine, M., Waguespack, M., Lomnicka, I., Barker, S. A., Da Silveira, D. X., and Chialvo, D. R. (2015). Acute biphasic effects of ayahuasca. *PLoS ONE*, 10(9):1–27.

Sereno, M. I., Pitzalis, S., and Martinez, A. (2001). Mapping of contralateral space in retinotopic coordinates by a parietal cortical area in humans. *Science*, 294(5545):1350–1354.

Seth, A. (2021). *Being You: A New Science of Consciousness*. Faber & Faber.

Seth, A. K., Dienes, Z., Cleeremans, A., Overgaard, M., and Pessoa, L. (2008). Measuring consciousness: relating behavioural and neurophysiological approaches. *Trends in Cognitive Sciences*, 12(8):314–321.

Setsompop, K., Kimmlingen, R., Eberlein, E., Witzel, T., Cohen-Adad, J., Mc-

Nab, J. A., Keil, B., Tisdall, M. D., Hoecht, P., Dietz, P., Cauley, S. F., Tountcheva, V., Matschl, V., Lenz, V. H., Heberlein, K., Potthast, A., Thein, H., Van Horn, J., Toga, A., Schmitt, F., Lehne, D., Rosen, B. R., Wedeen, V., and Wald, L. L. (2013). Pushing the limits of in vivo diffusion MRI for the Human Connectome Project. *NeuroImage*, 80:220–233.

Shew, W. L. and Plenz, D. (2013). The functional benefits of criticality in the cortex. *Neuroscientist*, 19(1):88–100.

Shew, W. L., Yang, H., Yu, S., Roy, R., and Plenz, D. (2011). Information capacity and transmission are maximized in balanced cortical networks with neuronal avalanches. *Journal of Neuroscience*, 31(1):55–63.

Shine, J. M. (2019). Neuromodulatory Influences on Integration and Segregation in the Brain. *Trends in Cognitive Sciences*, 23(7):572–583.

Shine, J. M., Breakspear, M., Bell, P. T., Ehgoetz Martens, K., Shine, R., Koyejo, O., Sporns, O., and Poldrack, R. A. (2019). Human cognition involves the dynamic integration of neural activity and neuromodulatory systems. *Nature Neuroscience*, 22(2):289–296.

Shriki, O., Alstott, J., Carver, F., Holroyd, T., Henson, R. N. a., Smith, M. L., Coppola, R., Bullmore, E., and Plenz, D. (2013). Neuronal avalanches in the resting MEG of the human brain. *The Journal of neuroscience : the official journal of the Society for Neuroscience*, 33(16):7079–90.

Sporns, O., Tononi, G., and Edelman, G. M. (2000). Connectivity and complexity: The relationship between neuroanatomy and brain dynamics.

Sporns, O., Tononi, G., and Kötter, R. (2005). The human connectome: A structural description of the human brain. *PLoS Computational Biology*, 1(4):0245–0251.

Srivastava, P., Nozari, E., Kim, J. Z., Ju, H., Zhou, D., Becker, C., Pasqualetti, F., Pappas, G. J., and Bassett, D. S. (2020). Models of communication and control for brain networks: Distinctions, convergence, and future outlook. *Network Neuroscience*, 4(4):1122–1159.

Stevner, A. B., Vidaurre, D., Cabral, J., Rapuano, K., Nielsen, S. F., Tagliazucchi, E., Laufs, H., Vuust, P., Deco, G., Woolrich, M. W., Van Someren, E., and Kringelbach, M. L. (2019). Discovery of key whole-brain transitions and dynamics during human wakefulness and non-REM sleep. *Nature Communications*, 10(1).

Swanson, L. R. (2018). Unifying theories of psychedelic drug effects. *Frontiers in Pharmacology*, 9(MAR):1–23.

Tagliazucchi, E., Balenzuela, P., Fraiman, D., and Chialvo, D. R. (2012). Criticality in large-scale brain fmri dynamics unveiled by a novel point process analysis. *Frontiers in Physiology*, 3 FEB:15.

Tagliazucchi, E., Carhart-Harris, R., Leech, R., Nutt, D., and Chialvo, D. R. (2014). Enhanced repertoire of brain dynamical states during the psychedelic experience. *Human Brain Mapping*, 35(11):5442–5456.

Tagliazucchi, E., Chialvo, D. R., Siniatchkin, M., Amico, E., Brichant, J. F., Bonhomme, V., Noirhomme, Q., Laufs, H., and Laureys, S. (2016a). Large-scale signatures of unconsciousness are consistent with a departure from critical dynamics. *Journal of the Royal Society Interface*, 13(114).

Tagliazucchi, E., Roseman, L., Kaelen, M., Orban, C., Muthukumaraswamy, S. D., Murphy, K., Laufs, H., Leech, R., McGonigle, J., Crossley, N., Bullmore, E., Williams, T., Bolstridge, M., Feilding, A., Nutt, D. J., and Carhart-

Harris, R. (2016b). Increased Global Functional Connectivity Correlates with LSD-Induced Ego Dissolution. *Current Biology*, 26(8):1043–1050.

Tagliazucchi, E., Siniatchkin, M., Laufs, H., and Chialvo, D. R. (2016c). The voxel-wise functional connectome can be efficiently derived from co-activations in a sparse spatio-temporal point-process. *Frontiers in Neuroscience*, 10(AUG):1–13.

Tewarie, P., Liuzzi, L., O'Neill, G. C., Quinn, A. J., Griffa, A., Woolrich, M. W., Stam, C. J., Hillebrand, A., and Brookes, M. J. (2019). Tracking dynamic brain networks using high temporal resolution MEG measures of functional connectivity. *NeuroImage*, 200:38–50.

Timmermann, C., Roseman, L., Schartner, M., Milliere, R., Williams, L. T., Erritzoe, D., Muthukumaraswamy, S., Ashton, M., Bendrioua, A., Kaur, O., Turton, S., Nour, M. M., Day, C. M., Leech, R., Nutt, D. J., and Carhart-Harris, R. L. (2019). Neural correlates of the DMT experience assessed with multivariate EEG. *Scientific Reports*, 9(1):1–13.

Timmermann, C., Roseman, L., Williams, L., Erritzoe, D., Martial, C., Cassol, H., Laureys, S., Nutt, D., and Carhart-Harris, R. (2018). DMT models the near-death experience. *Frontiers in Psychology*, 9(AUG):1424.

Tognoli, E. and Kelso, J. A. (2014). The Metastable Brain. *Neuron*, 81(1):35–48.

Tognoli, E. and Kelso, J. A. S. (2013). On the Brain's Dynamical Complexity: Coupling and Causal Influences Across Spatiotemporal Scales. *Advances in Cognitive Neurodynamics (III)*, pages 259–265.

Tononi, G. and Edelman, G. M. (1998). Consciousness and complexity.

Tononi, G. and Koch, C. (2008). The neural correlates of consciousness: An update. *Annals of the New York Academy of Sciences*, 1124:239–261.

Tournier, J. D., Smith, R., Raffelt, D., Tabbara, R., Dhollander, T., Pietsch, M., Christiaens, D., Jeurissen, B., Yeh, C. H., and Connelly, A. (2019). MRtrix3: A fast, flexible and open software framework for medical image processing and visualisation. *NeuroImage*, 202(January):116137.

Tozzi, A., Zare, M., and Benasich, A. A. (2016). New perspectives on spontaneous brain activity: Dynamic networks and energy matter. *Frontiers in Human Neuroscience*, 10(MAY2016):247.

Turkheimer, F. E., Hellyer, P., Kehagia, A. A., Expert, P., Lord, L. D., Vohryzek, J., De Faria Dafflon, J., Brammer, M., and Leech, R. (2019). Conflicting emergences. Weak vs. strong emergence for the modelling of brain function.

Turkheimer, F. E., Leech, R., Expert, P., Lord, L.-D., and Vernon, A. C. (2015). The brain's code and its canonical computational motifs. From sensory cortex to the default mode network: A multi-scale model of brain function in health and disease. *Neuroscience & Biobehavioral Reviews*, 55:1–12.

Turkheimer, F. E., Rosas, F. E., Dipasquale, O., Martins, D., Fagerholm, E. D., Expert, P., Váša, F., Lord, L. D., and Leech, R. (2021). A Complex Systems Perspective on Neuroimaging Studies of Behavior and Its Disorders. *Neuroscientist*.

Tzourio-Mazoyer, N., Landeau, B., Papathanassiou, D., Crivello, F., Etard, O., Delcroix, N., Mazoyer, B., and Joliot, M. (2002). Automated anatomical labeling of activations in SPM using a macroscopic anatomical parcellation of the MNI MRI single-subject brain. *NeuroImage*, 15(1):273–289.

Valle, M., Maqueda, A. E., Rabella, M., Rodriguez-Pujadas, A., Antonijoan, R. M., Romero, S., Alonso, J. F., Mañanas, M. A., Barker, S., Friedlander, P., Feilding, A., and Riba, J. (2016). Inhibition of alpha oscillations through

serotonin-2A receptor activation underlies the visual effects of ayahuasca in humans. *European Neuropsychopharmacology*, 26(7):1161–1175.

Van De Ville, D., Britz, J., and Michel, C. M. (2010). EEG microstate sequences in healthy humans at rest reveal scale-free dynamics. *Proceedings of the National Academy of Sciences of the United States of America*, 107(42):18179–18184.

van den Heuvel, M. P. and Hulshoff Pol, H. E. (2010). Exploring the brain network: A review on resting-state fMRI functional connectivity. *European Neuropsychopharmacology*, 20(8):519–534.

Van Essen, D. C., Smith, S. M., Barch, D. M., Behrens, T. E., Yacoub, E., and Ugurbil, K. (2013). The WU-Minn Human Connectome Project: An overview. *NeuroImage*, 80:62–79.

Vargas, C., López-Jaramillo, C., and Vieta, E. (2013). A systematic literature review of resting state network-functional MRI in bipolar disorder.

Vasa, F., Shanahan, M., Hellyer, P. J., Scott, G., Cabral, J., and Leech, R. (2015). Effects of lesions on synchrony and metastability in cortical networks. *NeuroImage*, 118:456–467.

Vidaurre, D., Smith, S. M., and Woolrich, M. W. (2017). Brain network dynamics are hierarchically organized in time. *Proceedings of the National Academy of Sciences*, 114(48):201705120.

Viol, A., Palhano-Fontes, F., Onias, H., de Araujo, D. B., and Viswanathan, G. M. (2017). Shannon entropy of brain functional complex networks under the influence of the psychedelic Ayahuasca. *Scientific reports*, 7(1):7388.

Vohryzek, J., Griffa, A., Mullier, E., Friedrichs-Maeder, C., Sandini, C., Schaer, M., Eliez, S., and Hagmann, P. (2019). Dynamic spatio-temporal patterns

of brain connectivity reorganize across development. *Network Neuroscience*, pages 1–39.

Vollenweider, F. X., Vollenweider-Scherpenhuyzen, M. F., Bäbler, a., Vogel, H., and Hell, D. (1998). Psilocybin induces schizophrenia-like psychosis in humans via a serotonin-2 agonist action. *Neuroreport*, 9(17):3897–3902.

Vos de Wael, R., Benkarim, O., Paquola, C., Lariviere, S., Royer, J., Tavakol, S., Xu, T., Hong, S. J., Langs, G., Valk, S., Misic, B., Milham, M., Margulies, D., Smallwood, J., and Bernhardt, B. C. (2020). BrainSpace: a toolbox for the analysis of macroscale gradients in neuroimaging and connectomics datasets. *Communications Biology*, 3(1).

Watts, D. J. and Strogatz, S. H. (1998). Collective dynamics of 'small-world' networks. *Nature*, 393(6684):440–442.

Williams, L. M. (2016). Precision psychiatry: A neural circuit taxonomy for depression and anxiety. *The Lancet Psychiatry*, 3(5):472–480.

Williams, P. E. and Shapley, R. M. (2007). A dynamic nonlinearity and spatial phase specificity in macaque V1 neurons. *Journal of Neuroscience*, 27(21):5706–5718.

World Health Organisation (2017). Depression and other common mental disorders: global health estimates. *World Health Organization*, pages 1–24.

Xing, X. X. and Zuo, X. N. (2018). The anatomy of reliability: a must read for future human brain mapping. *Science Bulletin*, 63(24):1606–1607.

Yang, H., Shew, W. L., Roy, R., and Plenz, D. (2012). Maximal Variability of Phase Synchrony in Cortical Networks with Neuronal Avalanches. *The Journal of Neuroscience*, 32(3):1061 –1072.

Yeo, B. T. T., Krienen, F. M., Sepulcre, J., Sabuncu, M. R., Lashkari, D., Hollinshead, M., Roffman, J. L., Smoller, J. W., Zöllei, L., Polimeni, J. R., Fischl, B., Liu, H., and Buckner, R. L. (2011). The organization of the human cerebral cortex estimated by intrinsic functional connectivity. *Journal of neurophysiology*, 106(3):1125–65.

Zalesky, A., Fornito, A., Cocchi, L., Gollo, L. L., and Breakspear, M. (2014). Time-resolved resting-state brain networks.

Zang, Y., Jiang, T., Lu, Y., He, Y., and Tian, L. (2004). Regional homogeneity approach to fMRI data analysis. *NeuroImage*, 22(1):394–400.

Zuo, X. N., Biswal, B. B., and Poldrack, R. A. (2019). Editorial: Reliability and reproducibility in functional connectomics. *Frontiers in Neuroscience*, 13(FEB):1–4.

# A | Supplementary Information

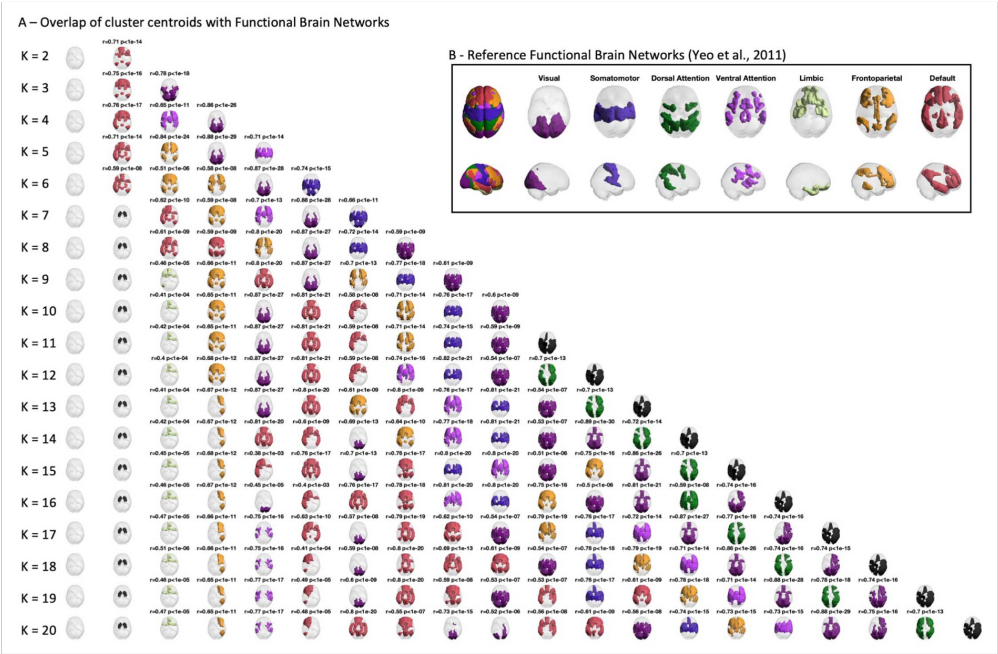



Figure A.1: ***Centroids Overlap with RSNs - Top view:*** **A)** representation of Figure 2.3. Representation of the centroids obtained for each k-means clustering solution with K ranging between 2 and 20. Centroids are represented in cortical space, rendering only the ROIs whose BOLD phase is shifted $\pm\pi/2$ with respect to the leading direction. ROIs are colored according to the Reference Functional Brain Network (shown in panel B) to which they most significantly relate with. Pearson's r and corresponding p-value are reported as a title only when surviving a conservative threshold of $p < 0.05/K$, to correct for the number of independent hypotheses tested in each partition model.Centroids not significantly overlapping with any of the reference functional net-works are colored in black. **B)** Reference functional brain networks estimated from 1000 subjects from correlation-based intrinsic FC (Yeo et al., 2011)

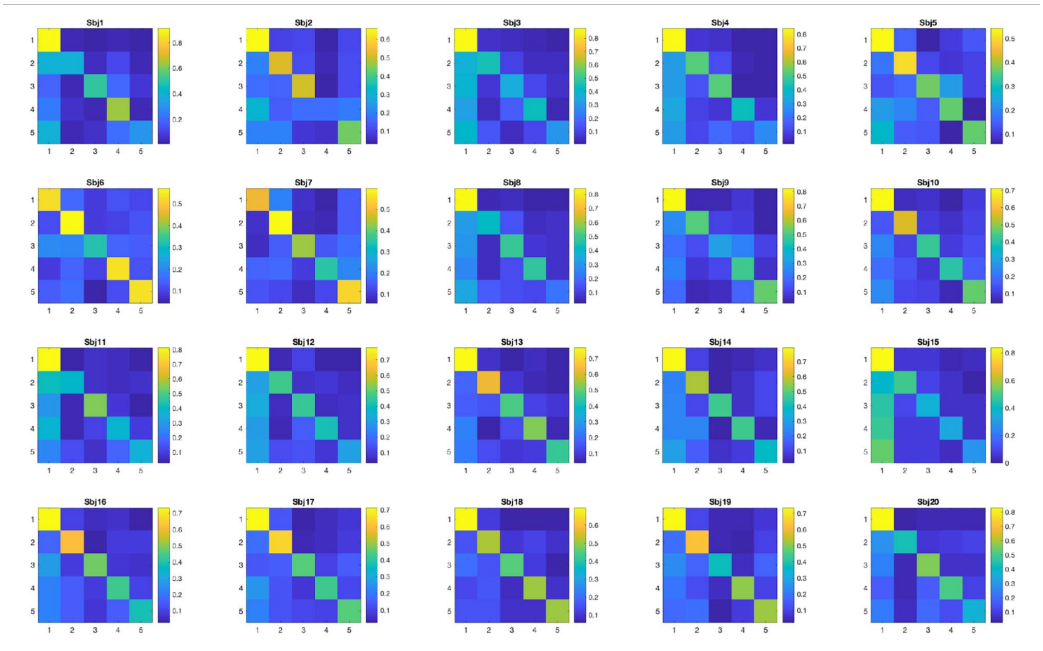



Figure A.2: ***Individual Transition Probability:*** Transition matrix quantifying the probability of the trajectory transiting from one substate to another as defined in Equation 2.4. Here, for the first 20 participants in the LR session.

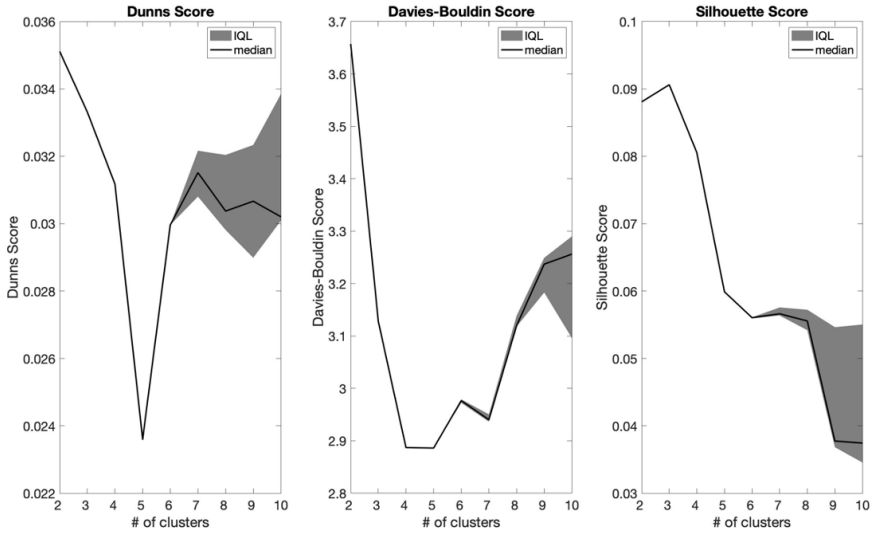



Figure A.3: ***Clustering Quality Measures:*** Three quality measures for th clustering solutions of Chapter 3 across runs of varying number of clusters. Here, Dunn's score, Davies-Bouldin and Silhouette scores are reported

.

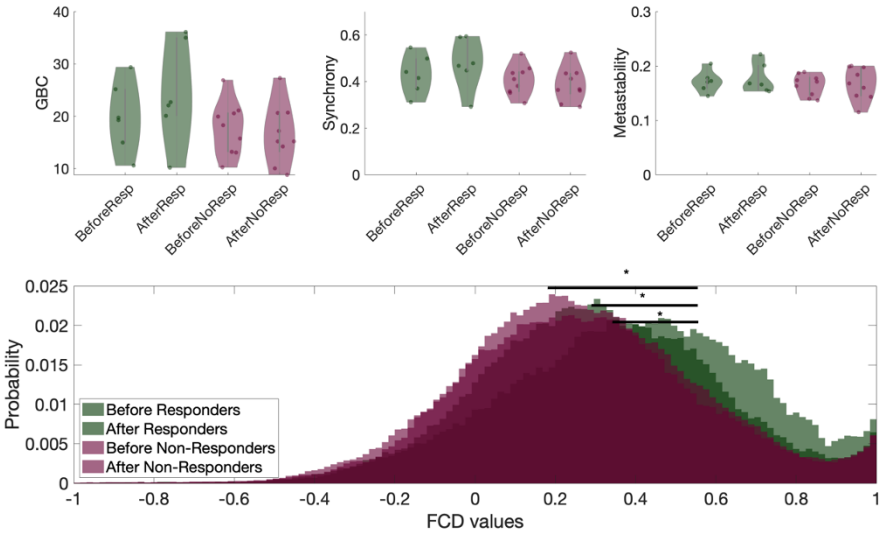



Figure A.4: ***Empirical Results - GBC, Synchrony, Metastability, FCD:*** Results of other measures between responders and non-responders to the psilocybin treatment. Here, non-significant differences reported for Global Brain Connectivity (GBC), Synchrony and Metastability. Furthermore, the mean histogram values of the FCD spectrum were found to be significant between pre- and post-treatment responders ($p = 0.0163$, signed rank-sum permutation test), and pre- and post-treatment non-responders with post-treatment responders respectively ($p = 0.0183$ and $p = 0.0273$, rank-sum permutation test), demonstrating the importance of taking into the consideration temporal fluctuations.

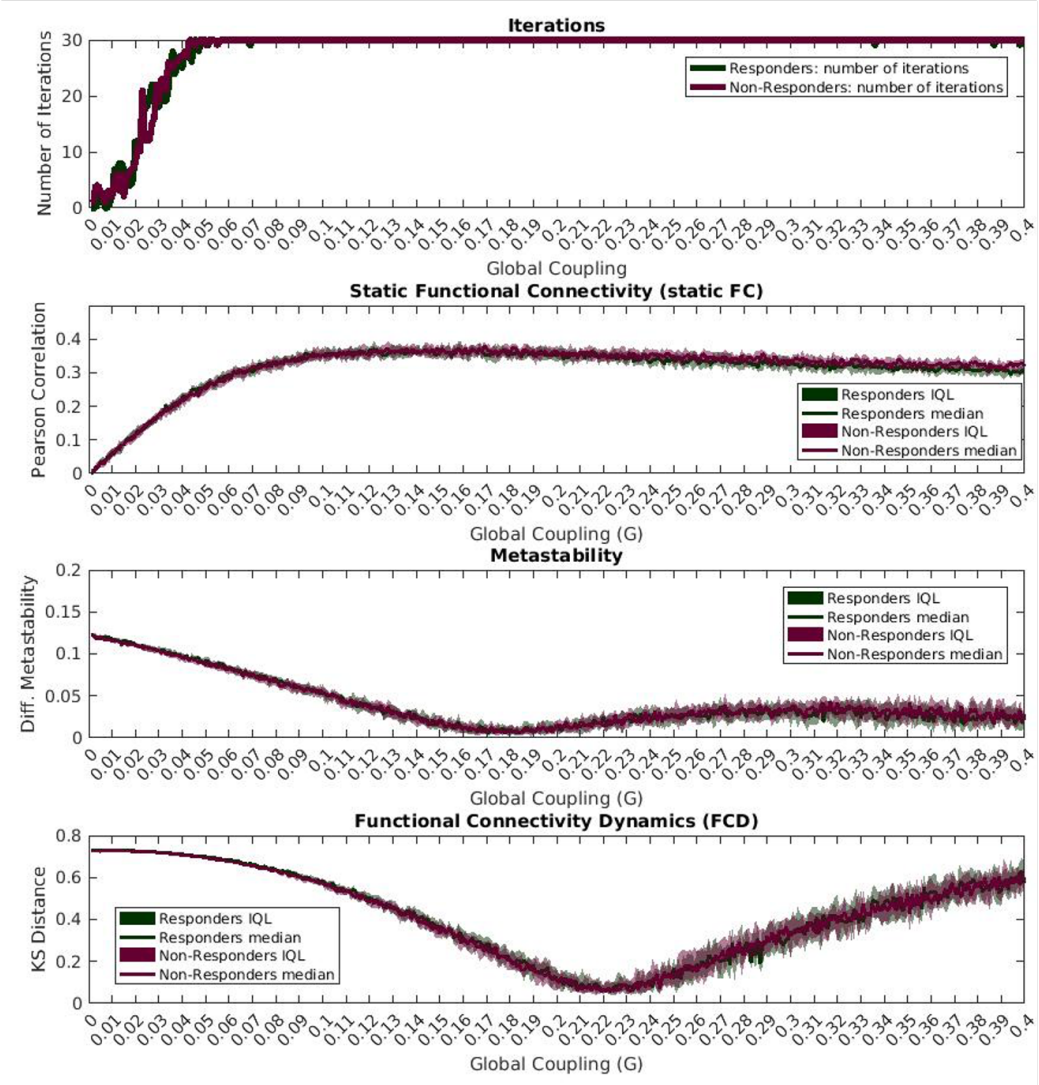



Figure A.5: ***Model Validation - GBC, Synchrony, Metastability, FC:*** The model validation was run over 30 iteration. Results for other objective functions: static FC (Pearson Correlation), Metastability (Difference in metastability) and Functional Connectivity Dynamics (KS-distance).

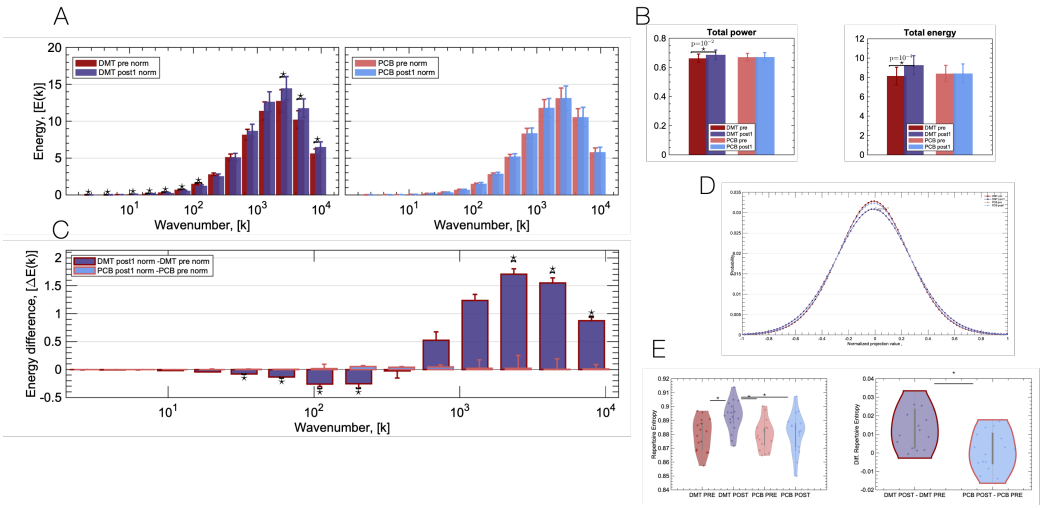



Figure A.6: ***Connectome Harmonic Decomposition Based on 32 HCP subjects; an Effect of Connectome Template:*** Analysis of the Chapter 4 results with a different structural connectivity template. Here I used diffusion spectrum and T2-weighted imaging from 32 HCP participants scanned for 89 minutes. Further details about the acquisition can be found in (Setsompop et al., 2013); the data are freely available on the Lead-DBS software website www.lead-dbs.org/ (A) A decrease of energy for low-frequency harmonics $k \in [1,...,10^2]$ (p-value < 0.05, Bonferonni-corrected paired t-test) and an increase of energy for high-frequency harmonics $k \in [10^3,...,10^4]$ (p-value < $10^{-2}$ and p-value < $10^{-4}$ respectively, Bonferonni-corrected paired t-test) were observed. (B) Total Power and Energy differences (p-value < $10^{-2}$ and p-value < $10^{-4}$ respectively, Bonferonni-corrected paired t-test) (C) Furthermore, energy differences between the DMT and placebo conditions were observed with decreases in low-frequency harmonics $k \in [1,...,10^2]$ (p-value < 0.05, Bonferonni-corrected paired t-test) and increases in high-frequency harmonics $k \in [10^3,...,10^4]$ (p-value < 0.05, Bonferonni-corrected paired t-test)). (D) Repertoire of connectome harmonics (pre/post DMT two-sample ks-test, p-value < $10^{-5}$). (E) Repertoire Entropy (Pre/Post DMT: p-value < $10^{-4}$,Pre PCB/Post DMT: p-value < $10^{-4}$, Post PCB/Post DMT: p-value < $10^{-4}$, paired t-test). Repertoire Entropy Difference (Diff. in Pre-Post DMT and Pre-Post PCB: p-value < $10^{-5}$, paired t-test). In this new analysis, I excluded the last bin, prone to spatial aliasing error, as done in (Aqil et al., 2021).

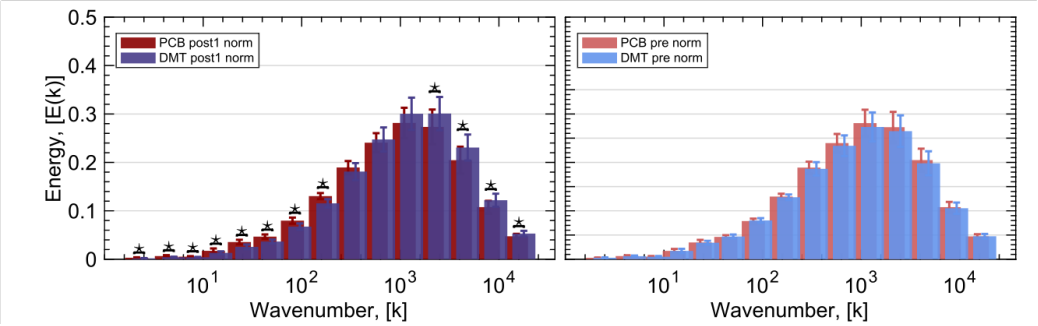



Figure A.7: ***Energy Spectrum of Connectome Harmonics Between Post-DMT and Post-placebo Conditions:*** (A) A decrease of energy for low-frequency harmonics $k \in [1,...,10^2]$ (p-value < 0.05, Bonferonni-corrected paired t-test) and an increase of energy for high-frequency harmonics $k \in [10^3,...,10^4]$ (p-value < $10^{-2}$ and p-value < $10^{-4}$ respectively, Bonferonni-corrected paired t-test) were observed. No statistically significant differences were observed in the pre DMT/PCB conditions.

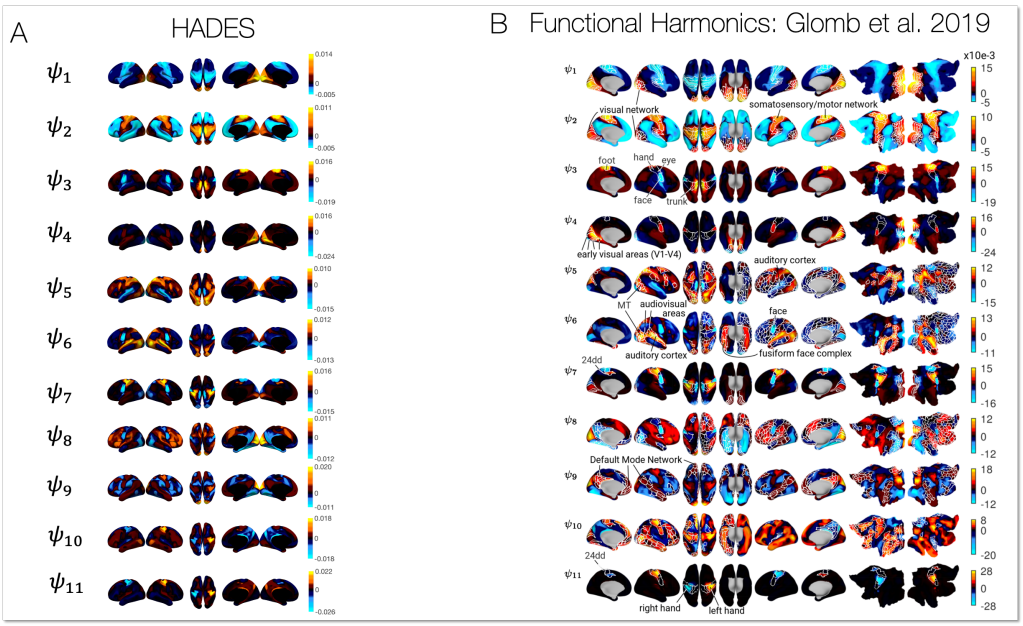



Figure A.8: ***Functional Harmonics of HADES and (Glomb et al., 2019):*** A Functional Harmonics derived from HADES. B Functional Harmonics reported by (Glomb et al., 2019) Both representations show consistency across Functional Harmonics, except for FH $\psi_{10}$. This could be due to different dense functional connectomes used - FHs in HADES are based on the HCP S1200 release with improved reconstruction software, whereas FHs in (Glomb et al., 2019) are computed from the original HCP S900 release.